Evaluation of the Effects of Tyrosine Kinase Inhibitors on the Metabolism of Human Tumor Cells using an NMR-based Biochemical Profiling Strategy

DISSERTATION

Zur Erlangung des Grades eines

Doktors der Naturwissenschaften

- Dr. rer. nat. -

Dem Fachbereich Biologie/Chemie der

Universität Bremen

vorgelegt von

Jelena Miljuš

Universität Bremen und University of Colorado Health Sciences Center, Denver

April, 2006

ZA MOJU VOLJENU MAMU

DANKSAGUNG

Mein besonderer Dank gilt meinem Doktorvater **Prof. Dr. Dieter Leibfritz** und **Frau Dr. Natalie Serkova** (UCHSC, Denver, USA).
Dank Prof. Leibfritz's Betreuung und hilfreichen Diskussionen war es möglich diese Arbeit anzufertigen. Vielen Dank für Ihr Vertrauen und Ermunterungen.
Bei Frau Dr. Serkova bedanke ich mich für die Themenstellung und freundliche Betreuung dieser Arbeit. Ich möchte mich weiterhin für die guten Arbeitsbedingungen und die finazielle Unterstützung bedanken.

Herrn Prof. Dr. Uwe Christians möchte ich für die Bereitschaft zur Begutachtung meiner Arbei danken. Seine Diskussionsbereitschaft und Ratschläge haben mir oft weiter geholfen.

Bei **Herrn Johannes Stelten** und **Dr. Wieland Willker** bedanke ich mich für deren Hilfe bei Lösungen NMR relevanter Probleme. Ausserdem danke ich allen weiteren Mitgliedern der Arbeitsgruppe von Prof. Dr. Leibfritz für die gute Zusammenarbeit.

I would like to thank **Prof. Dr. Thomas Henthorn** (chair) and all my other colleagues from the **Department of Anesthesiology** (Clinical Research and Development) at the UCHSC. My special thanks go to **Dr**. **Saskia Trump, Jaimi Brown, Jamie Bendrick-Peart, Dr. Yan-Ling Zhang and Jessica Collins** for their help and support, and their friendship.

Danke Jost ♥

ABBREVATIONS

Ab	Antibody
ADP	Adenosine Diphosphate
Ala	Alanine
Asp	Aspartate
ATP	Adenosine Triphosphate
BSA	Bovine Serum Albumin
Cho	Choline-containing compounds
Cho(l)	Cholesterol
CML	Chronic Myeloid Leukemia
Cr	Creatine
COX-2	Cyclooxygenase-2
DAG	Diacylglycerol
EDTA	Ethylendiaminetetraacetate
EGF(R)	Epidermal Growth Factor (Receptor)
FA	Fatty Acids
FACS	Flow Cytometry
FBS	Fetal Bovine Serum
FT	Fourier Transformation
5-FU	5-Fluorouracil
Glc	Glucose
Glu	Glutamate
Gln	Glutamine
GLT	Glutathione
GSH	Reduced Glutathione
GSSG	Oxidized Glutathione
Gly	Glycine
GPC	Glycerophosphocholine
GPE	Glycerophospho-ethanolamine
HPLC	High Performance Liquid Chromatography
HRP	Horseradish Peroxidase
HSQC	Heteronuclear Single Quantum Correlation
Ile	Isoleucine
Lac	Lactate
LDH	Lactate Dehydrogenase
MDR	Multi-drug Resistance
MRM	Multiple Reaction Monitoring
MRS	Magnetic Resonance Spectroscopy
MS	Mass Spectrometry
MUFA	Monounsaturated Fatty Acids
myo-Ins	myo-Inositol
n.s.	not significant
NAD^+	Nicotineamide Adenine Dinucleotide (oxd)
NADH	Nicotineamide Adenine Dinucleotide (red)
NMR	Nuclear Magnetic Resonance
NSCLC	Non-Small Cell Lung Cancer
NTP	Nucleotide Triphosphate
PBS	Phosphate Buffered Saline
PC	Phosphocholine / Pyruvate Carboxylase
PCA	Perchloric Acid
PCr	Phosphocreatine
PDH	Pyruvate Dehydrogenase
PE	Phosphoethanolamine
P-gp	P-glycoprotein
Ph	Philadelphia Chromosome
P_i	Inorganic Phosphate
PDE	Phosphodiester
PME	Phosphomonoester
ppm	parts per million
PtdCho	Phosphatidylcholine
PUFA	Polyunsaturated Fatty Acids
ROS	Reactive Oxygen Species
RT-PCR	Real-time Polymerase Chain Reaction
SD	Standard Deviation
TAG	Triacylglycerol
TCA	Tricarboxylic acid
TMSP	Trimethylsilylpropionic-2,2,3,3-d_4-acid
TK	Tyrosine Kinase
TKI	Tyrosine Kinase Inhibitor
Tyr	Tyrosine
VEGF(R)	Vascular Endothelial Growth Factor

Chapter 1

1. ZUSAMMENFASSUNG

Chronisch myeloische Leukämie (CML) entsteht aus der genetischen Translokation zwischen dem langen bcr-Arm des Chromosoms 9 und dem kurzen abl-Arm des Chromosoms 22 (Philadelphia Chromosom). Das neugebildete Oncogen BCR-ABL exprimiert die tumorspezifische Proteinkinase Bcr-Abl, welche in großen Mengen in transformierten CML Zellen vorkommt. Die Wirkungsweise von Imatinib (Gleevec^{TM}, Glivec^{TM}) besteht in der kompetitiven Hemmung der ATP-Bindungsstelle des Bcr-Abl-Enzyms. Diese Bindung blockiert die Tyrosinphosphorylierung von Proteinen, welche in die Bcr-Abl Signaltransduktion involviert sind. Die Korrelation zwischen den molekularen Mechanismen (Hemmung der Tyrosinkinase-Aktivität) von Imatinib und seiner Effizienz in klinischen CML-Studien ist bereits etabliert. Das Hauptproblem in der klinischen Praxis besteht darin, dass die Leukämiezellen nicht auf das Medikament ansprechen oder im Verlauf der Behandlung eine Resistenz entwickeln (in 60% der Patienten). Die Entschlüsselung der molekularen Mechanismen könnte daher helfen, die Wirksamkeit der Therapie zu verbessern. Es gibt allerdings keinerlei Informationen bezüglich metabolischer Veränderungen in den Imatinib-behandelten Bcr-Abl positiven Zellen, die helfen könnten diese molekularen Mechanismen aufzuklären.

Das Ziel dieser Arbeit war es die metabolischen Profile der Imatinib-sensitiver, behandelter und Imatinib-resistenter Leukämiezellen zu analysieren, um dadurch tiefere Einblicke in die Wirkungsweise dieses Tyrosinkinasehemmers auf den Zellstoffwechsel zu erhalten. Es wurden die Änderungen im Zellstoffwechsel während der Imatinib-Therapie, in der Phase der Resistenzentstehung und am Ende dieses Prozesses verfolgt. Desweiteren wurden die Folgen des Imatinib-Entzugs an Kulturen resistenter Zellen untersucht. Für die Aufklärung wurden Kern-Magnetische Resonanzspektroskopie (NMR) und Massenspektrometrie (MS) angewandt. Neben diesen beiden Techniken wurden auch Western Blott Analyse, Polymerase Ketten Reaktion (PCR) und flow cytometrische Analysemethoden benutzt. Für die Messungen der intra- und

extrazellulären Imatinibkonzentrationen wurde eine empfindliche Hochleistungsflüssigkeitschromatographie – Massenspektrometrie (HPLC-MS) Methode entwickelt und validiert.

Zwei imatinib-sensitive und resistente Klone der Bcr-Abl positiven K562 und LAMA84 Zellen wurden paarweise für die Untersuchung der metabolischen Effekte der Imatinibresistenz benutzt. Der Mechanismus der Resistenzentwicklung in den beiden gegenüber 1 μM Imatinib resistenten Zellinien, K562-r und LAMA84-r Zellen, ist verbunden mit der Überexprimierung des Bcr-Abl und des p-Glykoproteins. In K562-R Zellen, die gegenüber 5 μM Imatinib resistent sind, sind die Ursachen für das Auftreten der Resistenz noch nicht aufgeklärt und sind möglicherweise auf die Exprimierung anderer Tyrosinkinasen zurückzuführen.

Bcr-Abl positive Leukämiezellen verhalten sich wie andere Tumorzellen: die zeigen eine schnelle Proliferationsrate, einen hohen Bedarf an Glukose und den Wechsel von der oxidativen zur anaeroben Glykolyse und Laktatproduktion (Warburg-Effekt) auf.

Die Behandlung mit Imatinib hemmte die Proliferationsraten der leukämischen Zellen und induzierte Zeit- und konzentrationsabhängig die Apoptose. Die ersten Zeichen apoptotischer Veränderungen wurden eine Woche nach Behandlung mit relativ geringer Imatinib Konzentration von 0.1 μM sichtbar. Die Geschwindigkeit nahm mit länger werdender Inkubationszeit zu. Bei Imatinib Konzentrationen von 1 μM und höher, zeigten die Zellen ähnliche, jedoch sich schneller entwickelnde Effekte.

In der frühen apoptotischen Phase führte die Behandlung mit Imatinib zu erhöhten ATP Konzentrationen, die darauf hindeuteten, dass die Zellen eher der Apoptose als der Nekrose unterliegen. Die Nekrose führt unmittelbar zu sinkender ATP Konzentration bevorzugt. Die mitochondriale Aktivität der Zellen, welche mit weniger als 0.4 μM Imatinib 24 Stunden lang oder mit 0.1 μM eine Woche lang behandelt wurden, war ebenfalls angeregt. Die Bcr-Abl Tyrosinkinase Aktivität, als Zeichen für die Effizienz der Behandlung, war bereits nach 24 Stunden mit 0.1 μM Imatinib vollständig gehemmt. Mit zunahmender Imatinibkonzentration nahm die Apoptoserate schnell zu. Die resultierenden metabolischen Änderungen, die mit Hilfe von NMR erfassbar waren, korrelierten mit den ablaufenden Zelltodprozessen. Sowohl die Phosphokreatinkonzentration, der Energiekurzzeitspeicher, als auch die Konzentrationen von Glutathion

und NAD^+ nahmen ab. Die Abnahme der NAD^+ Konzentration wurde in der Literatur als einer der ersten Schritte in der Auslösung von Apoptose bezeichnet. Die ATP Konzentration, die ihr Maximum in der frühen apoptotischen Phase erreicht hatte, nahm mit deren Weiterentwicklung ab. In derselben Zeit nahmen auch die mitochondriale und die glykolytische Aktivität ab. Die Menge des Glukosetransporters Glut-1 nahm ab und die Versorgung der Zelle mit Glukose war beeinträchtigt. Im nächsten Schritt der Apoptose, bilden sich apoptotische Körper aus. Für die Ausbildung dieser Ausstülpungen wird Membranmaterial benötigt, welches durch eine Steigerung der Lipidbiosynthese bereitgestellt wurde. Die Konzentrationen der am Kennedyzyklus teilnehmenden Substanzen Phosphocholin und Phosphatidylcholin waren reduziert. Als Folge kam es zur Akkumulation von Tri- und Diacylglyceriden. Dieser Anstieg wiederum bewirkte eine Zunahme der mehrfachungesättigten Fettsäuren. Die Expression des p-Glykoproteins (pgp), welches zur Gruppe der *multidrug resistence* (MDR) Proteine gehört und für den Export von Substanzen aus der Zelle hinaus sorgt, nahm proportional zur Behandlungsdauer sowie zunehmender Imatinibkonzentration ab. Dadurch erhöhte sich die effektive, intrazelluläre Imatinibkonzentration. Im lezten Schritt der Apoptose, der "sekundäre Nekrose", waren die mitochondriale und die glykolytische Aktivität der Zelle als Folge der Imatinib Behandlung drastisch reduziert und die resultierende Energieversorgung minimal.

Gemeinsames Merkmal aller drei untersuchten resistenten Zellsorten ist ihr hoher Verbrauch an Glukose. Die Bildung von Laktat ist stark erhöht und ebenso dessen Transport in den extrazellulären Raum. Die resistenten Zellen gleichen in dieser Hinsicht den sensitiven Leukämiezellen, wobei ihre Laktatproduktion sogar noch erhöhter war.

Der wesentliche Unterschied zwischen den K562 und LAMA84 resistenten Zellinien liegt in ihrer unterschiedlichen Entstehung. Sowohl K562-r als auch K562-R Zellen wurden von derselben Zellsorte, den K562-s Zellen abgeleitet. Diese weisen Unterschiede auf molekularer Ebene auf, wie zum Beispiel in der Expression der Bcr-Abl, Glut-1 oder der pgp Proteine. Ausserdem vermögen sie in der Gegenwart verschiedener Imatinibkonzentrationen (1 oder 5 μM) zu überleben. Dennoch weisen, wie mit NMR-Spektroskopie gezeigt, K562-r und K562-R Zellen fast nicht unterscheidbare Zellstofwechselprofile auf, ein Indiz dafür, dass beide Zellinien dieselben metabolischem

Veränderungen auf dem Weg zur Imatinibresistenz genommen haben. Diese beinhalten erniedrigte Konzentration an intrazellulärem Laktat (stark erhöhter Transport nach aussen in das Zellmedium), keine Änderung in der Citratzyklusaktivität und annähernd die gleichen erniedrigten Konzentrationen an Phosphocholin, Glycerophosphocholin und -ethanolamin.

Das metabolische Profil der LAMA84-r Zellen zeigt höhere Konzentrationen an Phosphocholin und Phosphatidylcholin, Zunahme der cytosolischen Glykolyserate und eine Verbesserung der mitochondrialen Metabolisierung and des Energiestatus der Zelle. Diese Änderungen resistenter LAMA84 Zellen stimmen mit den Ergebnissen anderer MDR überexprimierenden, resistenten Zellarten überein. Das metabolische Profil könnte als Profil der Imatinibresistenz oder allgemeiner Resistenz gegenüber Medikamenten dienen, bei welchem durch das pgp-Protein die effektive intrazelluläre Konzentration des Therapeutikums herabgesetzt wird.

Nach der einwöchigen Enfernung von Imatinib aus der Kultur unterlagen die resistenten Zellen den Folgen von Apoptose bzw. Nekrose / "sekundäre Nekrose". Die Zellen zeigten wieder einige der Eigenschaften wie die entsprechenden sensitiven Zellen (wie z.B. bezüglich der Laktatproduktion oder der Phosphodiesterkonzentrationen, deren Änderungen sich den Kontrollwerten wieder annährten). Diese Beobachtung könnte als nützliches Hilfsmittel bei der Erkennung des Phänomens der klinischen Imatinibresistenz dienen. Nachdem die Zellen durch den Entzug sensibilisiert wurden, konnten sie anschliessend wieder erfolgreich mit Imatinib behandelt werden. Die intrazelluläre Imatinib-Konzentration resistenter Zellen, die nach einem einwöchigen Imatinib Entzug wieder mit der selben Konzentration wie davor behandelt wurden, war geringer als vor dem Entzug. Dies kann mit dem Anstieg der MDR-Transporter (multi drug resistance), wie zum Beispiel des α1-sauren Glykoproteins erklärt werden. Dieses Glykoprotein transportiert bei hoher extrazellulärer Konzentration Imatinib aus der Zelle hinaus. Daher wäre eine Kombinationstherapie von Imatinib und glykoproteinhemmenden Substanzen vom Nutzen in der Behandlung der auftretenden Resistenz.

Ein weiterer spezifischer und umstrittener Tyrosinkinasehemmer, Gefitinib (ZD1839, Iressa^{TM}) hemmt den epidermalen Wachstumsfaktorrezeptor (EGFR). Dadurch

wirkt es insbesondere bei Krebsarten, die hohe Mengen an EGFR enthalten, wie z.B. der nicht-kleinzelligen Lungenkrebs (NSCLC). EGFR ist an vielen Zellprozessen beteiligt, wie z.B. an der Zellproliferation, Hemmung der Apoptose oder der Förderung der Angiogenese und Metastasenbildung.

Das Ziel dieser Studie war es, metabolische Unterschiede der verschiedenen Gefitinib-abgeleiteten Behandlungsstratgien aufzudecken, um diese *in vitro* Ergebnisse als Indikatoren für klinische Studien verwenden zu können.

Die Studie basierte auf NMR-Analysen kombiniert mit der flow-cytometrischen Analyse von Proteinen. Zwei Darmkrebszellinien, HCT-116 und HT-29, wurden mit Gefitinib (15 μM), 5-Fluorouracil (5-FU, 1.5 μM) und Celecoxib (3.5 μM) 96 Stunden lang behandelt. Zusätzlich wurden die Effekte von Gefitinib und 5-Fluorouracil auf nicht-kleinzellige Lungenkrebszellen, H322 and H1334 untersucht.

Behandlung der Darmkrebs- und Lungenkrebszellen zeigte ähnliche metabolische Muster wie bei der Imatinibbehandlung: Abnahme der mitochondrialen und cytosolischen Aktivität, Abfall der Phosphokreatinkonzentration und Zunahme der Lipidbiosynthese gefolgt. Die Konzentrationen organischer Osmolyten nahm zu und die Zellen schrumpften. Andererseits nahm die Konzentration von Phosphocholin und Phosphatidylcholin ab. Die Verabreichung von Gefitinib alleine oder in Kombination mit 5-Fluorouracil hemmt die Zellproliferation und löst den apoptotischen Zelltod aus. Die kombinierte Gabe von Gefitinib, 5-Fluorouracil und Celecoxib, einem entzündungshemmenden Cycoloxygenase-2-Hemmer, führte zu interessanten Ergebnissen. Diese Dreifachkombination unterband die Zellproliferation, wirkte aber weniger cytotoxisch und hinterliess keine negativen Effekte auf die mitochondriale Aktivität und Energieproduktion. Gleichzeitig wurde eine Verbesserung und Anhebung der totalen Glutathionkonzentration auf das Niveau unbehandelter Zellen beobachtet, weshalb eine Beteiligung von anti-ROS (reaktive Sauerstoffspezies) Mechanismen möglich ist. Dies führt zur Hypothese, dass Celecoxib die Zellen vom oxidativen Stress und den Schäden der ROS schützt, ohne die anti-proliferative Wirkung von Gefitinib zu beinflussen. Diese Ergebnisse deuten darauf hin, dass eine Kombination mit Cyclooxygenase-2-Hemmern besser tolerierte klinischen Behandlungsstrategien relvanter Krankheiten ermöglichen könnte.

Wie in dieser Arbeit gezeigt wurde, besitzt „metabolic profiling“ ein grosses Potenzial, die Entwicklung neuer klinischer Diagnostika zu verbessern, und somit zu helfen, Krankheitsbilder im früheren Stadium zu erkennen und zu verhindern, als dies mit herkömmlichen klinisch-diagnostischen Methoden derzeit möglich ist.

1. SUMMARY

.

Chronic myelogenous leukemia (CML) is triggered by a translocation of chromosome 22 onto chromosome 9 in white blood cells. This translocation, known now as the Philadelphia chromosome, creates the fused oncogene BCR-ABL that is expressed as a tyrosine kinase fusion protein. Imatinib (Gleevec^{TM}) functions through competitive inhibition at the ATP-binding site of the BCR-ABL, which leads to the inhibition of tyrosine phosphorylation of proteins involved in BCR-ABL signal transduction pathway. The major concern regarding imatinib treatment is the development of drug resistance in CML patients. During long-term therapy, resistant clones can emerge in more than 60% of patients treated with imatinib. Although the correlation between the molecular mechanisms and imatinib efficacy in clinical trials is well established, there is no precise information about the changes in cell metabolism in CML cells during exposure to the drug.

The goal of this project was to assess the metabolic profiles of sensitive, imatinib-treated and imatinib-resistant leukemia cells to gain mechanistic insights into the effects of tyrosine kinase inhibitors on cell metabolism during the therapeutic effect, during drug resistance and its development and after withdrawal of tyrosine inhibitors from sensitive and resistant cancer cell lines. Most studies were based on nuclear magnetic resonance (NMR) and mass spectrometry (MS) metabolic profiling. To further evaluate underlying mechanisms Western blotting, polymerase chain reactions (PCR) and flow cytometry-based assays were used. For the measurement of drug concentrations an automated, highly sensitive high-performance liquid chromatography- mass spectrometry (LC-MS) assay was developed and validated.

Two paired imatinib-sensitive and resistant clones of K562 and LAMA84 leukemia cell lines were used to evaluate metabolic effects of imatinib resistance. Both to 1 μM imatinib resistant K562-r and LAMA84-r cells were resistant due to Bcr-Abl and p-glycoprotein overexpression, the mechanism of the resistance in to 5 μM imatinib resistant K562-R cells is still unknown (and may be implicating other tyrosine kinases). Bcr-Abl positive leukemia cells behave like other cancer cells; they retain a high proliferation rate, require large amounts of glucose for energy production and growth and

exhibit a metabolic shift from oxidative to elevated anaerobic glycolysis and lactate production (Warburg effect).

Treatment of sensitive leukemia cells with imatinib inhibited the proliferation rate and time- as well as concentration-dependently induced cell death. Apoptosis induction appeared at low drug concentrations (0.1 μM) after one week. The rate continuously increased with a longer incubation time. Imatinib concentrations at 1.0 μM or above showed similar, but rapidly increasing effects on the cell viability.

In the early apoptotic stage, imatinib-treated cells showed elevated ATP concentrations, which play a critical role in determining the mode of cell death, apoptosis *vs.* necrosis under ATP-depleting conditions. The mitochondrial cell activity was increased as well, in case the cells were treated with less the 0.4 μM imatinib for 24 hours or when treated with 0.1 μM for 1 week. Bcr-Abl tyrosine kinase activity as a sign for the drug efficacy was completely inhibited after 24 hours with 0.1 μM imatinib. With an increase of imatinib concentrations during treatment, the process of cell death rapidly progressed and was linked to metabolic changes as assessed by NMR analysis. Total glutathione, phosphocreatine and NAD^+ concentrations started to decrease during the early apoptosis and were found to be associated with initiation of the apoptotic cascade. The ATP concentrations reached their maximum at this stage, and declined with progression of the apoptotic processes. Mitochondrial activities as well as the glycolysis rates were both reduced. We showed that glucose uptake was impaired, due to the down-regulation of the glucose Glut-1 transporter and its re-distribution from the cell membrane into the cytoplasm. In the next step, the formation of the necessary membrane materials for apoptotic bodies was produced by up-regulation of lipid synthesis. The concentrations of the Kennedy pathway intermediates, phosphocholine and phosphatidylcholine were reduced. This led to increased concentrations of triacylglycerol (and diacylglycerol) and implicated an increase in polyunsaturated fatty acids. Decreased expression of p-glycoprotein (pgp), a multidrug resistance (MDR) protein and drug efflux transporter, affected the intracellular imatinib concentrations that increased subsequently. The concentration of intracellular organic osmolytes increased, indicating cell shrinkage. In the last step of apoptosis, the ”secondary necrosis”, the mitochondrial and glycolytical activities were drastically reduced, die energy production was minimal, and the cell was

underlying the consequences of imatinib treatment.

A common characteristic of all three investigated imatinib-resistant cell lines is high glucose uptake and consumption and an increased lactate production. Regarding this metabolic aspect, the resistant cells act like their sensitive counterparts and reveal even higher anaerobic glycolysis rates than those (and Warburg Effect).

The major difference between the K562 and LAMA84 resistant cell lines certainly lies in their different origins. Both K562-resistant cell lines were derived from the same sensitive cell line. They are resistant to different imatinib concentrations (1 and 5 μM) and show differences in protein expression. Nevertheless, their metabolic profiles are very similar suggesting that both cell lines have gone through the same metabolic changes on their way to become resistant. The endpoints of their metamorphosis are represented in a lower intracellular lactate concentration (the transport into the extracellular room is highly elevated) and reduced concentrations of phosphocholine, glycerophosphocholine and -ethanolamine (which were almost the same in both K562-resistant cell lines). No differences in the TCA cycle activity between K562-sensitive and resistant cells were observed, but the energy balance was decreased in resistant clones.

Another metabolic profile of imatinib resistance was derived from a MDR protein expressing LAMA84-r cell line and corresponded very well with NMR-analysis reports from other resistant, pgp-overexpressing cell lines. This particular cell lines showed increased cytosolic glycolysis, improvement of mitochondrial metabolism and energy state of the cell and increased phosphocholine and phosphatidylcholine concentrations. These parameters could serve as a metabolic signature indicating development of imatinib resistance and is at least in part due to a decrease of effective intracellular drug concentrations.

Results from imatinib withdrawal studies based on for one week imatinib-depleted resistant cell lines, showed that the detected metabolic changes corresponded well to the apoptosis and necrosis/"secondary necrosis"- based observations previously made. It furthermore seemed that the cells were regaining some of the properties of their parental clones (e.g. lactate production decreased, while the phosphodiester concentration increased towards control values). This information can be used as a helpful tool to treat the phenomenon of imatinib-resistance. After resistant cells have been detected, they can

either be exposed to imatinib again or to other drugs. Additionally, the observation was made that the intracellular imatinib concentration was much lower in cells being withdrawn from imatinib and re-exposed to the drug. If the assumption is correct that this observation resulted from an increase in drug-transporter activity, a combination therapy with agents inhibiting p-glycoprotein could be useful to overcome imatinib resistance. It has been seen that during exposure to high concentrations, the intracellular imatinib concentrations were much lower than expected and a possible involvement of other drug transporters such as α1-acid glycoprotein has been discussed.

Another specific and controversial tyrosine kinase inhibitor, approved for treatment of non-small cell lung cancer in 2003, is gefitinib (ZD1839, Iressa^{TM}). It inhibits the activity of EGFR (epidermal growth factor receptor), which contributes to uncontrolled cell proliferation, inhibition of apoptosis, promotion of angiogenesis and metastasis and thus making it an attractive agent for anticancer therapies.

The goal of this project was to distinguish the differences in metabolic pathways during different gefitinib-based treatment types in colon cancer cells and to use these *in-vitro* results as predictors for following clinical trials.

The study included NMR-based approach combined with flow cytometric assays on protein expression. Two human colorectal cell lines, HCT-116 and HT-29, were used to evaluate the effects of gefitinib (15 μM), 5-Fluorouracil (5-FU, 1.5 μM) and Celecoxib (3.5 μM) after 96 hours of incubation. In addition, effects of gefitinib and 5-FU on two non-small lung cell lines, H322 and H1334, were investigated as well.

The colon cancer and non-small lung cells treated with gefitinib revealed metabolic patterns very similar to imatinib-treated cells. Decreased mitochondrial and cytosolic activity, a reduction of phosphocreatine concentrations and changes in lipid metabolism were seen. More membrane material has been produced for apoptotic bodies formation, under decrease of phosphocholine and phosphatidylcholine concentrations. Gefitinib alone and in combination with 5-Fluorouracil, successfully inhibited cell proliferation and induced apoptosis.

Interesting results were perceived by combining gefitinib with 5-Fluorouracil and Celecoxib, an anti-inflammatory cyclooxygenase-2 inhibitor. This “TRI”-combination

treatment disrupted cell proliferation, but seemed to be less cytotoxic. It did not show a negative impact on the TCA cycle activities or the energy balance of the cells. Due to an improvement of total glutathione concentration back to normal values, the involvement of different mechanisms including the inhibition of reactive oxygen species production was discussed, but will need to be further investigated. If the hypothesis that Celecoxib prevented the cells from oxidative stress damage without reducing the anti-proliferative action of gefitinib and 5-Fluorouracil is correct, this may provide a platform strategy for developing combination therapies for different diseases with improved safety and tolerability.

These findings and observation may be important in the evaluation, identification, prediction of patients developing resistance and treatment of cancer. Based on these results, metabolic profiling of blood from imatinib-treated patients has the potential to be developed into a diagnosis tool to detect the development of resistant leukemia cells at an early stage. Furthermore, preclinical models of human cancer and their metabonome analysis suggest potential benefits of combined targeting of proteins for cancer prevention.

Chapter 2

2. INTRODUCTION

2.1. Blood cancer: an overview

The history of leukemia began in 1845, when Rudolph Virchow, a young Berlin pathologist, was puzzled by the strange symptoms displayed by one of his patients. He was amazed to discover that the patient's blood had a lack of red blood cells and an excess of white or colorless cells. Virchow coined the term "leukemia" ("white blood"). By 1900, leukemia was no longer seen as a single disease, but was rather viewed as a tree with two main limbs that in turn have two primary branches (acute or chronic), all of which reflect the type of blood cell leukemia originates from (lymphocytic or myelogenous).

There are four common types of leukemia:

- Chronic lymphocytic leukemia (chronic lymphoblastic leukemia, CLL) accounts for about 9,700 new cases of leukemia each year in the U.S. Most frequently it is diagnosed in patients over the age of 55 years.
- Chronic myeloid leukemia (chronic myelogenous leukemia, CML) accounts for about 4,600 new cases of leukemia each year in the U.S. It affects mainly adults.
- Acute lymphocytic leukemia (acute lymphoblastic leukemia, ALL) accounts for about 4,000 new cases of leukemia each year in the U.S. It is the most common type of leukemia in young children, but it also affects adults.
- Acute myeloid leukemia (acute myelogenous leukemia, AML) accounts for about 11,900 new cases of leukemia each year in the U.S. It occurs in both adults and children.
- Hairy cell leukemia is a rare type of chronic leukemia.

All facts and numbers were obtained from http://www.leukemia-lymphoma.org and http://www.cancer.gov, an official homepage of the U.S. National Cancer Institute.

An important clue that guided the discovery of the genetic origin of chronic myeloid

leukemia (CML) was that exposure to high amounts of radiation damaged the gene-harboring chromosomes of survivors and made them prone to developing CML.

2.1.1. Chronic myeloid leukemia (CML): Background

CML accounts for about 20% of newly diagnosed cases of leukemia in adults. About 20 to 30% of people who have CML die within 2 years after the diagnosis, and about 25% die each subsequent year (The Merck Manual of Medical Information — Second Home Edition, 2003). Today, allogenic bone marrow transplantation is the only proven curative treatment for CML. Allogenic bone marrow transplantation, however, is restricted to a small number of CML patients. Allogenic stem cell transplantation is a promising therapeutic strategy for patients with a suitable human leukocyte antigens (HLA)-matched donor and acceptable health conditions to tolerate the transplantation procedure (Hehlmann et al., 2000). However, up to 65% of the younger patients do not have suitable HLA-matched donors. Meta analysis of clinical trials showed that transplant-related mortality differs between 18 to 68% and is strongly associated with increasing age (Savage and Antman, 2002). Standard treatment with busulfan or interferon treats the symptoms, but does not prolong life. In addition, interferon therapy is associated with severe side effects. To develop more targeted and non-toxic treatments for CML, scientists needed to delve deeper into the conundrum of what exactly causes leukemia.

The Philadelphia chromosome (Ph) was originally described as a chromosomal abnormality in 1960 by Nowell and Hungerford. In 1973, Rowley reported that this abnormal chromosome, found in most patients with chronic myeloid leukemia (CML), has an apparent loss of the long arm of chromosome number 22 and is the result of reciprocal translocation involving the long arms of chromosomes 9 and 22, t(9;22) (Rowley, 1973). On the molecular level, the Ph chromosome results in juxtaposition of bcr and abl sequences, leading to a protein termed Bcr-Abl (Heisterkamp et al., 1983) (Figure 2.1). The BCR–ABL fusion results in the production of a constitutively active cytoplasmic tyrosine kinase that does not block differentiation, but enhances proliferation and viability of myeloid lineage cells. BCR–ABL is likely sufficient to cause CML, but over time other genetic events occur and the disease progresses to an acute leukemia.

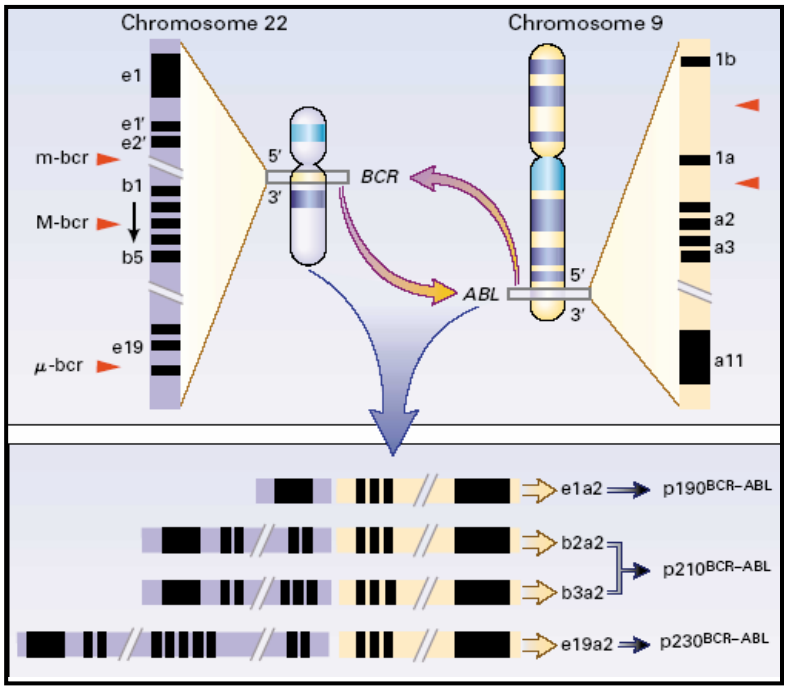

Figure 2.1: Philadelphia chromosome translocation and BCR-ABL formation. The kinase activity of Bcr-Abl is 5 to 10-fold higher than the kinase activity of c-Abl (adapted from hematology.im.wustl.edu/conferences/ presentations/uy043004.ppt).

2.1.2. Regulation of normal tyrosine kinase activity

Tyrosine kinases (TKs) are divided into two main classes, receptor and non-receptor TKs. Receptor TKs are transmembrane proteins with a ligand-binding extracellular domain and a catalytic intracellular kinase domain, whereas non-receptor TKs lack transmembrane domains and are found in the cytosol, the nucleus, and the inner surface of the plasma membrane. The enzymatic activities of both types of TKs are under tight control, so that non-proliferating cells have very low levels of tyrosyl-phosphorylated proteins (Krause and Van Etten, 2005).

In the absence of ligand, receptor TKs are unphosphorylated and monomeric, and the kinase domains are inactive. Receptor TKs become activated when ligand binds to the extracellular domain. These changes lead to a reorientation of critical amino acid residues, thereby increasing the catalytic activity of the enzyme (Schlessinger J, 2000). After activation, autophosphorylation generates binding sites for signaling proteins, recruiting them to the membrane and activating multiple signaling pathways (Schlessinger J, 2000; Griffith et al., 2004).

The non-receptor TKs, typified by c-ABL, are maintained in an inactive state by cellular inhibitor proteins and lipids and through intramolecular autoinhibition (van Etten, 2003). Non-receptor TKs are activated by diverse intracellular signals through dissociation of inhibitors, by recruitment to transmembrane receptors (causing oligomerization and autophosphorylation), and through *trans*-phosphorylation by other kinases. TK signaling is terminated in part through the action of tyrosine phosphatases that hydrolyze tyrosyl phosphates and by the induction of inhibitory molecules (Krause and Van Etten, 2005; Van Etten RA, 2003).

2.1.3. Mechanisms of TK dysregulation in cancer

In cancer cells TKs are dysregulated and, through different pathways, lead to enhanced phosphorylating activity. A common mechanism of TK activation is the fusion of a TK with a partner protein, usually as a consequence of a balanced chromosomal translocation for example Ph chromosome, in which tetramerization domain in BCR overcomes autoinhibition of ABL catalytic activity through oligomerization and autophosphorylation (Smith et al., 2003). (Figure 2.1)

A second important mechanism of TK dysregulation is a mutation that disrupts auto-regulation of the kinase. For example, small deletions and point mutations in the kinase domain of epidermal growth factor receptor (EGFR) in a subset of non–small-cell lung cancers increase the sensitivity of the receptor to its ligand (Lynch et al., 2004) and alter receptor signaling (Pao et al., 2004; Sordella et al., 2004).

A third mechanism of TK dysregulation is increased or aberrant expression of a receptor TK, its ligand, or both. Lastly, increased TK activity can result from a decrease in factors that limit TK activity, such as impaired tyrosine phosphatase activity or decreased expression of TK inhibitor proteins (Watanabe et al., 2004). Aberrant TK activation can increase the survival, proliferation, and cytotoxic drug resistance of malignant cells, and in tumors it can increase angiogenesis, invasiveness, and metastatic potential (Krause and Van Etten, 2005).

2.1.4. Strategies to target TKs in cancer therapy

TKs can be inhibited pharmacologically through multiple mechanisms. The major idea

behind anti-TK drug discovery is to find small molecules that directly inhibit the catalytic activity of the kinase by interfering with the binding of ATP or substrates (Sawyer TK, 2004; Paul and Mukhopadhyay, 2004; Sawyers CL, 2002). Other anti-TK drugs may inhibit activation of fusion TKs by blocking their dimerization. Antibodies against receptor TKs or their ligands interrupt TK signaling through neutralization of ligand, blockade of ligand binding, receptor internalization, and perhaps antibody-mediated cytotoxicity (Bennasroune et al., 2004; Craven et al., 2003). An important advantage of TK-directed therapy is that it is possible to perform pharmacodynamic studies that correlate inhibition of the targeted TK in cancer cells with clinical responses to the drug.

2.2. Imatinib Mesylate: The first successful small molecule TK inhibitor

2.2.1. Imatinib: mechanism of action

In 1996, Novartis Pharmaceuticals (Basel, Switzerland) in collaboration with Druker and colleagues developed the experimental drug CGP57148B that today is known as imatinib mesylate (imatinib, STI571, Gleevec®/Glivec®) (Figure 2.2).

Imatinib is an ABL tyrosine kinase inhibitor of the 2-phenylamino pyrimidine class (4-[(4-methyl-1-piperazinyl)methyl]-N-[4-methyl-3-[4-(3-pyridinyl)-2-pyrimidinyl]amino-phenyl] benzamide methanesulfonate) that was created using the structure of the ATP binding site of the ABL protein kinase (Druker et al., 1996; Buchdunger et al., 2000). Imatinib binds to and stabilizes the inactive form of BCR–ABL. Functionally, imatinib acts by revoking the effects of the BCR–ABL oncoprotein through inhibition of BCR–ABL autophosphorylation and substrate phosphorylation, inhibition of proliferation, and induction of apoptosis (Druker et al., 1996; Gambacorti-Passerini et al., 1997; Deininger et al., 1997) (Figure 2.3).

Despite the apparent specific anti-leukemic effect of imatinib in CML through inhibition of the ABL protein kinase, it also possesses inhibitory properties against other members of the tyrosine kinase family including PDGFRα/β and c-kit (Buchdunger et al., 1996).

Imatinib has the potential to be a curative drug and can be used as a first line treatment in the management of CML. However, the long-term effects of imatinib and its ability to cure CML as a single agent are unknown. It is still unclear as to whether or not imatinib

is sufficient to eradicate the disease; in addition, there is well-documented proof of primary and secondary resistance of leukemia cells to imatinib.

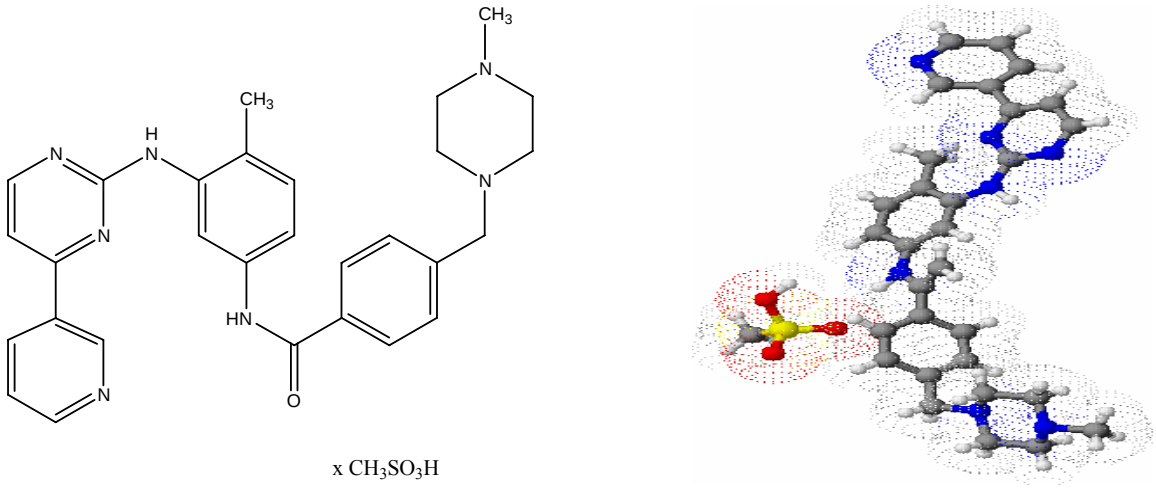

Figure 2.2: Chemical structure of imatinib mesylate, Gleevec™, ($C_{30}H_{35}N_7O_4S$; molecular weight 589.71 g/mol).

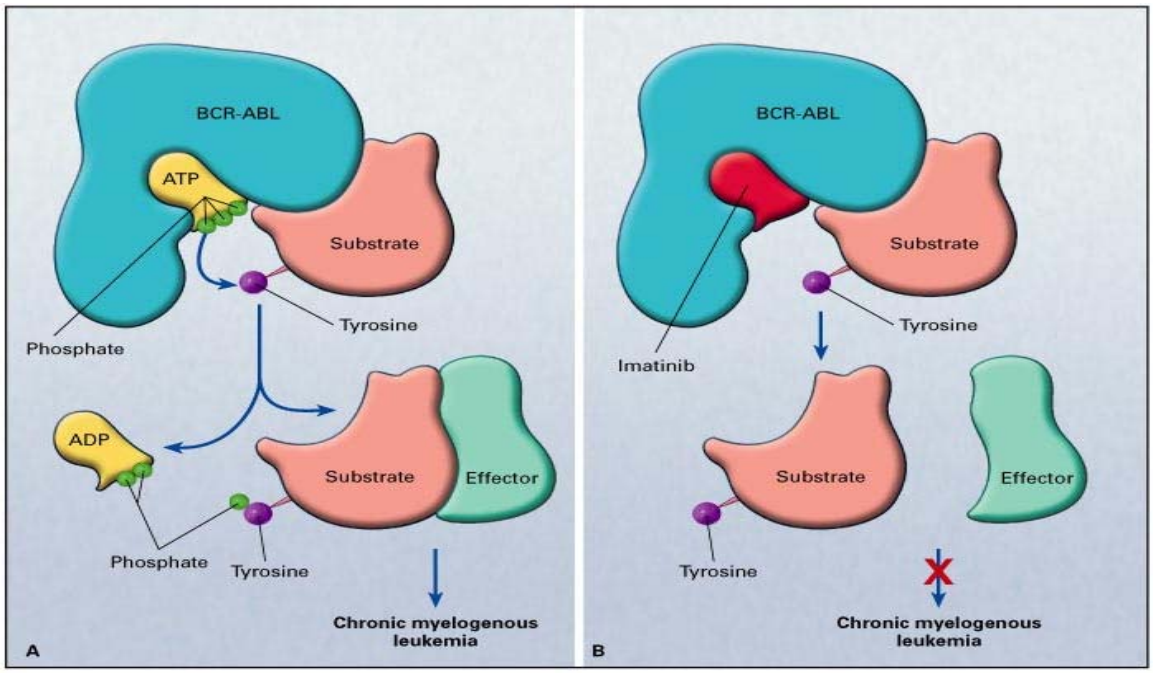

Figure 2.3: The activation gatekeepers are TKs molecules; cytokines or ligands that signal for replication bind to TKs, activating their ATP binding sites (A). By blocking ATP binding sites on specific mutant tyrosine kinases, imatinib directly interferes with the downstream propagation of signaling pathways to the nucleus that promote the growth of tumor cells (B) (adapted from Goldman and Melo, 2001).

The primary effect of imatinib on BCR–ABL expressing progenitor cells seems to be inhibition of proliferation rather than induction of apoptosis (Holyoake et al., 2001; Bhatia et al., 2003). As imatinib holds the activity of BCR–ABL dormant, it is possible that a single drug may not be sufficient to completely eradicate the tyrosine kinase positive stem cells from the body. Despite successful results in patients with early stages of CML, the unsatisfying activity of imatinib in advanced stages of CML (Hughes et al., 2003; Talpaz et al., 2002; Kantarjian et al., 2002) raised the need to identify novel drugs that are more potent against ABL and that are also effective in regards to resistant patients, particularly those with point mutations.

2.2.2. Imatinib Resistance

Resistance to imatinib can be defined as the lack of complete hematological response in patients with chronic phase disease or as a lack of return to chronic phase for patients in acute phase, in blast crisis CML, or with Ph positive ALL (Talpaz et al., 2002; Kantarjian, Sawyers et al., 2002). Depending on the time of onset, two categories of resistance can be distinguished:

- If there is no response after initial treatment, resistance is described as primary or extrinsic.
- In contrast, secondary or intrinsic resistance is present if resistance develops after achieving an objective response. Development of resistance to imatinib in advanced CML is frequent. Seventy % of patients with acute leukemia develop resistance within the first 6 months of treatment (Ottmann et al., 2002).

Potentially the most frequent clinically relevant mechanisms that change imatinib sensitivity in BCR–ABL transformed cells are mutations within the ABL kinase, affecting several of its properties (Figure 2.4) (Gorre et al., 2001; Hochhaus et al., 2002).
Point mutations can directly influence the proper binding of imatinib to the target molecule, as well as the binding of ATP (Roumiantsev et al., 2002; von Bubnoff et al., 2002). Furthermore, mutations can lead to conformational changes of the protein, affecting binding of either imatinib or ATP in an indirect way (Branford et al., 2002; Shah et al., 2002; Nagar et al., 2002). Imatinib-resistant mutations are likely to be induced by imatinib itself, due to selection of BCR–ABL expressing clones that harbor

the point mutation. In these particular cells, imatinib is unable to efficiently bind and thus permits a growth advantage due to lack of ABL kinase inhibition (Pricl et al., 2005; Gorre et al., 2001; von Bubnoff et al., 2002). This is consistent with the finding that resistance-mediating mutations can be found at very low levels in patients prior to clinical imatinib resistance (Branford et al., 2003; Hofmann et al., 2003).

Five different point mutations resulting in four distinct amino acid exchanges within the ATP-binding site and activation loop of Bcr-Abl have been recorded (von Bubnoff et al., 2002). From these mutations, the Thr315Ile (threonine 315 to isoleucine) seems to play the crucial role in resistance development to imatinib, which predicted threonine 315 to be a key requirement for imatinib to bind to and to inhibit the Abl. In addition, a recent study reported two new mutations (Phe311Leu and Met351Thr), which were not restricted to the accelerated phase of CML (Roche-Lestienne et al., 2002). These two mutations were present even prior to imatinib treatment, probably as second mutational events during the course of CML. Von Bubnoff and colleagues (2002) summarized that a patient could be resistant to imatinib by acquisition of different individual point mutations within the ATP-binding pocket or activation loop of Bcr-Abl, which could make it difficult to overcome imatinib resistance by use of alternative kinase inhibitors.

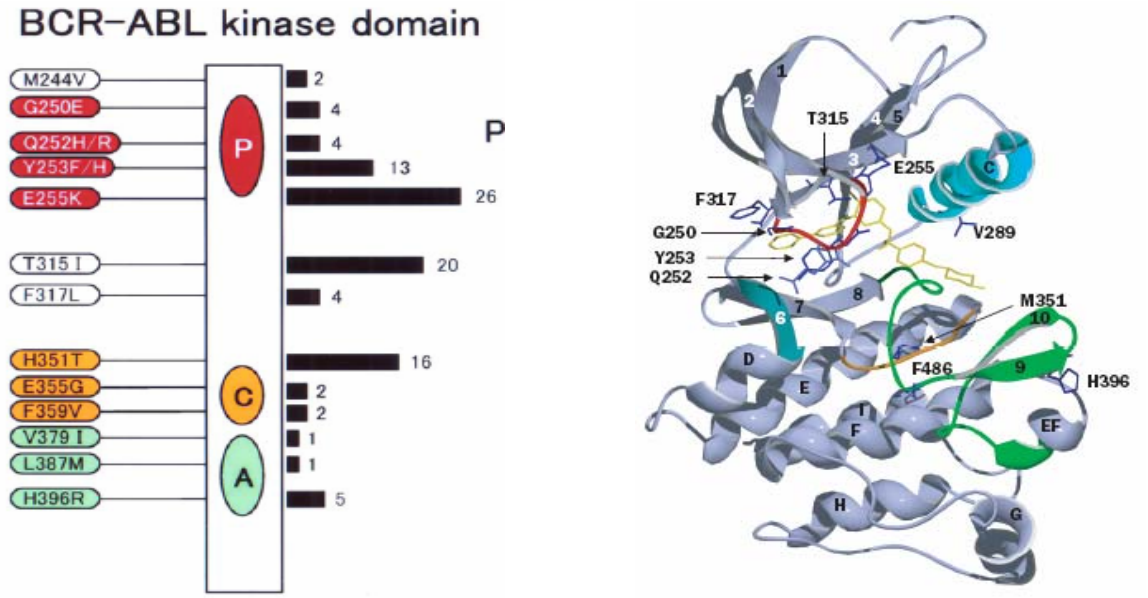

Figure 2.4: Different point mutations in the Bcr-Abl kinase domain and their influence on the proper binding of imatinib to the target molecule (adapted from *hematology.im.wustl.edu/conferences/ presentations/uy043004.ppt*).

Resistance to imatinib can also be caused by overexpression of the BCR–ABL protein due to *gene amplification of the BCR–ABL gene*. This mechanism was initially described in the LAMA84-r cell line with a 4.6-fold increase in mRNA levels (Le Coutre et al., 2000). Furthermore, it can be caused by imatinib's binding to the inactive conformation of BCR-ABL (Van Etten et al., 2004).

Like most other small molecule drugs, imatinib needs to pass through the plasma membrane to reach its target protein. In many cases of drug resistance, transmembrane proteins involved in ion transport across the plasma membrane (or pumps) have been implicated in mediating drug resistance. Many changes are associated with *multidrug resistance (MDR)* of tumor cells (Lehnert et al., 1994; Zgurskaya et al., 2000). There are several efflux pumps, such as p-glycoprotein (pgp) or multidrug resistance protein (MRP), which can decrease drug accumulation in cells and make therapy ineffective (Clynes et al., 1998). Both pgp (p170, which is encoded by the multidrug resistance *ABCB1 (formerly MDR-1)* gene) or A1-acid glycoprotein (AGP, which is present in the plasma and can bind to imatinib, thus possibly reducing its intracellular concentration at high plasma levels) are involved in imatinib resistance (Mahon et al., 2003; Gambacorti-Passerini et al., 2000). Since pgp and AGP, are both ATP-dependant transporters (Davidson, 2002; Higgins and Linton, 2004; Fournier et al., 2000) a limitation in ATP supply could make *ABCB1* over-expressing and resistant cells more susceptible to the toxic effects of drugs.

Although the correlation between the molecular mechanisms and imatinib efficacy in clinical trials is well established, there is no precise information about the changes in cell metabolism during exposure to the drug or in imatinib resistance. Previously, Barnes et al., 2005 and Gottschalk et al., 2004, showed that inhibition of Bcr-Abl activity by imatinib in K562 cells caused significant changes in cellular glucose metabolism. Bcr-Abl positive cells express high affinity Glut-1 glucose transporter and demonstrate high glucose uptake, therefore effects of imatinib on glucose flux and metabolism are important in understanding resulting cell changes, from apoptosis to resistance occurrence. Clinical studies of patients with imatinib-resistant c-KIT-positive tumors

have furthermore demonstrated increased glucose uptake in PET scan studies (Van den Abbeele et al., 2000).

Remarkably, in tumor cells, the development of drug resistance has been associated with changes in their plasma membrane lipids composition. For example, daunomycin-resistance in P338 cells is associated with lower drug concentrations in resistant cells than in their sensitive counterparts and the resistant cells were shown to have higher cholesterol contents in their membrane than sensitive cells (Escriba et al., 1990).

Most MRP or pgp overexpressing multi-drug resistant cell lines display changes in lipid composition compared with drug-sensitive counterparts (Lavie et al., 1996; Kok et al., 2000; Ferte et al., 2000). It has long been recognized that the lipid phase of the plasma membrane plays an important role in respect to multidrug resistance and pgp:

- the compounds involved in the multi-drug resistant phenotype are hydrophobic and diffuse passively through the membrane;
- pgp domains involved in drug binding are located within the putative transmembrane segment;
- pgp activity is highly sensitive to its lipid environment; and pgp may be involved in lipid trafficking and metabolism.

Pgp has been reported to localize in low-density, decreased membrane fluidity, cholesterol-enriched membranes (Lavie et al., 1998; Hinrichs et al., 2005). In adriamycin- and taxol-resistant K562 cells, both resistant cell lines showed lower fatty acid methylene/methyl ratios and higher choline/methyl ratios than sensitive cells as shown using NMR spectroscopy (Le Moyec et al., 1996).

The success of Gleevec in the treatment of chronic myelogenous leukemia has provided proof of principle that cancer can be treated by identifying the underlying molecular defects and designing drugs to correct those. Promising results in trials with other molecularly targeted drugs, such as gefitinib (ZD1839, Iressa^{TM}), have given further encourage-ment for such approaches. And with genomics and proteomics technologies poised to have an increasing impact, it seems a new era in anticancer therapy is beginning.

2.3. Gefitinib (Iressa™): Small molecule inhibitor of EGFR

Epidermal growth factor receptor (EGFR) is overexpressed, mutated, or both in many solid tumors e.g. non-small cell lung cancer (NSCLC) with 40-80% expression or colorectal cancer with 25-77% expression if EGFR (Salomon et al., 1995). Expression correlates with disease progression, poor survival, and poor response to therapy and resistance to cytotoxic agents (Arteaga, 2002). EGFR is a transmembrane glycoprotein comprising an extracellular ligand-binding domain, a transmembrane hydrophobic domain and an intracellular domain with tyrosine kinase activity involved in signal transduction (Figure 2.5).

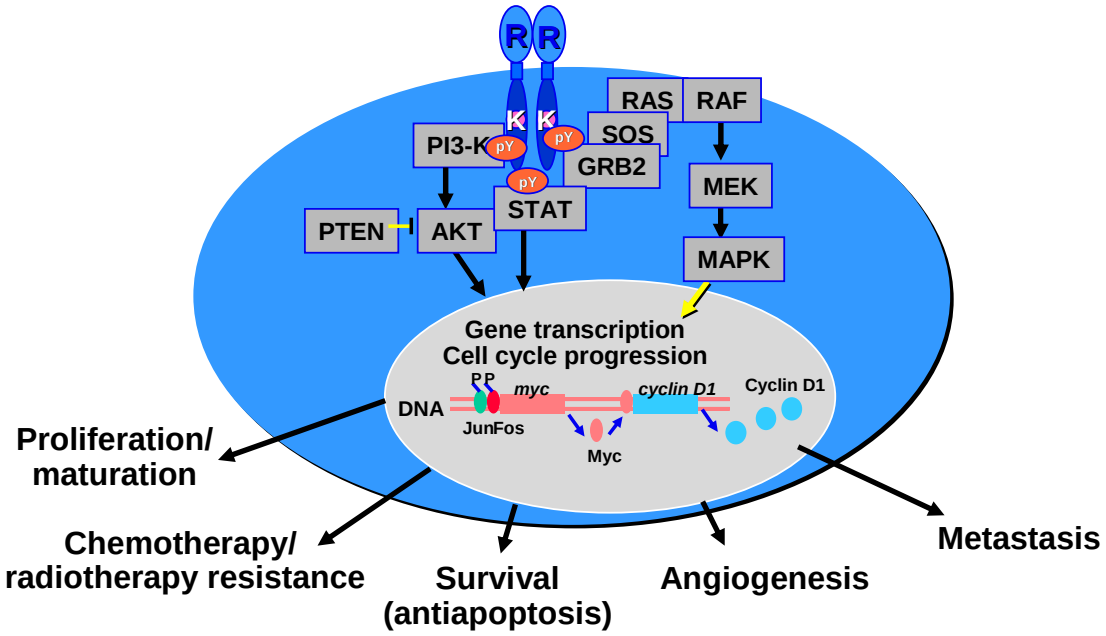

Figure 2.5: EGFR signaling. Upon ligand binding, receptor dimerization activates tyrosine kinase activity and tyrosine autophosphorylation. This initiates a signaling cascade that leads to cell proliferation, chemotherapy / radiotherapy resistance, increased angiogenesis, invasion and metastasis as well as decreased apoptosis (adapted from Baselga, 2002).

2.3.1. Gefitinib: Mechanism of action

Gefitinib (Iressa™, ZD1839, AstraZeneca, Sweden) is an anilinoquinazoline (Figure 2.6) that is a specific, competitive inhibitor of ATP binding by EGFR (Figure 2.7).

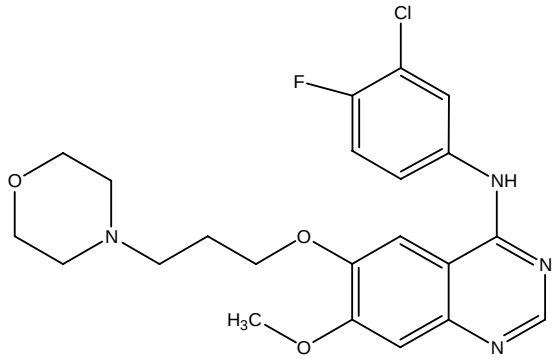

Figure 2.6: Chemical structure of gefitinib (ZD1839, $C_{22}H_{24}ClFN_4O_3$, MW 446.91 g/mol).

It was approved by the Food and Drug Administration (FDA) in 2004 for refractory locally advanced or metastatic non–small-cell lung cancer. Gefitinib led to partial responses in 11 to 19 percent of patients with refractory disease in phase 2 trials (Kris et al., 2003).

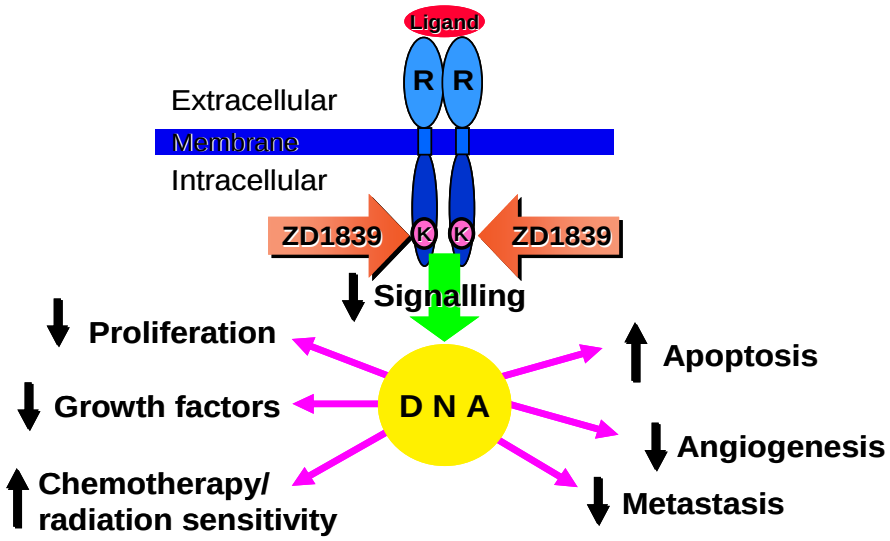

Figure 2.7: Mechanism of action of gefitinib (ZD1839) by competitive inhibition of ATP binding.

Disappointingly, the addition of gefitinib to chemotherapy in the initial treatment of non–small-cell lung cancer did not yield any additional benefit (Herbst et al., 2004; Giaccore et al, 2004). A small subgroup of patients with non–small-cell lung cancer who frequently had adenocarcinomas and most of whom were Asian, female, and nonsmokers had dramatic and sometimes long-term responses to gefitinib monotherapy. Sequencing of the *EGFR* gene in tumor tissue from these patients revealed somatic gain-of-function

mutations clustered around the ATP-binding pocket of the kinase domain of the EGFR protein in most cases (Lynch et al., 2004; Paez et al., 2004). Unlike c-KIT mutations in GIST (gastrointestinal stromal tumor), these EGFR mutations do not cause constitutive activation; rather, they enhance the responsiveness of the receptor to EGF ligand and increase its sensitivity to inhibition by gefitinib (Lynch et al., 2004; Pao et al., 2004). They also may preferentially activate anti-apoptotic signaling pathways in the tumor cells (Sordella et al., 2004). Studies from Asia, where *EGFR* mutant tumors are more prevalent, have found significant increases in response rates and overall survival among patients with *EGFR*-mutant tumors treated with gefitinib (Han et al., 2005; Mitsudomi et al., 2005). Additional prospective studies are needed to determine as to whether analysis of *EGFR* expression and mutation in tumors should be used to select patients with non–small-cell lung cancer for EGFR-inhibitor therapy.

2.3.2. Combination therapy: gefitinib with chemotherapeutics and COX-2 inhibitors

5-Fluorouracil (5-FU) (Figure 2.8) is usually given in combination therapy (Sun, 2002). Various mechanisms including inhibition of thymidylate synthase (TS) by 5-fluoro-2'-deoxyuridine-5'-monophosphate (FdUMP), incorporation of 5-fluorouridine-5'-triphosphate (FUTP) into RNA and incorporation of 5-fluoro-2'-deoxyuridine-5'-triphosphate (FdUTP) into DNA have been reported (Leichman et al., 1997; Salonga et al, 2000). Although TS inhibition and its expression have been related to the antitumor effect of 5-FU, it has not yet been demonstrated clinically as to whether incorporation into RNA or DNA contribute to its antitumor effect.

Tumor cell proliferation and survival depend on vasculature to supply adequate oxygen and nutrients. *In vivo* and *in vitro* studies showed that prostaglandins, which are being produced by stimulation of cyclooxygenase-2 (COX-2), can up-regulate vascular endothelial growth factor (VEGF), as a potent angiogenic growth factor (Cheng et al., 1998). Further, in colon cancer, COX-2 up-regulation seems to be an important early event in colon carcinogenesis. It appears that COX-2 is an activator of angiogenesis necessary for tumors to grow beyond $2mm^3$ (Form and Auerbach, 1983; Hanahan and Folkman, 1996). Because of these observations, many investigators think of COX-2 inhibitors, such as Celecoxib (Celebrex^{TM,} Pfizer, USA) (Figure 2.8), as chemopreventive

agents that are able to reduce inflammation (and pain) while minimizing undesired side effects (such as stomach ulcers) that can occur with non-selective NSAIDs (non-steroidal anti-inflammatory drugs). Celecoxib mechanism of action is believed to be due to inhibition of prostaglandin synthesis, primarily via inhibition of COX-2 (Vane, 1971; Laine et al., 1999; Emery et al., 1999).

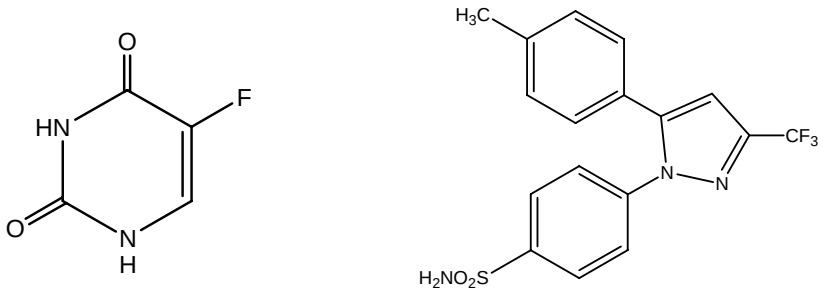

Figure 2.8: Chemical structures of 5-Fluorouracil (5-FU, $C_4H_3FN_2O_2$, MW 130.08 g/mol, left) and Celecoxib (Celebrex™, $C_{17}H_{14}F_3N_3O_2S$, MW 381.38 g/mol, right).

2.4. Magnetic Resonance Spectroscopy (MRS) in biological systems

MRS has developed over the years into the principal method for evaluating molecular structure and conformation. More recently, it has matured into a non-invasive and non-destructive technique that can help physicians diagnose disease.

The physical principle first proposed by Bloch in 1946 to describe the behavior of nuclei in a magnetic field has been a very important rational in understanding the magnetic resonance phenomena. This rapid and non-invasive technique produces a characteristic spectrum of specific nuclei, such as proton (^{1}H), carbon (^{13}C) or phosphorous (^{31}P). Using modern multi elemental techniques, we can use MRS to examine energy levels, changes in glucose metabolization, cell volume or amino acids concentrations in cultured cells, body fluids or perfused organs (Kaplan et al., 1992; Ross BD, 1992; Lundberg et al., 1990).

In addition to mass spectrometry, MRS is one of the basic technologies driving the rapidly growing field of metabonomics with broad applications in tumor diagnostics. Metabonomics can provide real biological endpoints and is defined as “the quantitative measurement of the time-related multiparametric metabolic response of living systems to pathophysiological stimuli or genetic modification” (Nicholson et al., 1999; 2002).

The validity of metabonomics research strategies is based on the fact that in most cases disease, drugs and toxins cause perturbations of the concentrations and fluxes of metabolites involved in key cellular pathways. For example, MRS has successfully been used as a tool evaluating the efficacy of anti-cancer therapies based on the altered metabolic network of oncogenesis (Mountford et al., 1997; Gillies et al., 2000; Evelhoch et al., 2000). Variations in the rate of cell proliferation, cell-cycle progression, and apoptosis cause changes in glucose cell metabolism (Griffin and Shockcor, 2004). Moreover, the metabolic response to anti-cancer treatments resulting in apoptosis and necrosis through the specific inhibition of a signal transduction pathway often occurs before morphological, molecular or histological changes are evident (Shih et al., 2005).
MRS-based metabonomics also plays an increasing role in drug development. Due to a wide range of metabolites screened by MRS and advanced data analysis techniques, drug candidates can be ranked by their toxicity and mechanisms of action.

2.5. Aims of the Study and Research Strategies

This thesis was mainly focused on:

I. Metabolic effects of tyrosine kinase inhibitors;
II. Resistance to tyrosine kinase inhibitors.

I. One of the central aims of this project was to investigate and compare the effects of tyrosine kinases imatinib (Gleevec^{TM}) and gefitinib (Iressa^{TM}) on metabolism of cancer cells. It was furthermore attempted to find correlations between the metabolic profiles and the efficacy and outcome of the treatment. For example, the establishment of different metabolic signatures of *in vitro* models exposed to diverse drug-combination and treatment types could be used as predictors for combination therapies in following clinical trials. They furthermore could help to early predict a success or a failure of the therapy sequence, and therefore supplying enough time for employment of other treatment strategies. The current studies were based on human leukemia cell lines exposed to imatinib and colon and non-small lung cancer cells treated with gefitinib.

MRS-studies on glucose-derived amino acid synthesis, lipids and fatty acids production and drug-effects on energy-state of cells were performed. The results were correlated to the changes in cell processes (e.g. proliferation, cell death or changes in protein expression). In case of imatinib, its anti-proliferative and pro-apoptotic effects were assessed on the cell morphological level, as well as on the level of intracellular changes in metabolic profiles and pathway.

II. The occurrence of resistance is the major problem for patients treated with imatinib. Therefore, MRS-based profiling was used for the identification of new biomarkers for imatinib resistance in order to better predict, clinically detect and even treat drug resistance. Understanding the biochemical mechanisms underlying and typical for drug resistance has the potential for early detection of the development of imatinib resistance, to develop alternative strategies for prevention and to overcome resistance by combination with other targeted agents.
Detection of metabolite markers and their application to clinical monitoring of leukocytes using a combination of metabonomics-based strategies allowed for investigating a large number of signaling pathways and their connection to metabolic changes.

It was our goal to use additional technologies such as flow cytometry, polymerase chain reactions (PCR) and Western blotting to further assess and understand mechanisms and to support and explain metabolic profiling results. For example, one of the mechanisms of imatinib resistance is the overexpression of p-glycoprotein, a drug-efflux transporter. Therefore, besides measuring protein expression, a fully validated HPLC/MS/MS method was developed. It allowed performing measurements and tracking the changes in effective intracellular imatinib concentrations during various treatments.

Chapter 3

3. RESULTS AND DISCUSSION

3.1. Imatinib resistance development: Long-term incubation of leukemia cells

During the time of resistance development to imatinib, K562 and LAMA84 leukemia cells were changing; not only their morphology but also their metabolic profile and metabolic activity changed. Experiments in which the cells were continuously exposed to increasing imatinib concentrations resulted in metabolic differences compared to the untreated, sensitive controls.

Long-term imatinib incubations were carried out for 4 weeks and subsequently cell extracts, lipids and media fractions were analyzed by MRS. The idea behind the time schedule was the attempt to make K562 cells resistant to 1.0 μM imatinib. According to the treatment schemes of other research groups, who have succeeded to isolate cells resistant to 1μM imatinib, our cells were treated the same way: with a 0.1 μM weekly increase in concentration of imatinib (starting from 0.1 μM to 1.0 μM).

K562, LAMA84 (both Bcr-Abl positive) and HC-1 (Bcr-Abl negative) cells were incubated with increasing imatinib concentrations starting at 0.1 μM in the first week (cells were collected after 96 hours and 1 week). As mentioned, imatinib concentrations were increased weekly by 0.1 μM. In addition, cells were collected after 2 (0.2 μM) and 4 weeks (0.4 μM imatinib).

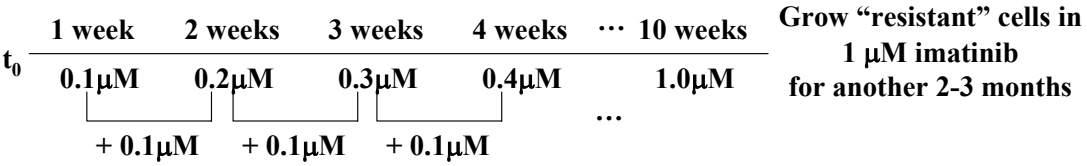

After 5 weeks more than 70% of the treated K562 cells were dead, while HC-1 cells were not affected in terms of their growth or differentiation. Due to the insufficiency of cell material further MRS analysis was not performed. For the LAMA84 cell line, only cell

media related glucose-uptake MRS experiments were performed.

3.1.1. Imatinib influence on cell proliferation and viability

Proliferation and viability of imatinib-treated K562 and LAMA84 leukemia cells was assessed as a function of time. The results are presented in Figures 3.1 and 3.2 and clearly distinguished short- from the long-term treatment, whereas no differences were observed between the two Bcr-Abl positive cell lines. Both cell lines have comparable doubling times and IC_{50} values regarding imatinib treatment (K562 cells: 0.51 μmol/l; LAMA84 cells: 0.48 μmol/l). Exposure to 0.1 μM imatinib in the first 96 hours led to neither significant change in cell proliferation nor in cell cycle distribution in any of the three examined cell lines.

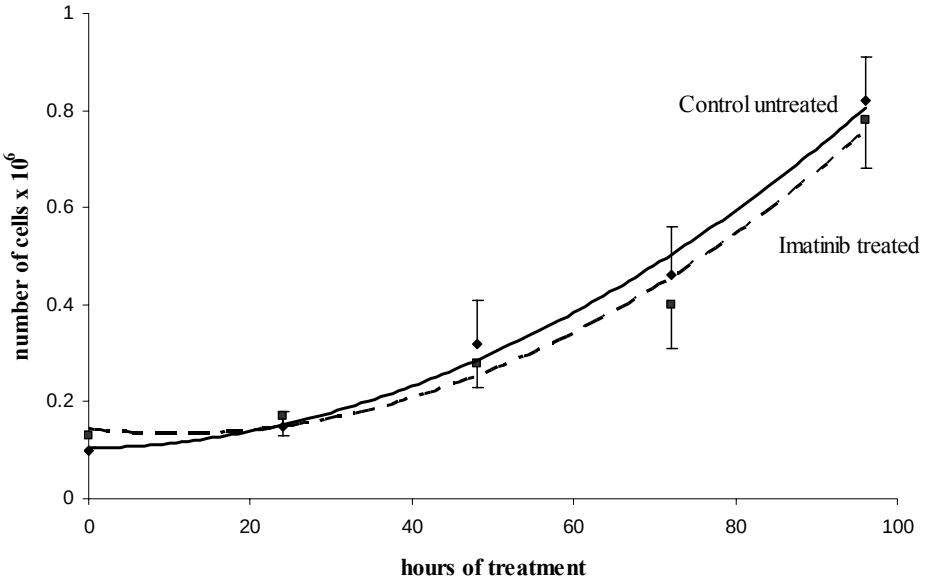

Figure 3.1: Proliferation of K562 leukemia cells. Comparison between untreated control cells and cells treated with 0.1μM imatinib (mean of n=4 experiments; control and imatinib treated values are presented as means + SD and means – SD, respectively).LAMA84 and HC-1 cells proliferation rates were also not significantly affected by addition of imatinib.

Imatinib's mechanism of action includes induction of apoptosis in Bcr-Abl expressing human CML lines (Fang et al., 2000). In our studies, significant apoptosis induction started after 96 hours of incubation with 0.1 μM imatinib and increased when cells were treated longer and/or after the drug concentration was increased (weekly increase by 0.1 μM imatinib) (Figure 3.2). After 4 weeks and 0.4 μM imatinib, 44% cell death was

detected in K562 cells, while no changes were observed in the HC-1 cell line. LAMA84 cells were treated with 0.1 μM imatinib for one week, during which flow cytometry analysis of apoptosis and HPLC/MS analysis of high-energy phosphates were performed.

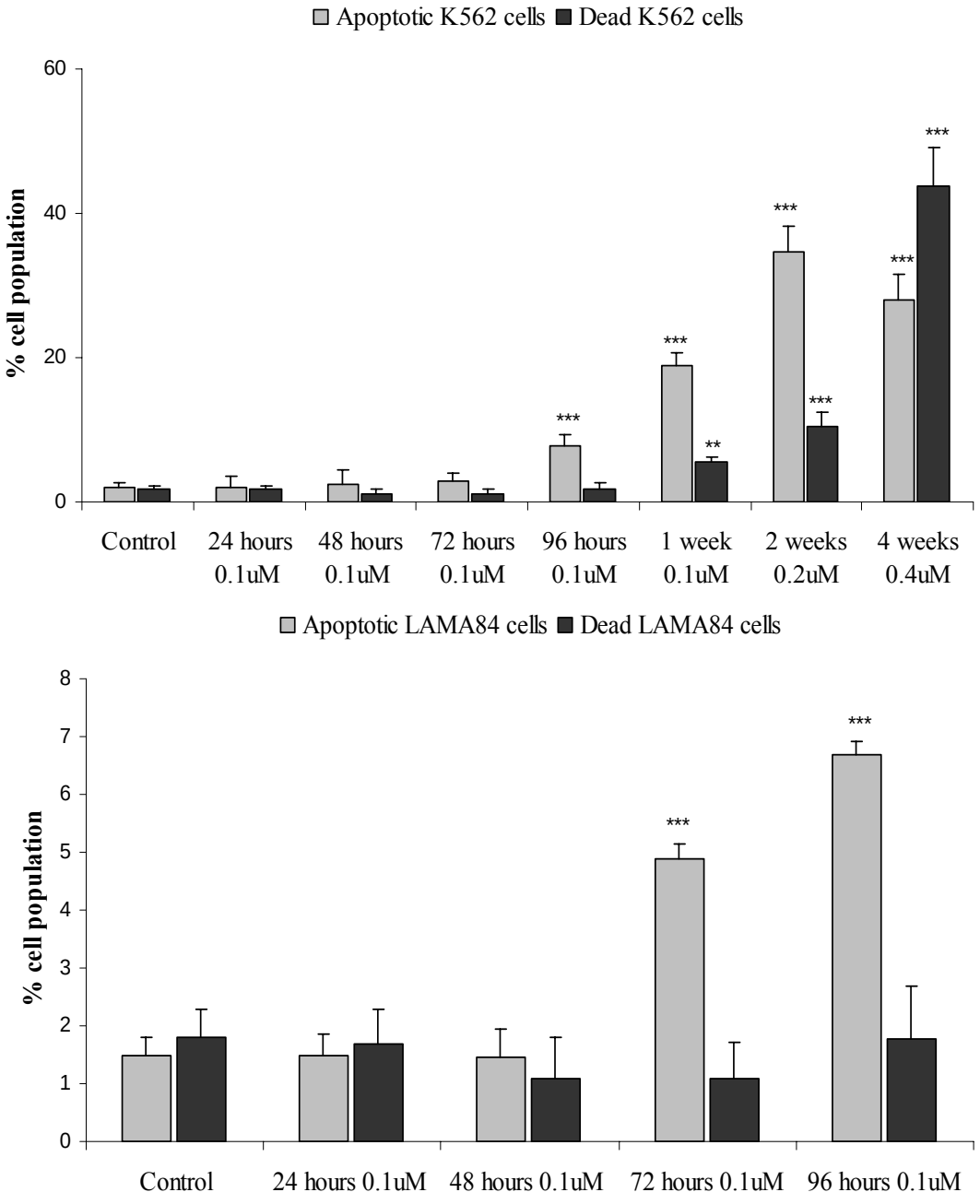

*Figure 3.2: Apoptotic and dead cells number in K562 (top) and LAMA84 (bottom) cells increased with longer treatment time and higher imatinib concentration. The data are presented as means + SD of three independent experiments and are given as % of cell population (set at 100%); significance levels: *p<0.05; **p<0.005; ***p<0.001.*

Another method used for measurements of cell viability and membrane stability was staining with Trypan-Blue. Trypan-Blue belongs to the group of dyes which are able to cross a "holey" but not an intact membrane, therefore allowing for distinction of living and dead cells.

In contrast to apoptotic cells, in which the loss of membrane integrity happens during a period of "secondary necrosis", the last step in the cell disruption process, necrotic cells exhibit an early break-down in their membrane integrity. Therefore, they absorb the dye molecules while apoptotic cells remain unstained.

Our K562 cells were periodically examined by Trypan-Blue exclusion during the time of resistance development. A significant increase in the number of stained, dead cells was not noticed until 2 weeks. At this time point ca. 20% dead cells were observed (from the total cell population), which corresponded to the results obtained from flow cytometry analysis (11% dead cells, Figure 3.2). Hereafter, the number of dead cells increased exponentially. As aforementioned, after 5 weeks more then 70% of cells were dead.

3.1.2. Glucose and energy metabolism in K562 leukemia cells / Changes after long-term imatinib treatment

Glucose metabolism after imatinib treatment. After 96 hours of imatinib treatment with 0.1 μM and 4 hours of incubation with 5 mM [1-^{13}C] glucose, glucose metabolism in K562 cells started to change from anaerobic glycolysis, as indicated by predominantly lactate production, towards the mitochondrial Krebs cycle (as indicated by predominantly glutamine and glutamate synthesis). The ^{13}C-enrichment of lactate slightly decreased to 84% of control after 96 hours of incubation ($p<0.05$, $n=4$), indicating a decreased cytosolic glycolytic activity. In parallel, the ratio of mitochondrial Krebs cycle activity relative to glycolysis (indicated by an increase in C4-glutamate and a decrease in C3-lactate concentration, both produced from the metabolism of 1-^{13}C-glucose) increased to 138% ($p<0.05$, $n=4$) of controls (Figure 3.4). Three more days of treatment with 0.1 μM imatinib (total of 1 week incubation) showed almost no changes in the ^{13}C-lactate production and a maximum increase in the TCA cycle/glycolysis ratio (Figure 3.4). After 2 weeks of treatment with an imatinib concentration of 0.2 μM, the trends changed and

TCA cycle activity started to decrease (to 87% of control, Figure 3.4). The minimal value of 68% ($p<0.005$, n=3) was reached after 4 weeks and 0.4 μM imatinib (Figure 3.4).

Increased production of labeled glutamate indicated increased utilization of the mitochondrial glucose pathway with glutamate as a major detectable metabolite.

The percentage ^{13}C-enrichments in individual carbons, i.e. in the C2-, C3- or C4-glutamate positions after addition of [1-^{13}C] glucose, depend on the relative fluxes through TCA cycle enzymes. The ratio [glutamate (C2+C3)/C4] did not change significantly in any of the treatment groups, even though the absolute concentrations decreased. This labeling pattern of the glutamate carbons can be used to estimate the relative glucose flux / turnover rates *via* pyruvate carboxylase (PC, anaplerotic pathway) and pyruvate dehydrogenase (PDH, oxidative pathway) activities into the tricarboxylic (TCA) cycle (Figure 4.11) (Lapidot and Gopher, 1994). Thus, our results indicated that the total mitochondrial activity was diminished, and not the activity of the two enzymes located at the entrance of the Krebs cycle. An exact quantification of the anaplerotic pathway is difficult, since the label of glutamate in C2 may also increase during the second PDH turn. However, the incubation time with [1-^{13}C] glucose was 4 hours, which reduces the possibility of the second turn.

	Glu C4	**Glu C2**
Control	**4.89±0.58**	**0.77±0.05**
96 hours 0.1 μM	**6.96±0.92***	**0.87±0.05***
1 week 0.1 μM	**7.39±0.64*****	**1.20±0.11****
2 weeks 0.2 μM	**4.00±0.52**	**0.71±0.05**
4 weeks 0.4 μM	**2.81±0.59***	**0.23±0.09*****
ANOVA	***p<0.001***	***p<0.001***

*Table 3.3: The percentage of ^{13}C-enrichments in C2- and C4-glutamate; calculated by integration of specific signals in ^{13}C-MRS spectra obtained from control and imatinib treated K562 cell extracts after 4 h incubation with 5 mM [1-^{13}C] glucose. The values are given as means ± SD of 3 independent experiments (n=6 for control, n=4 for 96 hours). Significance levels *p<0.05; **p<0.005; ***p<0.001 were determined by ANOVA (with post-hoc pairwise multiple comparison Tukey-test).*

Furthermore an increased ^{13}C-enrichment in alanine was detected after 96 hours of imatinib treatment (131% of controls, $p<0.05$, n=4); but with increase of imatinib concentrations, areas under the alanine signal decreased to 49% of the controls after 4 weeks of treatment ($p<0.001$, n=3).

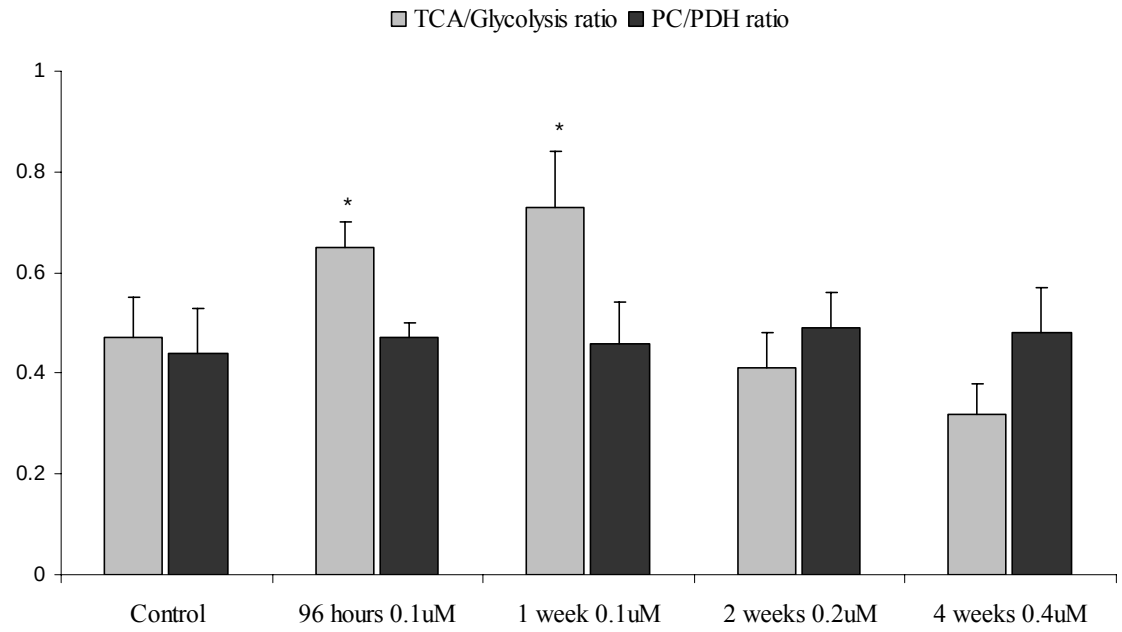

*Figure 3.4: Effects of imatinib on TCA cycle (primarly Gln and Glu) to glycolysis (lactate + alanine) and PC/PDH ratios (Glu (C2+C3)/C4)) as calculated from the ^{13}C-MRS spectra of K562 cell extracts. The values are given as means + SD of 3 independent experiments (n=6 for control and n=4 for 96 hours with 0.1 μM imatinib). Significance levels (*p<0.05) were determined by ANOVA (with post-hoc pairwise multiple comparison Tukey-test). ANOVA value for TCA/Glycolysis ratio p<0.001.*

Energy state after imatinib treatment. The increase in mitochondrial glucose metabolism was accompanied by a higher energy state in Bcr-Abl positive K562 cells. The cell energy NTP/NDP-ratio (nucleoside triphosphate/nucleoside diphosphate) increased from 6 to 8.4 after 96 hours compared to the untreated control cells ($p<0.05$, n=3, Figure 3.5). Higher TCA activity did not cause any further improvement of the energy balance after 1 week of treatment. The energy balance stayed unchanged and was reduced after 2 and 4 weeks in comparison to cells incubated for 1 week. The minimum NTP/NDP ratio of 2.5 was observed after 4 weeks of treatment and 0.4 μM imatinib

(Figure 3.5).

The same directional changes were also seen in case of NAD(H) concentrations: a slight increase after 96 hours and 1 week of incubation with 0.1 μM imatinib in comparison to untreated controls and a significant reduction in concentrations after 4 weeks of treatment (Figure 3.5). During the same time a noticeable decrease of phosphocreatine concentrations (and PCr/Cr ratios, Figure 3.5) was observed compared to after 1 week of incubation. Phosphocreatine was almost undetectable after 4 weeks of treatment.

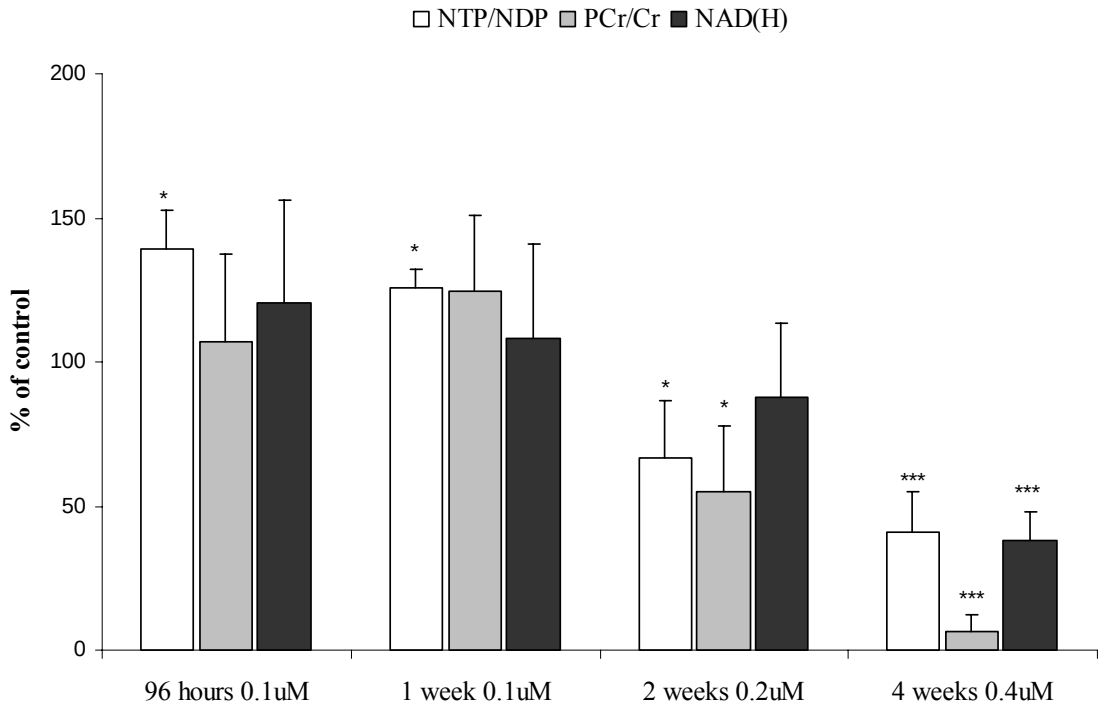

*Figure 3.5: Concentration ratios of high-energy phosphates and NAD(H) as calculated from the ^{31}P-MRS spectra of K562 cell extracts (untreated controls and with imatinib treated cells). The values were calculated per μmol/g cell wet weight and are given as % of control (concentrations in the control cells were set to 100%) and represent means + SD of 3 independent experiments (n=6 for control). Significance levels: *p<0.05; **p<0.005; ***p<0.001 were determined by ANOVA (with post-hoc pairwise multiple comparison Tukey-test).Comparison by ANOVA indicated statistically significant differences with p<0.001 for NTP/NDP, PCr/Cr and NAD(H).*

As observed in previous studies (Hatse et al., 1999) and in our experiments, based on the whole cell trinucleotides contents, K562 and LAMA84 cells contain approximately 55% ATP and 20% UTP or GTP. Since the magnetic field employed for our ^{31}P-MRS experiments could not resolve specific trinucleotides, the HPLC/MS analyses were

performed in order to determinate concentrations of specific nucleotides. The results are presented in Figure 3.6 and show an even higher increase of ATP/ADP ratios and energy charge (calculated as [(ATP+0.5*ADP) / (AMP+ADP+ ATP)]) than indicated by the NTP/NDP ratios previously calculated from ^{31}P-MRS spectra. Based on HPLC/MS analysis, not only was the ATP/ADP ratio found increased but also the ratios of the other nucleoside tri- and diphosphate pairs studied (Figure 3.6). Our results indicated that imatinib-treated cells accumulated high-energy phosphates during the first week of treatment. In the following time period, this energy was used mainly for fatty acid (membrane) synthesis and apoptosis processes (*vide infra*).

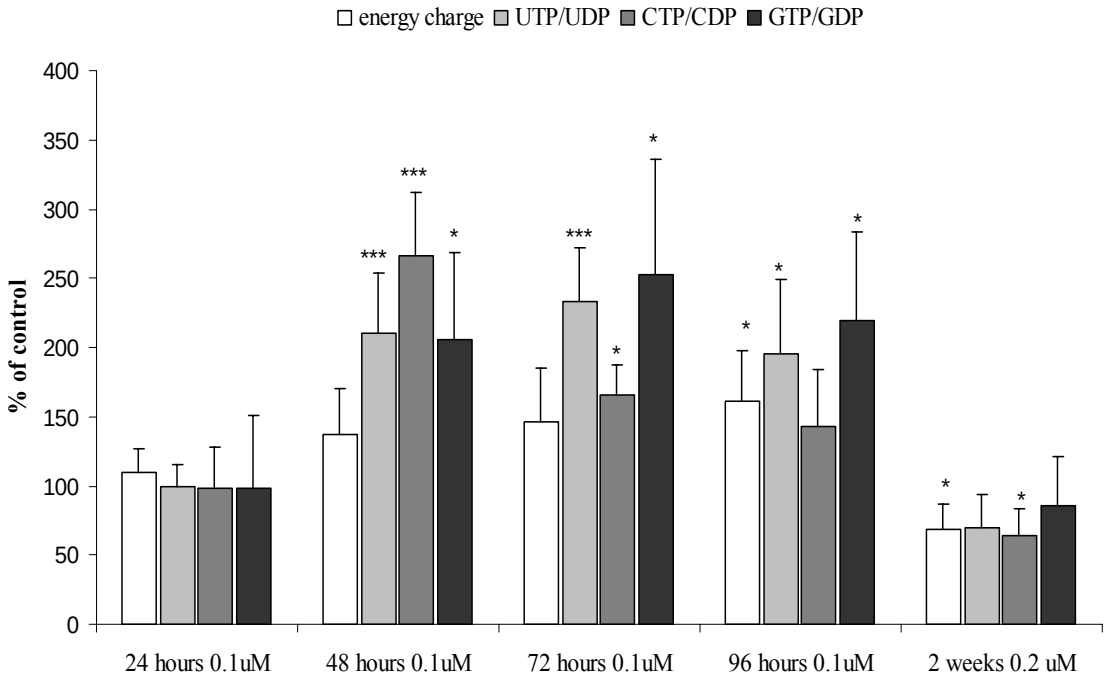

*Figure 3.6: Concentration ratios of high-energy phosphates as calculated from the HPLC/MS data of K562 cell extracts (untreated and with imatinib treated cells). Energy charge was calculated as [(ATP+0.5*ADP)/(AMP+ADP+ATP)]. The values were calculated per number of cells (x 10^7) and are given as % of control set to 100% and represent means + SD of 3 independent experiments. Significance levels: *p<0.05; **p<0.005; ***p<0.001 were determined by ANOVA (with post-hoc pairwise multiple comparison Tukey-test).Comparison by ANOVA indicated statistically significant differences with p<0.05 for energy charge and GTP/GDP and p<0.001 for UTP/UDP and CTP/CDP.*

HPLC/MS analysis of high-energy phosphate concentrations in LAMA84 cell extracts

revealed a pattern similar to K562 cells. Only the metabolic changes occurred faster. The ATP/ADP ratios increased to a maximum within 48 hours of incubation and almost reached the values of the controls after 96 hours (Figure 3.7). During further incubation the energy balance of the cells was reduced, as seen after 2 weeks of treatment.

It is currently assumed that the apoptotic process can be divided into at least three distinct functional phases (Kroemer, 1997; Constantini et al., 2000): the induction, effector and "beyond the point of no return" degradation phase. During the induction phase, cells receive the death-inducing stimulus such as triggered by imatinib. Previous studies showed that other antitumor agents initiate the apoptotic cascade by decreasing NAD^+ concentrations (Wosikowski et al., 2002), followed by disruption of the mitochondrial membrane potential and, subsequently, DNA degradation.

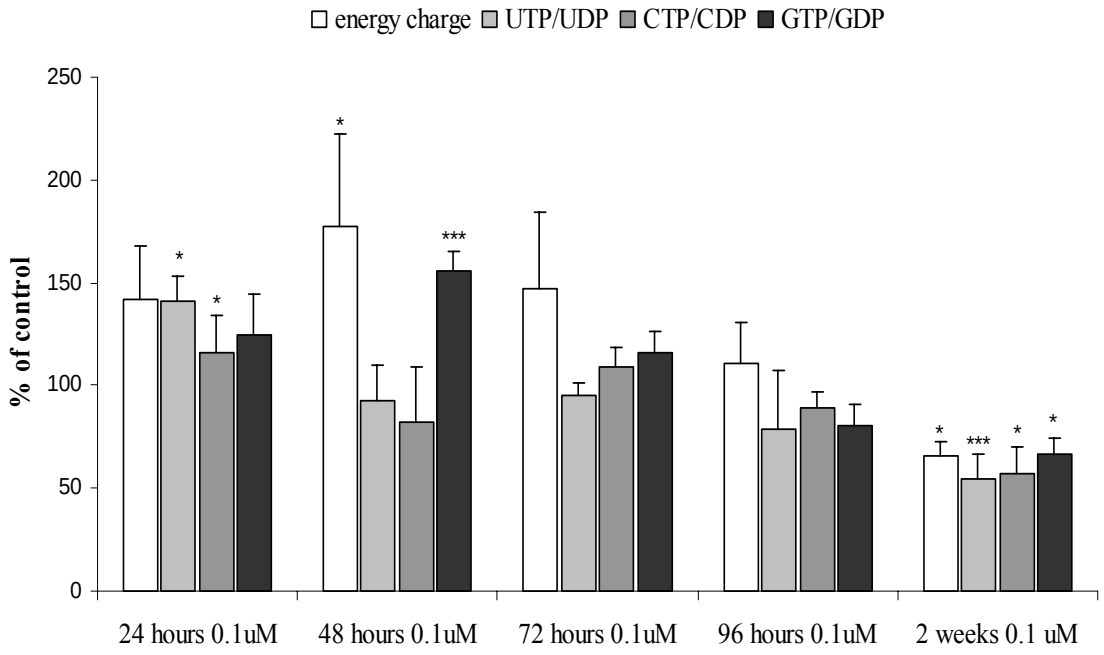

*Figure 3.7: Concentration ratios of high-energy phosphates as calculated from the HPLC/MS data of LAMA84 cell extracts (untreated controls and with imatinib treated cells). Energy charge was calculated as [(ATP+0.5*ADP)/(AMP+ADP+ATP)]. Values were calculated per number of cells (x 10^7) and are given as % of control and concentrations found in the controls were set to 100%. Relative concentrations are presented as means + SD of 3 independent experiments. Significance levels: *p<0.05; **p<0.005; ***p<0.001 were determined by ANOVA (with post-hoc pairwise multiple comparison Tukey-test).Comparison by ANOVA indicated statistically significant differences with p=0.01 for energy charge and p<0.001 for UTP/UDP, CTP/CDP and GTP/GDP.*

Thus, HPLC/MS was used for determination of NAD^+ concentrations which cannot be derived from MRS spectra. As expected based on the literature, we observed decreasing NAD^+ concentrations in our human leukemia cell model. Treatment with imatinib reduced the intracellular NAD^+ concentrations from 1.3 to 0.5 μmol/l per 10^7 cells in K562 and from 1.7 to 0.9 μmol/l per 10^7 cells in LAMA84 cells after 2 weeks (Figure 3.8)

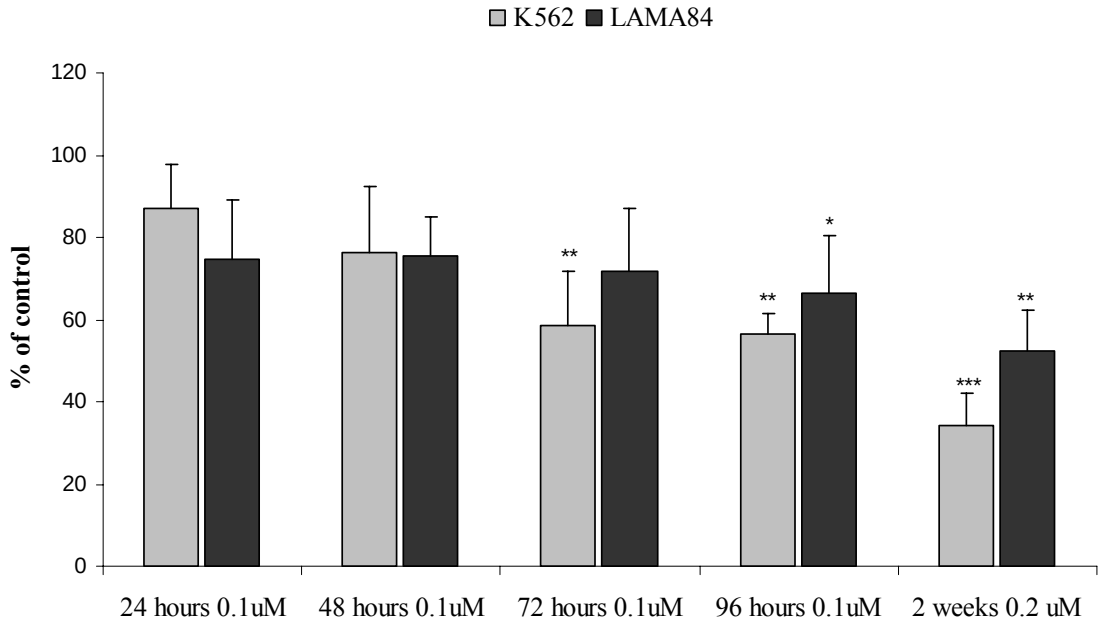

*Figure 3.8: NAD^+ concentrations started to decrease after 96 hours of drug treatment as calculated from the HPLC/MS data of K562 and LAMA84 cell extracts (untreated control and with imatinib treated cells). The values were calculated per number of cells (x 10^7) and are given as % of control. Concentrations in the controls were set to 100% and relative concentrations are presented as means + SD of 3 independent experiment. Significance levels: *p<0.05; **p<0.005; ***p<0.001 were determined by ANOVA (with post-hoc pairwise multiple comparison Tukey-test). .Comparison by ANOVA indicated statistically significant differences with p<0.001 for K562 and p=0.009 for LAMA84 cells.*

3.1.3. Changes in lipids metabolism in K562 cells after long-term imatinib treatment

Changes in phospholipids metabolism. Another significant difference in metabolic response of imatinib-treated K562 cells was a decrease of phosphocholine and phosphatidylcholine. Phosphocholine signals as calculated from the ^{31}P-MRS spectra of

PCA cell extracts decreased to 43% after 96 hours ($p<0.005$, n=3) and to 31.2% of the controls after 2 weeks ($p<0.005$, n=3) (Figure 3.9). Phosphocholine (PC) is a precursor of membrane phospholipids, and increased concentrations of PC are a marker for various cancer types with high proliferation rates including leukemia cells (Ackerstaff et al., 2003; Franks et al., 2002). Phosphocholine is synthesized from choline. The nucleotide cytidine triphosphate (CTP) reacts with phosphocholine and CDP-choline is produced. For the synthesis of phosphatidylcholine, CDP-choline reacts with diacylglycerol, catalyzed by the enzyme CDP-choline: 1,2-diacylglycerol cholinephosphotransferase (CT) (Kent C, 1995).

Moreover, the concentrations of phosphatidylcholine as measured by ^{1}H-MRS of lipid extracts (Table 3.10) decreased and reached its minimum of 42% of the controls after 4 weeks of treatment ($p<0.005$, n=3), indicating inhibition of PC-biosynthesis (Table 3.10). Phosphatidylcholine (PtdCho) is a phospholipid that is a major component of cell membranes and is necessary for the structure and function of all cells and crucial for sustaining life (Kent, 1995; Zeisel and Blusztajn, 1994).

Glycerophosphocholine (GPC) is an intermediate of membrane catabolism and a metabolite produced by membrane degradation processes. No significant changes in GPC or GPE (glycerophosphoethanolamine) concentrations were found. The concentration rather decreased (78% and 69% of control after 1 and 2 weeks, respectively, $p<0.08$ not significant, n=3, Figure 3.10) than increased as expected based on the literature (Evelhoch et al., 2000). The ratio phosphomonoester (PME) to phosphodiester (PDE), an indicator of the turnover of the choline-pool, was decreased by 15-20% after 96 hours and 1 week of treatment. After 2 weeks, PC/GPC ratios decreased to 73% of the controls (statistically not significant: $p<0.07$, n=3).

An unidentified signal (X) (Figure 3.9) in ^{31}P-MRS spectra at 0 ppm was detected. A previous study (Henke, 1998) had also reported the appearance of a signal at 0 ppm that was found in the cell extract fraction containing DNA fragments and apoptotic bodies. Its chemical shift reveals that the compound belongs to the group of phosphodiesters (excluding PtdCho, PtdS and PtdE) and could potentially serve as a metabolic marker for apoptosis.

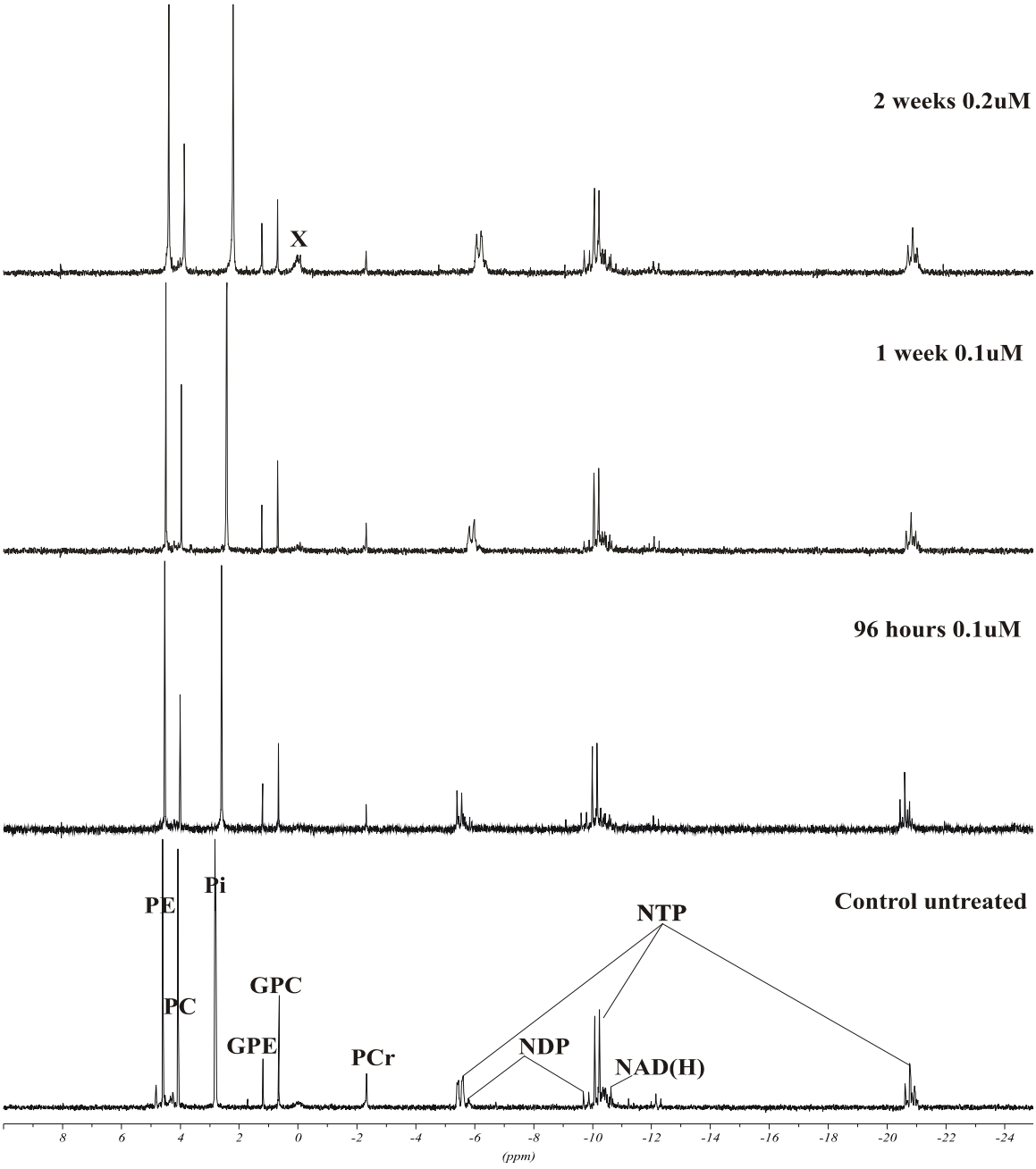

Figure 3.9: Representative ^{31}P-MRS spectra of K562 cell extracts. Cells were incubated with 0.1 μM imatinib for 96 hours or 1 week and with 0.2 μM imatinib for 2 weeks and compared to untreated controls. Peak assignment: PC: phosphorylcholine, PE: phosphorylethanolamine, Pi: inorganic phosphate, GPC: glycerylphosphocholine, GPE: glycerylphosphoethanolamine, PCr: phosphocreatine, NAD(H): nicotine amide adenine dinucleotide, NTP: nucleotide triphosphates, NDP: nucleotide diphosphates, X: unknown signal (previously also described in apoptotic bodies, identified as a phosphodiester by Henke, 1999). The spectra were normalized to the methylene diphosphonic acid (MDP) signal at 21ppm.

Changes in neutral lipids and fatty acids. PUFAs (polyunsaturated fatty acids) play a major role in membrane constitution and function and are one of the main targets of lipoperoxidative processes caused by reactive oxygen species.

With increasing apoptosis rate, changes in signal intensities at 2.8 (PUFA) and 3.23 (PtdCho) ppm were observed (as calculated from ^{1}H-MRS spectra of lipid extracts). No significant changes were seen after 96 hours of treatment; but the reduction of glutathione concentrations after 2 to 4 weeks of treatment (*vide infra*) was accompanied by an increase of PUFA and PtdCho signals to 121% (1 week, $p<0.05$, n=3) and 181% (4 weeks, $p<0.005$, n=3) of control (Table 3.10).

	Cho C19	**F_{mix}**	**PUFA**	**PtdCho**
Control	**0.63±0.05**	**134.52±4.00**	**2.51±0.26**	**2.35±0.43**
96 hours 0.1 μM	**0.68±0.11**	**145.62±11.05**	**3.11±0.49**	**2.32±0.14**
2 weeks 0.2 μM	**0.76±0.16**	**185.97±13.80*****	**3.18±0.29***	**1.79±0.29***
4 weeks 0.4 μM	**0.85±0.14***	**230.37±8.53*****	**4.78±0.23*****	**1.18±0.22****
ANOVA	***p=0.04***	***p<0.001***	***p<0.001***	***p=0.003***

*Table 3.10: Changes in lipids signals as calculated by integration of specific signals in ^{1}H-MRS spectra obtained from lipid extracts of untreated and imatinib-treated K562 cells. Peak assignments: Cho(lesterol) C19 at 0.9 ppm; F_{mix}: $CH_2\mathbf{CH_2}CH_2$ (largely 18:1 and 18:2) at 1.3 ppm, PUFA (polyunsaturated fatty acids) at 2.8 ppm; and PtdCho (phosphatidylcholine) at 3.23 ppm. The values are given as means ± SD of 3 independent experiments (n=6 for control and n=4 for 96 hours with 0.1 μM imatinib). Significance levels: *p<0.05; **p<0.005; ***p<0.001 were determined by ANOVA (with post-hoc pairwise multiple comparison Tukey-test).*

^{13}C-MRS experiments on lipid extracts to verify if in our model imatinib reduces PC and PtdCho concentrations and causes an increase in other substrates of PtdCho-synthesis, diacylglycerol (DAG) and, subsequently, in triacylglycerol (TAG) have not yet been carried out. Corresponding findings were observed in various cell types undergoing apoptosis (Engelmann et al., 1996; Finstad et al., 1998; Al-Saffar et al., 2002; Listenberger et al., 2003).

De novo DAG and TAG synthesis could not be studied, but the integration of a TAG-

signal in ^{1}H-MRS spectra of lipids (at 5.3 ppm) showed that its total concentration increased to 121% ($p<0.05$, n=3) and 181% ($p<0.05$, n=3) of the controls after 2 and 4 weeks of imatinib-treatment, respectively. Those results indicated that in our model the increasing rate of apoptosis rate was reflected by increasing total TAG concentrations as well.

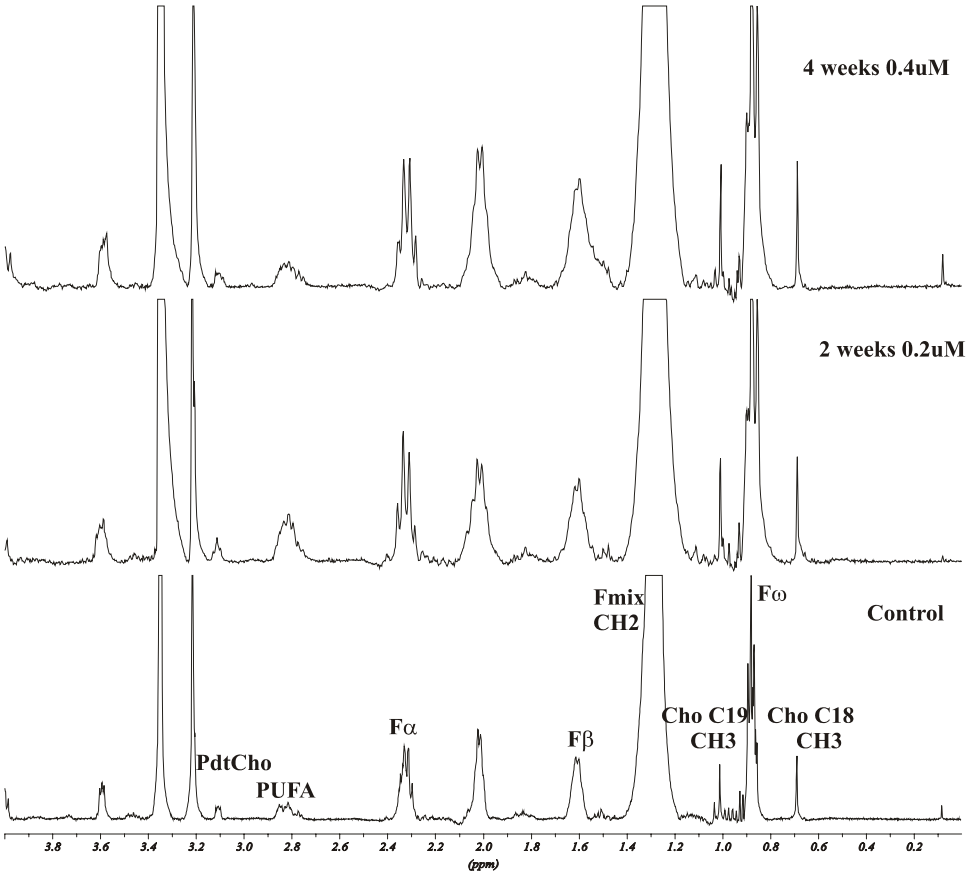

Figure 3.11: Representative ^{1}H-MRS spectra of K562 lipid extracts. Cells were incubated with 0.1 μM imatinib for 1 week, after which the drug concentration was increased weekly by 0.1 μM. The resulting final concentrations were 0.2 μM after 2 weeks and 0.4 μM imatinib after 4 weeks. All treated cells were compared to untreated controls. Peak assignment: PdtCho: phosphatidylcholine, PUFA: polyunsaturated fatty acids, Cho: cholesterol; F: fatty acid side chain F_{mix}: -(CH_2)n-; Fω: methyl group.

3.1.4. Changes in cell volume in K562 cells after long-term imatinib treatment

Changes in concentration of osmoregulators, such as taurine, myo-inositol, glycine or GPC, can be detected and quantified using MRS. Their increase or decrease is a result of

the adaptive volume regulation upon cell shrinkage or swelling and is responsible for a variety of cellular processes. The organic osmolytes play a decisive role in cell volume regulation: upon shrinkage, they accumulate inside the cells, in response to cell swelling they can be released from the cells via osmoregulated membrane channels (Burg MB, 1995; Lang et al., 1998). Lymphocytes undergo apoptosis in response to glucocorticoids and exhibit cell shrinkage, nuclear condensation, internucleosomal DNA fragmentation, and apoptotic body formation (Green and Reed, 1998; Wyllie et al., 1980; Compton MM, 1992). Exposure of cells to apoptotic stimuli induces a rapid loss of cell volume (apoptotic volume decrease) that plays a pivotal role in the decision of a cell to undergo apoptosis (Okada and Maeno, 2001; Lang et al., 2004; Green and Reed 1998).

While after 96 hours of treatment with 0.1 μM imatinib no significant changes in myo-inositol concentrations were observed, further treatment for up to 2 weeks led to a signal increase to 133% of controls ($p<0.05$, n=3). This indicated that under imatinib treatment cells were shrinking. Unfortunately, taurine signal was not high enough to enable appropriate quantitation.

3.1.5. Changes in amino acid concentrations after long-term imatinib treatment

The concentration of total glutathione (both oxidized and reduced forms: GSSG+GSH) decreased to 60% (after 1 week, $p<0.005$, n=3) and even further in the following 3 weeks of treatment. Glutathione is an important water-phase antioxidant and essential cofactor for antioxidant enzymes. It also provides protection for mitochondria against endogenous oxygen radicals. A trend towards lower glutathione levels may indicate increased oxidative stress and/or a decrease in anti-oxidative defense.

Furthermore, a decrease in alanine concentrations was observed. Those dropped from 71% (not significant, n=3) after 96 hours to 38% ($p<0.005$, n=3) of controls after 2 weeks of imatinib treatment.

In contrast, the acetate signals significantly increased to 232% ($p<0.005$, n=3) of controls after 96 hours but returned to control values after 2 weeks.

3.1.6. Changes in Bcr-Abl protein expression and protein phosphorylation

K562 and LAMA84 cells both contain the fusion protein Bcr-Abl. Since imatinib

specifically reduces the tyrosine kinase activity of Bcr-Abl, we evaluated its effect on the level of tyrosine phosphorylation (p-tyr) via flow cytometry of permeabilized cells. Incubation with imatinib significantly reduced the fluorescence intensity of the p-tyr staining in both cell lines. Western blot analysis showed that the p-tyr band (at 210 kDa) completely disappeared after 24 hours with 0.1 μM imatinib in both cell lines. Flow cytometry revealed a significant decrease to less then 30% of the controls' expression after 96 hours of incubation ($p<0.0001$, $n=3$ for K562 and LAMA84 cells).

In the K562 CML cell line, the level of c-Abl protein (as assessed by Western blotting of cell lysates and normalized to β-actin as housekeeping protein) was almost three-fold higher then in the controls after 24-48 hours, but decreased to control values after 96 hours of treatment. The LAMA84 cell line does not contain a normal ABL gene. Therefore the level of Bcr-Abl overexpression in LAMA84 cells was examined by flow cytometry of permeabilized cells with an anti-Abl monoclonal antibody. Short incubation times led to an increase in protein expression with maximum values after 48 hours of incubation. However, after 96 hours expression was down-regulated to control values as well.

3.1.7. Glucose uptake studies and Glut-1 transporter expression levels (total protein and m-RNA expression) after long-term imatinib treatment

Glucose uptake / lactate release: MRS and enzymatic approach. Time-dependency of imatinib effects on glucose uptake/lactate release was studied in a new set of experiments. Media aliquots from untreated K562 and LAMA84 cells and cells treated with 0.1 μM imatinib were taken after 24, 48, 72 and 96 hours of incubation. Cells had been counted and had been incubated with 5mM [1-1^3C] glucose for 4 hours before sample collection. Subsequently, ^{1}H-MRS analysis was performed. Concentrations determined by integration of ^{1}H-MRS signals were normalized to the number of cells. In order to obtain valid ^{1}H-MRS spectra, a water presaturation sequence was used. Therefore, the presaturation effect on quantitation of nearby glucose signals was evaluated based on the previously performed experiments.

In both cell lines the time course was the same: from 48 hours (minimal glucose uptake and lactate release) to 96 hours, less glucose was taken up and less lactate was released

into the media compared to the controls (Figure 3.12).

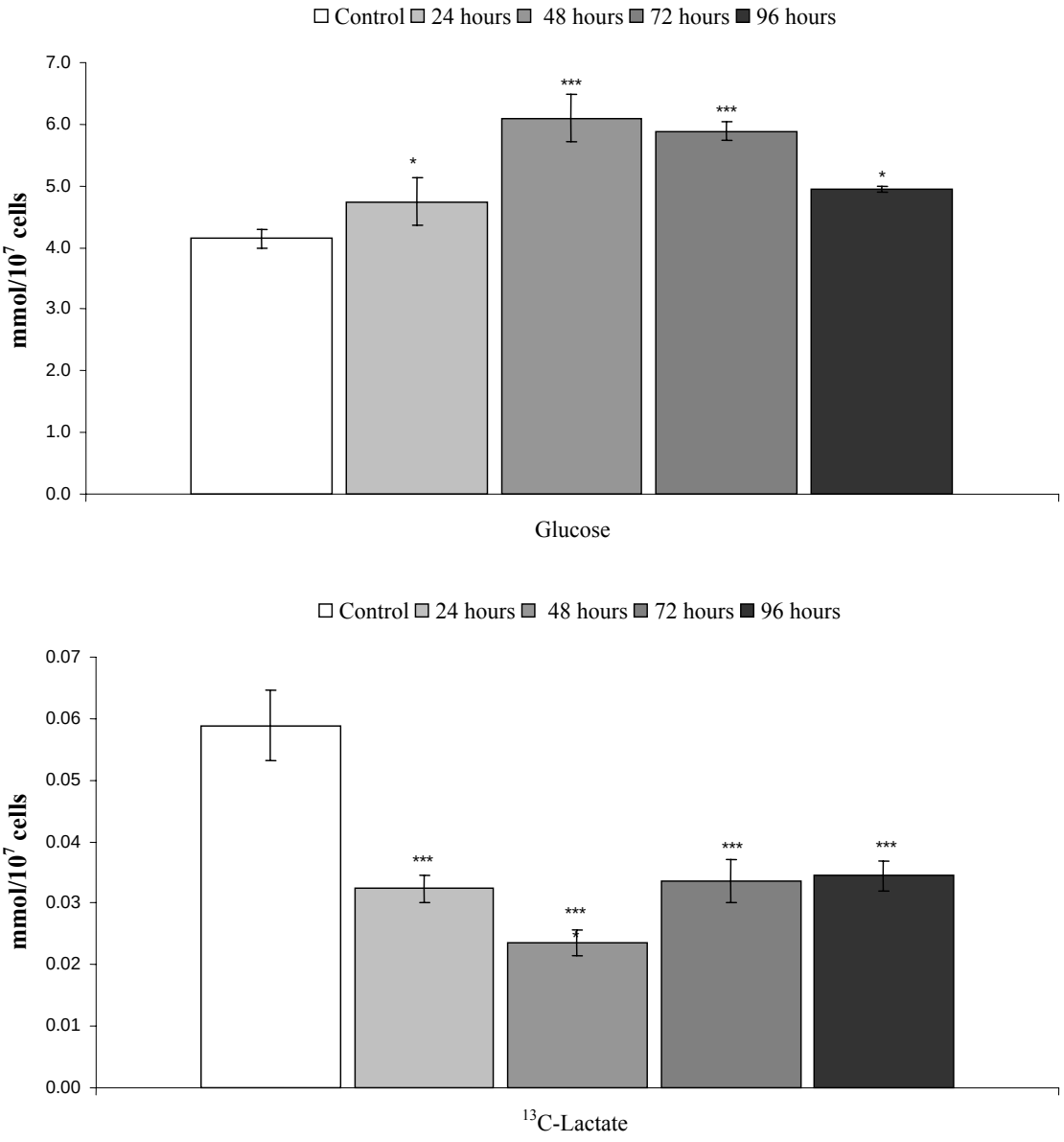

*Figure 3.12: Glucose and de novo produced ^{13}C-lactate concentrations as calculated from the ^{1}H-MRS spectra of LAMA84 media (untreated controls and LAMA84 cells treated with 0.1 μM imatinib). The cells were incubated with 5mM [1-1^{3}C] glucose for 4 hours. The values were calculated per number of cells (x 10^{7}) and represent means ± SD of 4 independent experiments. Significance levels: *p<0.05; **p<0.005; ***p<0.001 were determined by ANOVA (with post-hoc pairwise multiple comparison Tukey-test). Comparison by ANOVA indicated statistically significant differences with p<0.001.*

To validate MRS-based quantification, the same media samples were also analyzed using enzymatic glucose and lactate assays. The results showed 10-15% deviation compared to when being analyzed by MRS. However, the same trends in both, glucose and total lactate concentration, were observed. The comparison between the enzymatic assay and MRS results is a useful tool to compare the accuracy of both methods. The concentrations calculated from the ^{1}H-MRS spectra were 10-15% lower than the values from the glucose and lactate enzymatic assays (different sources of error could make the difference e.g. it could originate from the lyophylization process prior to MRS analysis or due to cross-reactivity of enzymatic assays). However, a deviation of 10-15% between two assays with a day-to-day precision of approximately ±10% during a one-time comparison is an acceptable result (CDER, 2001).

Glucose is the primary source of carbon for *de novo* synthesis of nucleic acids, lipids and amino acids and is the major source for energy production. The increased concentration of glucose in the media of imatinib-treated cells correlated with previous findings (Gottschalk et al., 2004). Prior studies reported that imatinib regulated glucose flux through down-regulation and translocation of Glut-1 transporters from the cell membrane into the cytoplasm in human leukemia cells (Boros et al., 2002; Boren et al., 2001; Prenen et al., 2005). Glucose uptake furthermore is increased in imatinib-resistant c-kit tumors, as observed in clinical studies based on PET-scans (Van den Abbeele, 2002).

2-Deoxyglucose uptake. Experiments studying 2-deoxyglucose uptake were performed at the radioactivity core laboratory of the University of California at San Diego. K562 cells were incubated with 2-deoxyglucose plus 0.1 μM imatinib for 24 hours. Media and cell aliquots were taken in 10 minutes intervals during the first 60 minutes (after 0, 10, 20, 30, 40, 50 and 60 minutes) and between the 23rd and the 24th hour of incubation (also in 10 minutes intervals: 23 hours + 0, 10, 20, 30, 40, 50, 60 minutes = 24 hours). The results showed that 0.1 μM imatinib did not significantly affect glucose uptake in the first 60 minutes (1.95 vs. 1.93 nmol/min/10^6 cells); but after 24 hours of incubation, uptake was significantly decreased (1.99 vs. 1.86 nmol/min/10^6 cells, $p=0.05$, $n=4$).

Glut-1 transporter total protein and m-RNA expression. Flow cytometry analysis of time-dependent total Glut-1 protein expression was measured in K562 and LAMA84 cells. After 96 hours, the expression was slightly down-regulated compared to the

controls. After 2 weeks of imatinib-treatment only half the protein expression than in the controls was observed (Figure 3.13). One of the reasons for the difference between the observed decreased glucose uptake (already significant after 24 hours of imatinib treatment) and Glut-1 transporter expression in "short-term" experiments could be that, even though the amount of protein did not change, its location may have. Previous studies on Glut-2 expression changes in GIST cells after 24 hours of imatinib treatment showed that the transporter migrates from the membrane away into the inner cell, with no changes in its total expression (Prenen, et al., 2005). The same could be happening in our studies as well and will need to be investigated in the future. After 2 weeks, Glut-1 expression was significantly reduced.

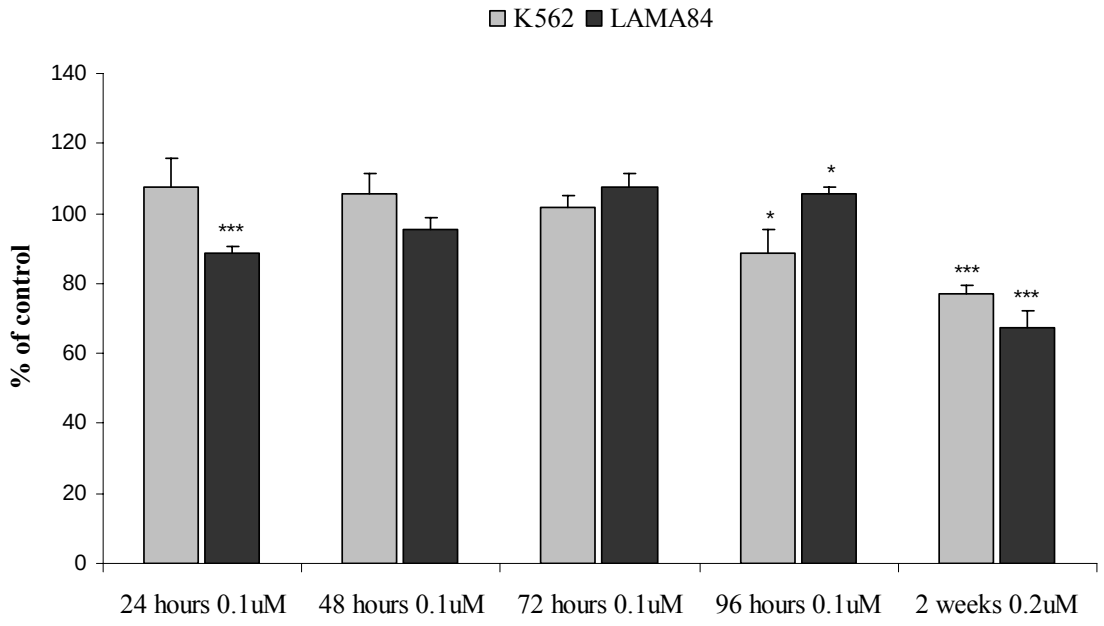

*Figure 3.13: Glut-1 glucose transporter expression as calculated from flow cytometry analysis of K562 and LAMA84 cells. Cells were incubated with 0.1μM imatinib for 1 week, after which the imatinib concentration was increased to 0.2 μM (second week). The cells were fixated, permeabilized and stained with Glut-1 antibody. The values were calculated as % of control and represent means + SD of 3 independent experiments (only n=2 for 2 weeks treatment). Significance levels: *p<0.05; **p<0.005 were determined by ANOVA (with post-hoc pairwise multiple comparison Tukey-test). Comparison by ANOVA indicated statistically significant differences with p<0.001.*

Reverse-transcription polymerase chain reaction (RT-PCR) is the most sensitive

technique for mRNA detection and quantitative analysis of gene expression. We used quantitative RT-PCR for quantification of Glut-1 mRNA levels in K562 and LAMA84 cells. After 96 hours of imatinib treatment in K562 cells, no significant changes were seen (at 79.3±14.6% of control, n=3). In LAMA84 cells, the mRNA concentration decreased to 69.0±11.1% of control ($p<0.05$, n=3) (followed by a subsequent decrease in protein expression after 2 weeks of treatment, Figure 3.13).

3.1.8. Changes in intracellular imatinib concentration and p-glycoprotein expression

HPLC/MS-measurements of intra- and extracellular imatinib concentrations. A fully validated, automated HPLC/MS method (according to the US Federal Drug Agency (FDA) approved Bioanalytical Method Validation Guidance for Industry; CDER, 2001) for the quantification of imatinib in human blood, and cultured blood cells media was developed (4.3.8).

Intracellular imatinib concentrations did not significantly change between 24 and 72 hours of treatment, but significantly increased after 96 hours in both cell lines (Figure 3.14). Interestingly, when after 2 weeks the concentration of imatinib was doubled to 0.2 μM, the intracellular concentration in LAMA84 cells showed an even higher increase (< factor 2). The change between 96 hours with 0.1 μM and 2 weeks with 0.2 μM imatinib was 0.0111±0.0009 vs. 0.0273±0.0013 μM imatinib per 10^7 cells ($p<0.001$, n=4) (Figure 3.14). As it can be seen in Figure 3.14, K562 cells contained more imatinib than LAMA84 cells, possibly indicating higher imatinib efflux transporter expression / activity in LAMA84 cells.

After the first week, the cell media was changed and fresh 0.2 μM imatinib was added. The total imatinib concentration was again measured at the end of 2 weeks (calculated as the sum of intra- and extracellular concentrations) and showed that 20% of imatinib had degraded or been metabolized after this period of time.

The generally accepted action of pgp is to reduce intracellular drug accumulation through pgp-mediated efflux, thus hampering the achievement of effective drug levels at the target site. In their study, Mahon et al. (2003) demonstrated that *ABCB1* (*MDR1*) gene overexpression can confer resistance to imatinib in leukemia cell lines. The possible

importance of drug-transporter proteins was confirmed by demonstrating that imatinib was a substrate of pgp (Hegedus et al., 2002).

Experiments were performed in order to identify changes in pgp-protein expression (as measured by flow cytometry analysis of fixated cells). Assessment of the effects of incubation time and imatinib concentrations showed that K562 cells were not subject to any changes, but that in LAMA84 cells pgp expression was already increased after the initial 24 hours of treatment (123.9±9.6% of control, Figure 3.15). Pgp is exporting drugs from cells. The trend changed after 2 weeks, after which pgp expression decreased below control levels (from 119.6±4.4% after 96 hours to 83.1±7.7% of controls after 2 week).

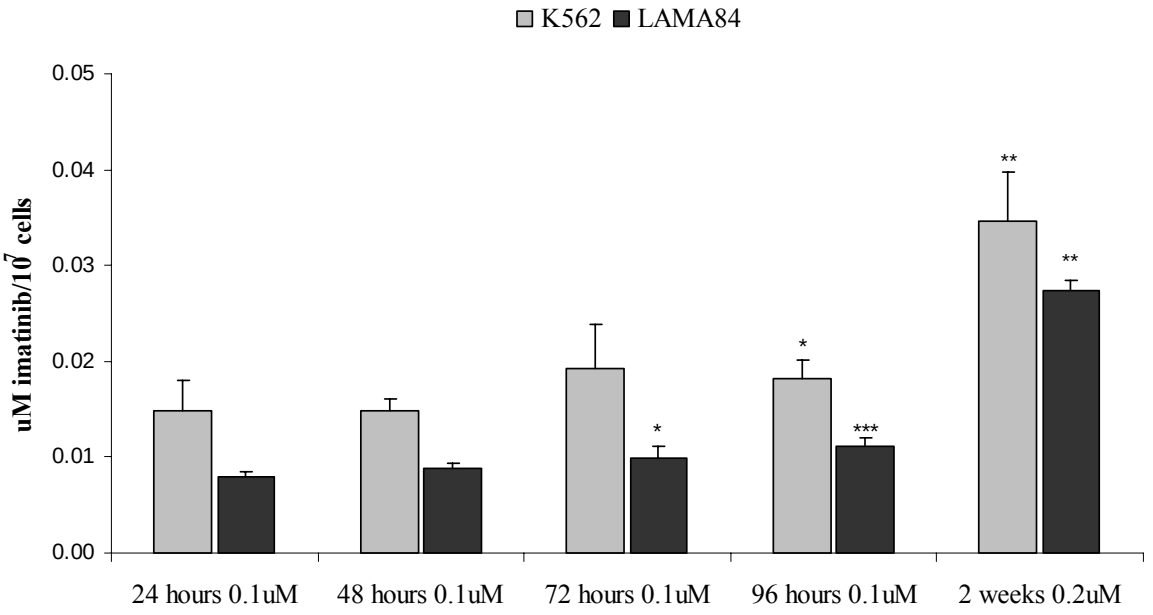

*Figure 3.14: Intracellular imatinib concentration as calculated based on HPLC-MS/MS data of intracellular concentrations in K562 and LAMA84 cells (treated with 0.1 and 0.2 μM imatinib). The values were calculated as μM imatinib per 10^7 cells and represent means + SD of 4 independent experiments. All values were highly significant when compared to untreated controls. Significances were determined by ANOVA (with post-hoc pairwise multiple comparison Tukey-test). In the figure, significances were given as *p<0.05; **p<0.005; ***p<0.001 when values were compared to the 24 hours value(s). Comparison by ANOVA indicated statistically significant differences with p<0.001.*

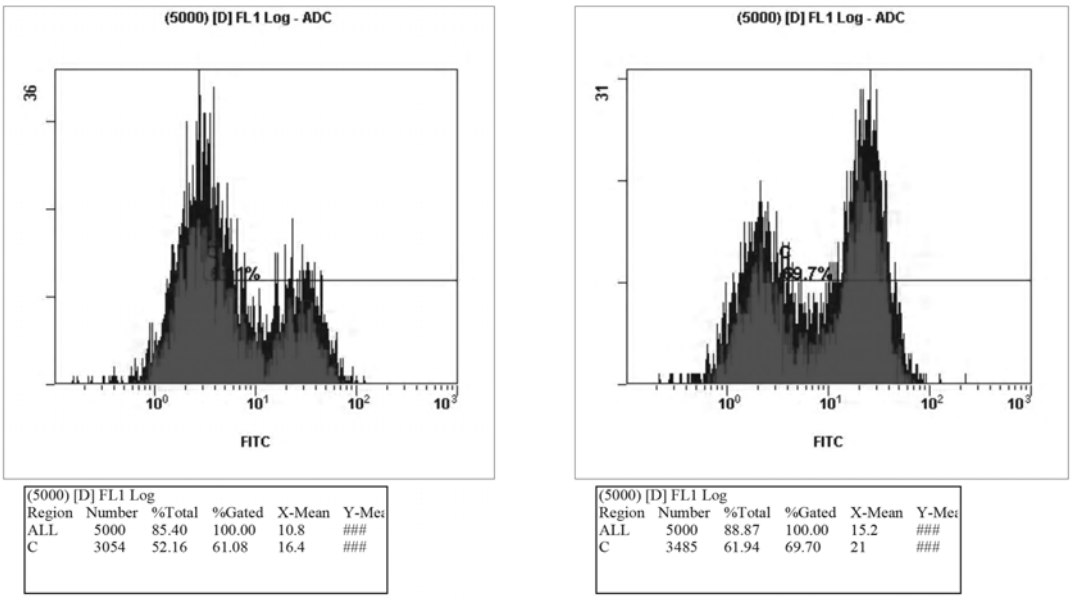

(5000) [D] FL1 Log					
Region	Number	%Total	%Gated	X-Mean	Y-Mea
ALL	5000	85.40	100.00	10.8	###
C	3054	52.16	61.08	16.4	###

(5000) [D] FL1 Log					
Region	Number	%Total	%Gated	X-Mean	Y-Mea
ALL	5000	88.87	100.00	15.2	###
C	3485	61.94	69.70	21	###

Figure 3.15: Flow cytometry plots of untreated LAMA84 cells (left) and of LAMA84 cells treated with 0.1 μM imatinib for 24 hours (right). All cells were fixated and permeabilized before staining with pgp- antibody. The mean fluorescence intensity (x-Mean ALL) was used to calculate pgp protein expression.

3.1.9. Discussion and Conclusions: Long-term imatinib treatment

The discovery and development of imatinib has shown that it is possible to produce rationally designed, molecular-targeted drugs for treatment of a specific cancer. Such designed compounds can affect not only one but several targets, allowing for therapeutic efficacy in several diseases.

One of the major concerns with imatinib treatment is the development of drug resistance (see chapter 2.2.2.). Previous research and clinical reports have indicated that changes in glucose metabolism may be related to or even be predictive for the development of imatinib resistance.

In this study cellular metabolic response including mitochondrial activity and glucose utilization, energy production, membrane biosynthesis and degradation to imatinib treatment were investigated. The imatinib concentration chosen (0.1 μM) was successfully used in previous studies (Gottschalk et al., 2004). This concentration was confirmed not to cause cytotoxic effects during short-term administration (up to 96

hours). However, long-term treatment (from 1 to 4 weeks) with increasing imatinib concentrations (0.1 μM imatinib increase per week) caused significantly higher apoptosis rates. After 5 weeks, more then 70% of treated-cells were dead.

Tumor cells exhibit elevated glycolysis rates under aerobic conditions, the so-called Warburg effect (Warburg, 1956). Increased expression of the glucose transporter Glut-1 and increased hexokinase activity appear to underlie the acceleration of glycolysis in tumors (Asano et al., 2000; Smith TA, 1998). Glut-1 is an important tumor biomarker, being overexpressed in a wide range of tumors, and correlating with poor prognosis (Airley et al., 2001). Glut-1 is composed of two subunits each possessing an active site to which AMP or ATP can bind. Binding of ATP to the site induces a conformational change that reduces glucose uptake. Imatinib targets the ATP-binding sites of c-kit or Bcr-Abl. Studies in gastrointestinal stromal tumors have shown a rapid decrease in fluorinated deoxyglucose (FDG) uptake, sometimes as early as 24 h after administration of imatinib. Previous studies have also reported that imatinib regulates glucose flux through down-regulation and translocation of Glut-1 transporters from the cell membrane into the cytoplasm in human leukemia cells (Boros et al., 2002; Boren et al., 2001; Prenen et al., 2005).

When treated with imatinib, leukemia cells showed decreased glycolysis rates. This observation was opposite to the Warburg effect. Additional reduction of Glut-1 protein expression and small changes in Glut-1 mRNA production were observed. The suppression of glycolysis resulted in decreased [1-^{13}C]glucose uptake from the incubation media, which correlated with previous findings (Gottschalk et al., 2004).

While the C3-lactate concentration was decreased, a simultaneous increase in C4-glutamate production was observed. Through increased mitochondrial activity, production of high-energy phosphates (PCr and NTP) was elevated. These observations and the suggestion that imatinib stimulates mitochondrial metabolism and reduces anaerobic glycolysis in Bcr-Abl positive leukemia cells confirmed the results reported by Gottschalk et al., 2004.

When cells are exposed to cytotoxic agents, there are two major types of cell death: apoptosis and necrosis. Cell shrinkage, DNA damage, chromatin condensation and

blebbing of the plasma, and alteration of plasma membrane phospholipids organization with phosphatidylserine externalization are major characteristics of apoptosis (Robertson and Orrenius, 2000). Necrosis is generally characterized by swelling of cells and mitochondria, scattered chromatin condensation, and loss of plasma membrane integrity due to an overwhelming physical cell injury (Nicotera and Lesia, 1997).

In the time period between 96 hours and 2 weeks of treatment, imatinib started to reveal its anti-proliferative and pro-apoptotic properties in our cell models. After the first week of treatment, decreased cell proliferation rate and increased number of apoptotic cells became detectable and were enhanced with longer incubation times and higher imatinib concentrations.

Short-term incubation with 0.1 μM imatinib led to an increase of mitochondrial activity and energy balance and/or charge. The maxima were reached after 1 week. Hereafter, both mitochondrial activities and energy charge started to decrease. When after 96 hours the first signs of apoptosis were observed, cells were highly active and have maintained their elevated mitochondrial activity. From the literature is known that the apoptotic process demands high energy for its development (Garland and Harlestrap, 1997; Eguchy et al., 2000; Zamaraeva et al., 2005).

Although most studies demonstrated that apoptotic stimulation reduced total cellular ATP levels to a certain extent, the fact that the cells can show the same or even better energy status was also reported (Leist et al., 1997; Budd et al., 2000; Zamaraeva et al., 2005). Such variability in ATP levels might be, at least in part, due to differences in the time period of apoptotic stimulation. Furthermore, it may also be explained by decreased energy utilization that results from inhibition of cell proliferation.

With an increasing number of apoptotic and dead cells, the NTP concentration decreased and was followed by an even more dramatic decrease of PCr. After 4 weeks of treatment, the NTP signal significantly declined, and PCr signals became even undetectable. Similar observations were made by Henke, 1996, and Henke et al., 1999, whose investigations on miltefosine- induced apoptosis revealed a “stable” NTP state, up to the point where the PCr concentration decreased below 50% of control and the cells underwent processes associated with “secondary necrosis”.

Phosphocholine (PC), a major precursor for membrane synthesis, is known to be increased in rapidly proliferating cancer cells, including leukemia cells (Ackerstaff et al., 2003; Franks et al., 2002). Its reduction was significant after the first week and even enhanced after 2-4 weeks of imatinib treatment. The reduction in PC is consistent with the findings for the response of other cell types and tumors to therapy (Evelhoch et al, 2000). Additionally, lower phosphocholine concentrations lead to a decrease in phosphatidylcholine. Phosphocholine is both, a precursor and a breakdown product of phosphatidylcholine.

Phosphatidylcholine (PtdCho) is a phospholipid that is a major component of cell membranes and that is necessary for the structure and function of all cells and crucial for sustaining life (Kent, 1995; Zeisel and Blusztajn, 1994; Cullis and Hope, 1991;).The fact that with advancing apoptosis stages, the concentration of PtdCho was lowered has already been observed (Engelmann et al., 1996; Williams et al., 1998). Possible involvement of 1,2-diacylglycerolcholine phosphotransferase (CT), the key enzyme in PtdCho synthesis, has previously been discussed (Geilen et al, 1992) and would need to be further investigated in case of imatinib induced apoptosis. With longer incubation times, we found that the concentrations of CTP were reduced. This may also interfere and reduce the production of CDP-choline, a precursor of PtdCho.

Products of choline phospholipid metabolism, such as PC, diacylglycerol, and metabolites synthesized from arachidonic acid may function as second messengers (Meves H, 1994; Goni and Alonso, 1999). In this study an increase in the concentration of triacylglycerol (TAG) (which is synthesized from diacylglycerol (DAG)) was observed. This has also been seen in various cell types undergoing apoptosis (Engelmann et al., 1996; Finstad et al., 1998; Al-Saffar et al., 2002; Listenberger et al., 2003).

PUFAs (polyunsaturated fatty acids) play a major role in membrane constitution and function and are one of the main targets of the lipoperoxidation process caused by reactive oxygen species. PUFAs can be synthesized from DAG (by DAG Lipase). In malignant cells and tumors, appearance of a lipid peak at 1.3 ppm from $CH_2\mathbf{CH_2}CH_2$ moieties (associated largely with 18:1 and 18:2 lipids) has commonly been associated with ongoing cell death processes (Griffin et al., 2003; Blankenberg et al., 1996, 1997;

Al-Saffar et al., 2002; Juhana et al., 2000; di Vito et al., 2001). Furthermore, an increase of bisallylic methylene fatty acyl protons at 2.8 ppm was observed by Hakumaki et al. (1999), who suggested that these protons correspond to PUFA and that their accumulation follows apoptosis.

Our study showed an increase in fatty acids synthesis: Increased methyl (Fω) and methylene (F_{mix}) signals were followed by increasing PUFA signals. The increase started at the time when the energy charge was still high in order to generate more lipids for the upcoming apoptotic body formation (larger cell surface for membrane folding during apoptosis).

Furthermore, decreased NAD^+ and glutathione concentrations could also serve as early indicators for ongoing imatinib-induced apoptosis. Previous studies have shown that other antitumor agents initiate the apoptotic cascade by decreasing NAD^+ concentrations (Wosikowski et al., 2002).

The generally accepted action of *ABCB1* (*MDR1*) is to reduce intracellular drug accumulation through pgp-mediated efflux, thus reducing drug concentrations at the intracellular effector sites. After 24 hours in LAMA84 cells, pgp-expression was already elevated, indicating enhanced active drug efflux. Longer-treatment periods, on the other hand led to a decrease in pgp-expression, followed by an increase in intracellular effective imatinib concentrations. Due to the formation of apoptotic bodies, the membrane becomes more porous and its fluidity increases, what lowers the possibility for pgp imbedding and localization (Kok et al., 2000; Ferté J, 2000).

The results show that multinuclear MRS is a valid method for studying apoptosis after drug exposure and therapy of tumor cells. Different metabolic markers, early and late, can be distinguished, and as demonstrated by our studies, show good correlation with molecular changes such as protein expression. Furthermore, the use of cell extracts for MRS investigations helps to evaluate the mode of action of anticancer drugs on the molecular level.

Pre-apoptosis	
Bcr-Abl phosphorylation	↓↓
intracellular lactate	↓
TCA-cycle activity	↑
energy balance	↑
Apoptosis	
intracellular lactate	↓
Glut-1 protein expression	↓
Extracellular glucose and lactate	↑ / ↓
TCA-cycle activity	–
energy balance	–
Phosphocreatine	↓
NAD^+	↓
Phosphocholine	↓
Phosphatidylcholine	↓
PUFA, F_ω, F_{mix}	↑
p-glycoprotein expression	↓
intracellular imatinib concentration	↑
cell volume	↓
Necrosis / "Secondary necrosis"	
TCA-cycle activity	↓
energy balance	↓
Phosphocreatine	↓↓
NAD^+	↓↓
phosphocholine, phosphatidylcholine	↓↓

Figure 3.16: Summary of metabolic effects after long-term imatinib treatment of K562 human leukemia cells. Metabolic changes after imatinib treatment were divided into 3 groups: pre-apoptotic stage (up to 1 week of treatment), apoptosis developing stage (up to 2 weeks of treatment) and necrosis / "secondary necrosis" development (after 3 weeks). Cells were treated with 0.1μM imatinib in the first week, after which the drug concentration was increased weekly (0.1μM imatinib per week).

3.2. Imatinib effects: Short-term incubation of leukemia cells

For the evaluation of short-term effects two cell lines: K562 and LAMA84 cells were incubated with 1 μM imatinib for 24 hours. The results of different experiments performed are demonstrated in the following.

3.2.1. Imatinib influence on cell proliferation and viability

In both Bcr-Abl positive cell lines, significant growth inhibition occurred after 30 hours (Figure 3.17). After 48 hours in K562 cells, 65% viable cells were counted. In LAMA84 cells, cell viability was lower with 55% (as determined by Trypan-Blue exclusion method).

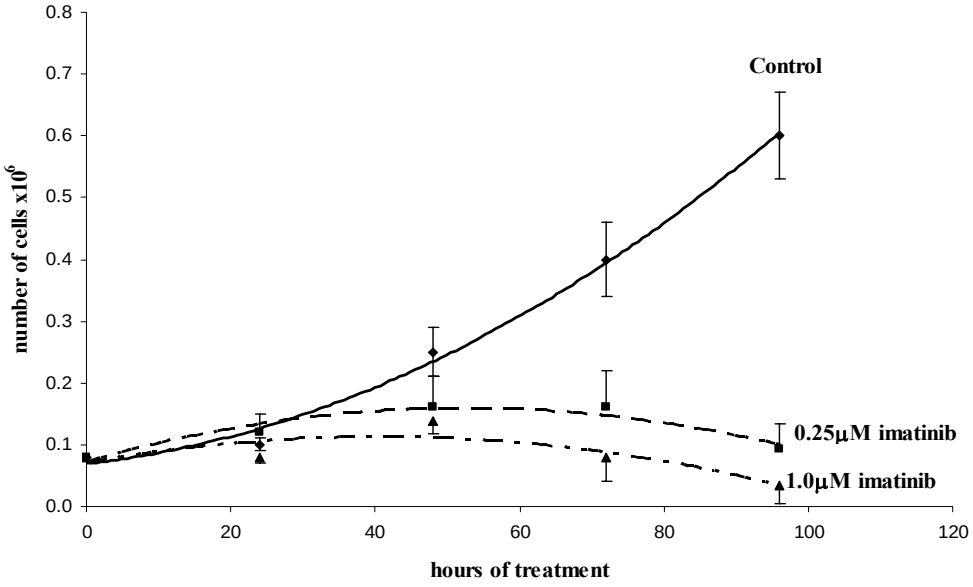

Figure 3.17: Proliferation curves of LAMA84 leukemia cells; comparison between untreated cells (control) and cells treated with 0.25μM and 1μM imatinib (mean of n=3 experiments). Control values are presented as means± SD; imatinib treated values are presented as means + SD (0.25μM imatinib) and means – SD (1μM imatinib)). Effects of imatinib on the proliferation rates of K562 cells were similar.

Apoptotic processes were already induced after 24 hours causing an increase of 27% in apoptosis ($p<0.0005$, n=4) in the K562 and of 18% ($p<0.005$, n=4) in the LAMA84 total cell populations (Figure 3.18). Increases in imatinib concentrations up to 5.0μM (for 24h) caused an increase in the number of apoptotic cells as well. In K562 cells 38.5%

($p<0.0001$, n=4) and in LAMA84 cells 29.7% apoptotic cells (from the total cell population) were measured.

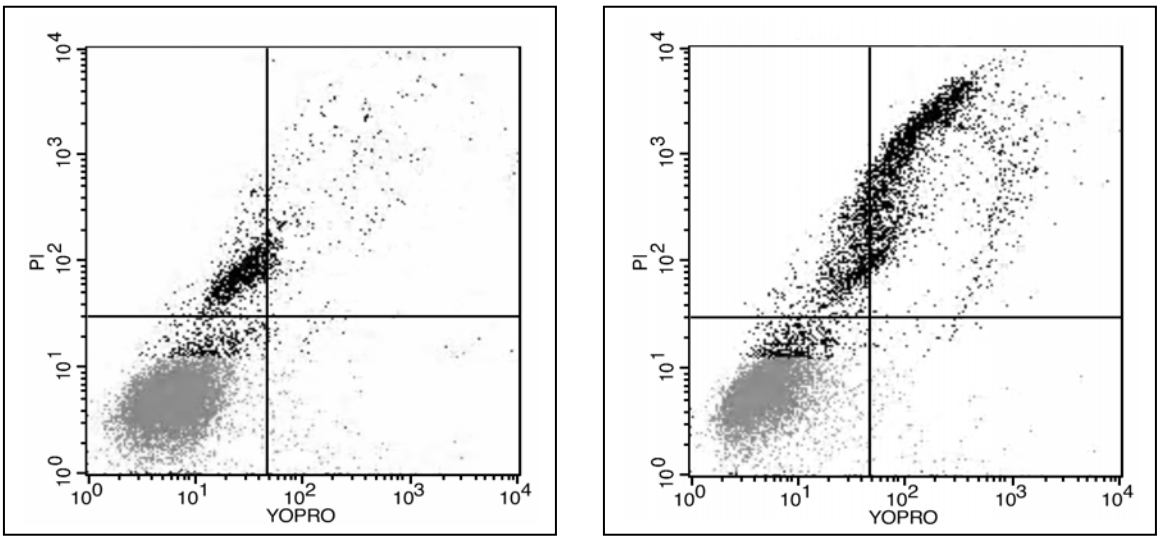

Figure 3.18: Flow cytometry plots of untreated (left) and K562 cells treated with 1 μM imatinib (24 hours) (right). The cells were stained with YOPRO-1 and propidium iodide. Lower left: live, upper left: necrotic, lower right: early apoptotic, upper right: apoptotic cells.

3.2.2. Glucose and energy metabolism in K562 leukemia cells / Changes after short-term imatinib treatment

Glucose metabolism. The cellular response to imatinib reflects a similar metabolic pattern in both Bcr-Abl positive cell lines. After 24 hours of incubation with imatinib, energy producing pathways, anaerobic glycolysis (lactate production) and mitochondrial Krebs cycle (glutamine and glutamate production), were down-regulated. As previously described, cells undergoing apoptosis have limited their glucose uptake; therefore intracellular glucose concentrations decreased to 39% and 59% of controls in imatinib-treated LAMA84 and K562 cells. Not only that the cells had less glucose available, they also had significantly reduced their ^{13}C-lactate production (Table 3.19). The extracellular lactate concentration (lactate release) was lowered as well. Simultaneously, Krebs cycle activity was inhibited. *De novo* synthesis and the percentage of ^{13}C-enrichments in individual carbons were decreased; for example the signal of C4-glutamate was reduced to 57% ($p<0.05$, n=6) in K562 and 65% in LAMA84 cells in comparison to controls ($p<0.005$, n=6) (Table 3.19). The ratio [glutamate (C2+C3)/C4] = PC/PDH did not

significantly change in K562 cells, but did decrease from 0.59 to 0.40 ($p<0.05$, n=6) in LAMA84 cells, indicating a distribution change between anaplerotic and oxidative pathways.

	^{13}C-enrichment	Concentration (nmol/g) [^{13}C}
Lactate C3	**26.1±3.3** ***19.61±3.4****	**515.0±143.8** ***352.6±59.6****
Glutamate C2	**3.3±1.1** ***1.8±0.6****	**91.1±32.5** ***40.0±28.9****
Glutamate C3	**2.2±1.0** ***1.0±0.3****	**59.8±28.2** ***25.7±15.3****
Glutamate C4	**9.5±2.2** ***6.7±1.4****	**253.7±49.8** ***164.1±31.5****
Glutamine C2	**4.0±1.6** ***8.3±3.6****	**30.6±9.3** ***47.3±25.5***
Alanine C3	**17.2±2.5** ***14.6±4.5***	**25.3±12.0** ***22.1±10.5***

*Table 3.19: The absolute amounts of ^{13}C (nmol/g cell wet weight) and the percentage of ^{13}C-enrichments in individual carbon position of amino acids calculated by integration of signals in ^{13}C-MRS spectra obtained from control (bold) and with 1 μM imatinib treated (bold italic) LAMA84 cell extracts after 4 h incubation with 5 mM [1-^{13}C] glucose. The values are given as means ± SD of 6 independent experiments; significance *p<0.05; **p<0.005; ***p<0.001 determined by TTest.*

Energy state after imatinib treatment. Increased apoptosis rate and decreased mitochondrial glucose metabolism were not accompanied by lower energy state in imatinib-treated cells. Absolute concentration of high energy phosphates and, subsequently, the energy balance as calculated from the NTP/NDP ratio decreased, but the difference did not reach statistical significance in either of the cell lines. The concentrations of phosphocreatine that had been previously shown to decrease faster than

ATP during apoptotic processes (in long-term imatinib treatment experiments), highly decreased to 53% of control in K562 ($p<0.005$, n=6) and to 65% in LAMA84 treated cells ($p<0.05$, n=6).

HPLC-MS analyses showed the same results regarding the changes in ATP/ADP ratios as ^{31}P-MRS (not significant at 86% of control in LAMA84 and 79% in K562 cells, n=4). In addition, no significant changes were seen in either of the nucleoside tri- to diphosphate ratios (CTP/CDP, GTP/GDP or UTP/UDP, n=4). The ratios showed tendencies towards being reduced (60-80% of control cells) but these differences did not reach significance.

The NAD^+ concentrations decreased to 72% and 68% ($p<0.05$, n=4) of control K562 and LAMA84 cells. The observation that NAD^+ concentrations change more quickly than the concentrations of NTP (ATP) had already been made in long-term imatinib-treated cells.

3.2.3. Changes in lipids metabolism after short-term imatinib treatment

Changes in phospholipids metabolism. Over the past decade, one common feature consistently revealed by magnetic resonance spectroscopic studies is the elevation of phosphocholine (PC) and total choline-containing metabolites [tCho, glycerophosphocholine (GPC) + PC + free choline] in cancer cells and solid tumors.

The total choline concentration was calculated from ^{1}H-MRS spectra of water-soluble PCA extracts and showed a significant increase in both imatinib-treated cell lines, mostly resulting from an increase in GPC concentrations. In imatinib-treated K562 cells, total choline concentrations reached 137% of the controls ($p<0.05$, n=6); in LAMA84 cells the increase was even more evident reaching 210% of the controls ($p<0.005$, n=6).

In sensitive cells, treatment with 1 μM imatinib for 24 hours significantly decreased PC concentrations. The decrease was more pronounced in K562 (45% of control, $p<0.005$, n=6) then in LAMA84 cells (72%, $p<0.05$, n=6). The decrease of PC was followed by a subsequent decrease of phosphatidylcholine (PtdCho) concentration, which decreased to 58% in K562 and to 73% in LAMA84 cells (both as % of control, $p<0.05$, n=6).

The decrease of the phosphomonoester's (PC) was accompanied by an increase in phosphodiester (PDE) signals (Figure 3.20). GPE and GPC concentrations after 24 hour incubation with 1μM imatinib were highly increased in LAMA84 cells compared to untreated cells (343 ± 150 *vs.* 117 ± 57 nmol/g, $p<0.05$, n=6; and 861 ± 217 *vs.* 122 ± 34

nmol/g, $p<0.0005$, n=6). In K562 cells the increase in GPC concentrations was less extensive with 133% of control ($p<0.05$, n=6).

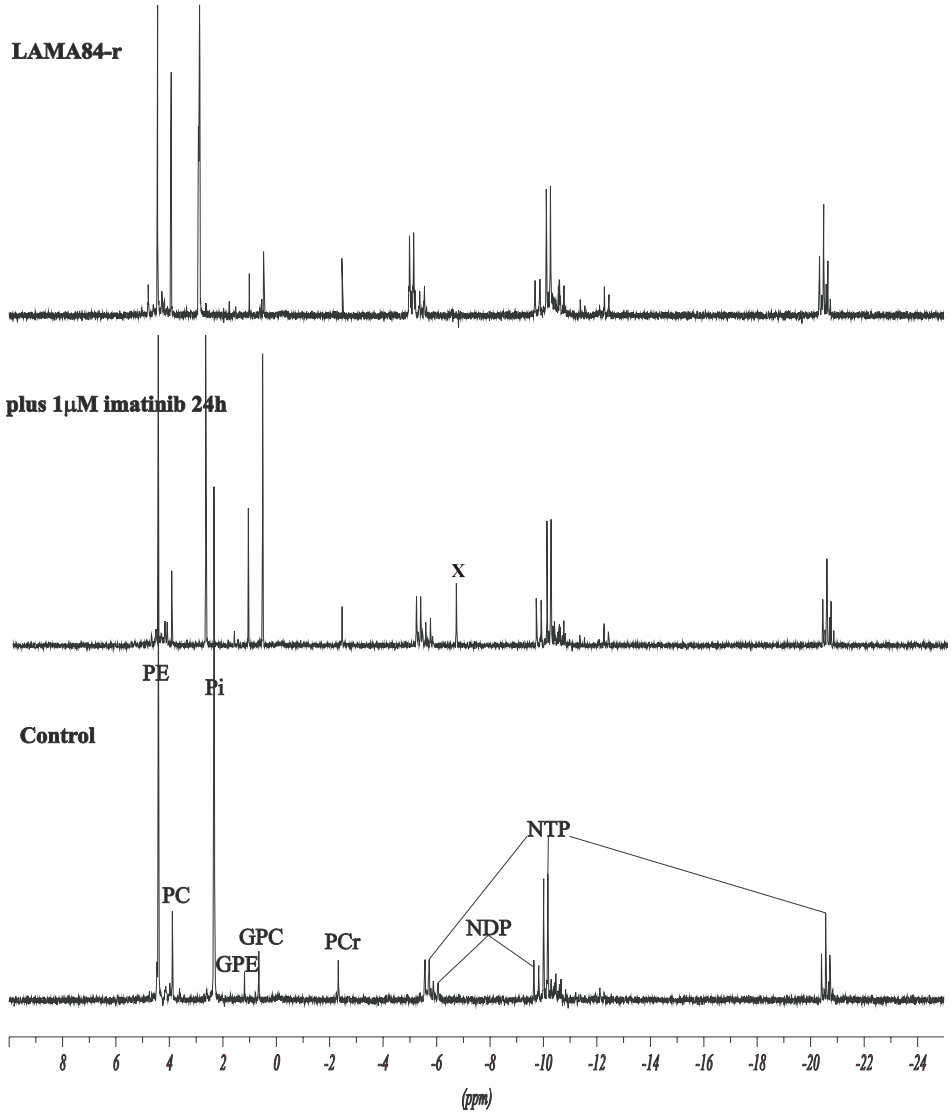

Figure 3.20: Representative ^{31}P-MRS spectra of LAMA84 and LAMA84-r (to 1μM imatinib resistant) cell extracts. Sensitive cells were incubated with 1μM imatinib for 24 hours and compared to untreated controls. Resistant cells were compared to their sensitive counterparts. Peak assignments: PC: phosphorylcholine, PE: phosphorylethanolamine, Pi: inorganic phosphate, GPC: glycerylphosphocholine, GPE: glycerylphosphoethanolamine, PCr: phosphocreatine, NTP: nucleotide triphosphates, NDP: nucleotide diphosphates, X: unknown signal (appeared in 2 of 6 spectra).

Changes in neutral lipids and fatty acids. The signals of polyunsaturated fatty acids

(PUFA) and cholesterol C18/C19 concentrations were elevated in with 1 μM imatinib treated K562 cells. Their concentrations had previously been shown to increase with increasing apoptosis rate (in long-term imatinib treated cells). Metabolic patterns in LAMA84 cells were the same, but due to a high standard deviation, were not statistically significantly different.

3.2.4. Changes in amino acid concentrations after short-term imatinib treatment

The concentration of total glutathione (both oxidized and reduced forms: GSSG+GSH) was reduced in both cell lines. In imatinib-treated K562 cells, the concentrations were at 650±274 nmol/g compared to 1254±410 nmol/g in controls; in LAMA84 cells it was 745±265 (treated) *vs.* 1002±177 nmol/g (control cells).

3.2.5. Changes in Bcr-Abl protein expression and protein phosphorylation

Inhibition of cell proliferation and occurrence of apoptosis in both Bcr-Abl positive cell lines was accompanied by inhibition of p-tyrosine protein expression. Western-blot results showed a total disappearance of the 210 kDa band specific for phosphorylated Bcr-Abl (Figure 3.21).

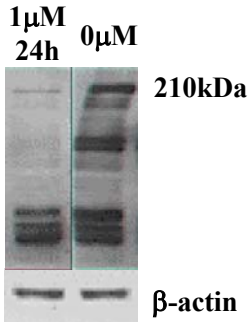

Figures 3.21: Western-blot on Bcr-Abl phosphorylation (p-tyrosine, p-tyr) (protein band at 210 kDa) in K562 control (right) and with 1.0 μM imatinib (24 hours) treated cells.

When treated with 1 μM imatinib, LAMA84 cells showed a 2-fold increase in Bcr protein levels compared to their sensitive control ($p<0.05$, $n=4$), while the changes in K562 cells did not reach statistical significance.

3.2.6. Glucose uptake and Glut-1 transporter expression after short-term treatment

Glucose uptake / lactate release: MRS and enzymatic approaches. In both cell lines after treatment with 1 μM imatinib, extracellular glucose concentrations were higher than

in untreated controls. Due to decreased glucose uptake, release of ^{13}C-lactate was significantly lower with 71% and 75% of untreated K562 and LAMA84 cells ($p<0.05$, n=6). This was followed by an increase in the extracellular glucose/lactate ratios (178% and 163% of K562 and LAMA84 treated cells ($p<0.005$, n=6)). Due to a lower glycolysis rate, extra- and intracellular ^{13}C-lactate concentrations were reduced as well.

Additionally performed enzymatic assays to quantify glucose and lactate in media confirmed those MRS results.

Imatinib effects on glucose uptake/lactate release experiments were also performed as a function of time. Media aliquots from untreated and with 1 μM imatinib treated K562 cells were taken after 2, 4 and 24 hours of incubation (Figure 3.22 A and B). Already after 2 hours of imatinib treatment, significant changes in glucose uptake were observed. While after 24 hours the glucose signal was not detectable in untreated cells, imatinib-treated cells showed higher glucose peaks and a significantly lower ^{13}C-lactate signal.

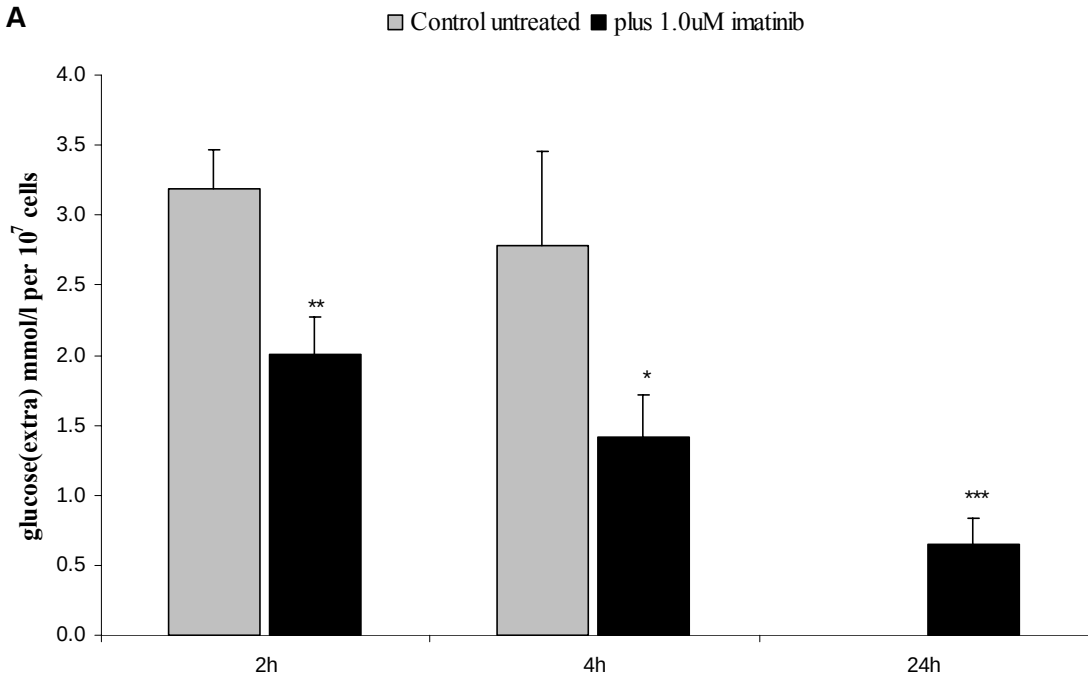

Figures 3.22 A: (for description see below).

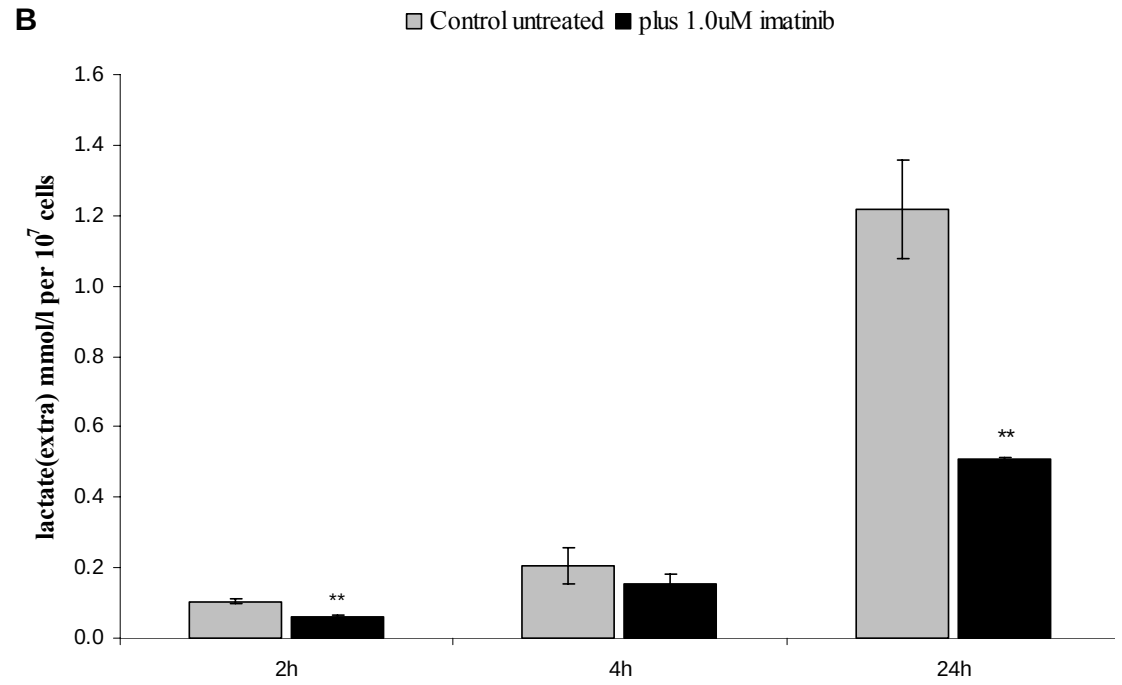

*Figures 3.22 A and B: Glucose and de novo produced ^{13}C-lactate concentrations as calculated from the ^{1}H-MRS spectra of K562 media (untreated controls and cells treated with 1 μM imatinib for 24 hours). The cells had been incubated with 5mM [1-1^{3}C] glucose for 4 hours. The values were calculated per number of cells (x 10^{7}) and represent means ± SD of 4 independent experiments; significance *p<0.05; **p<0.005; ***p<0.001 for untreated vs. treated cells. .Comparison by ANOVA indicated statistically significant differences with <0.001 when cells treated for 2h, 4h and 24h and untreated cells were compared.*

2-Deoxyglucose uptake. As previously seen from the MRS results, imatinib-treated cells showed a significantly lower deoxyglucose uptake rate, which was noticeable after the first 60 minutes of incubation and clearly distinguished them from the control cells after a longer period of time (24 hours) (Figure 3.23). In comparison, the relative uptake rate was higher in K562 then in LAMA84 cells.

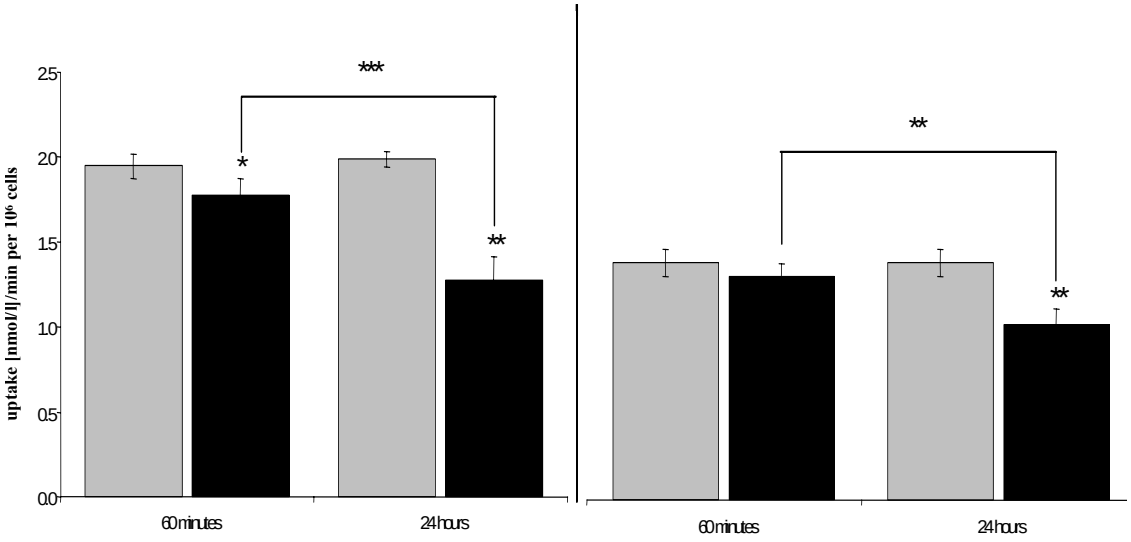

*Figure 3.23: 2-Deoxyglucose uptake [(nmol/mL)/min] per 10^6cells of K562 (left) and LAMA84 cells (right). Untreated controls are gray bars and with 1μM imatinib (24 hours) treated cells are represented by black bars. The cells had been incubated with 2-deoxyglucose for 1 to 24 hours. The values represent means ± SD of 4 independent experiments; significance *p<0.05; **p<0.005 determined by TTest.*

Glut-1 transporter total protein and m-RNA expression. Treatment with 1μM imatinib for 24 hours resulted in down-regulation of Glut-1 protein. Its expression was reduced to 77% of controls in K562 cells ($p<0.001$, n=4) (Figure 3.24) and to 82% in LAMA84 cells ($p<0.005$, n=4).

In addition, RT-PCR experiments based on imatinib-treated cells showed no significant changes in Glut-1 mRNA levels.

3.2.7. Changes in intracellular imatinib concentrations and p-glycoprotein expression

Intracellular imatinib concentrations were measured as a function of time. The experiments revealed that on K562 cells the concentration significantly increased between 4 hours and 24 hours of exposure to 1 μM imatinib (Figure 3.25), although no significant changes in pgp expression were observed at those time points.

In both cell lines, K562 and LAMA84, treatment with 1μM imatinib for 24 hours resulted in a slight, but not significant decrease of pgp expression.

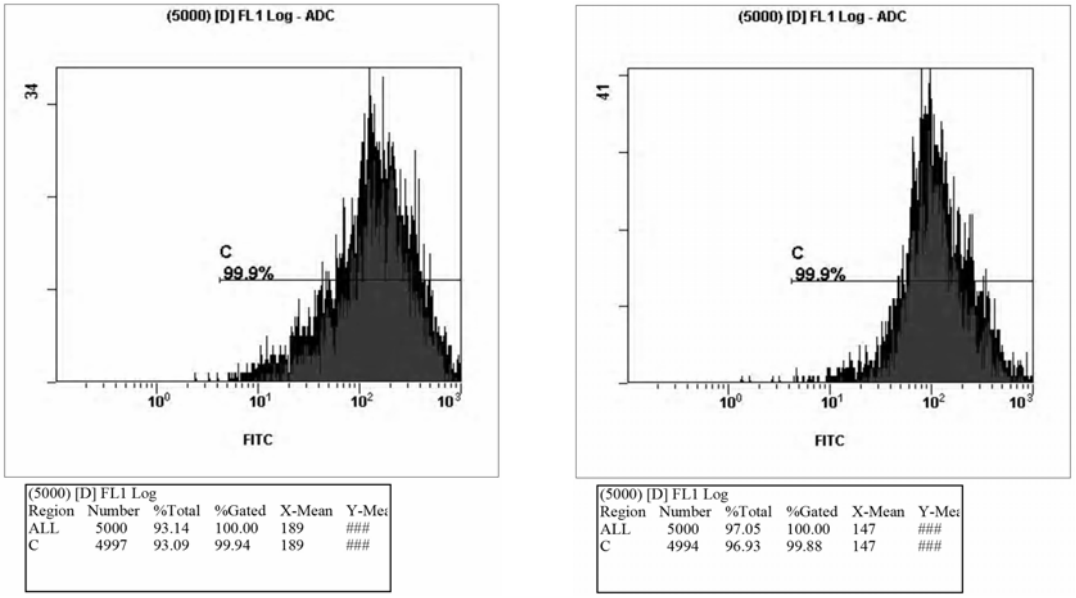

(5000) [D] FL1 Log

Region	Number	%Total	%Gated	X-Mean	Y-Mea
ALL	5000	93.14	100.00	189	###
C	4997	93.09	99.94	189	###

(5000) [D] FL1 Log

Region	Number	%Total	%Gated	X-Mean	Y-Mea
ALL	5000	97.05	100.00	147	###
C	4994	96.93	99.88	147	###

Figure 3.24: Flow cytometry plots of untreated (left) and K562 cells treated with 1μM (24 hours, right). The cells had been fixated and permeabilized before staining with Glut-1. The mean fluorescence intensity (x-Mean ALL) was used to calculate Glut-1 protein expression.

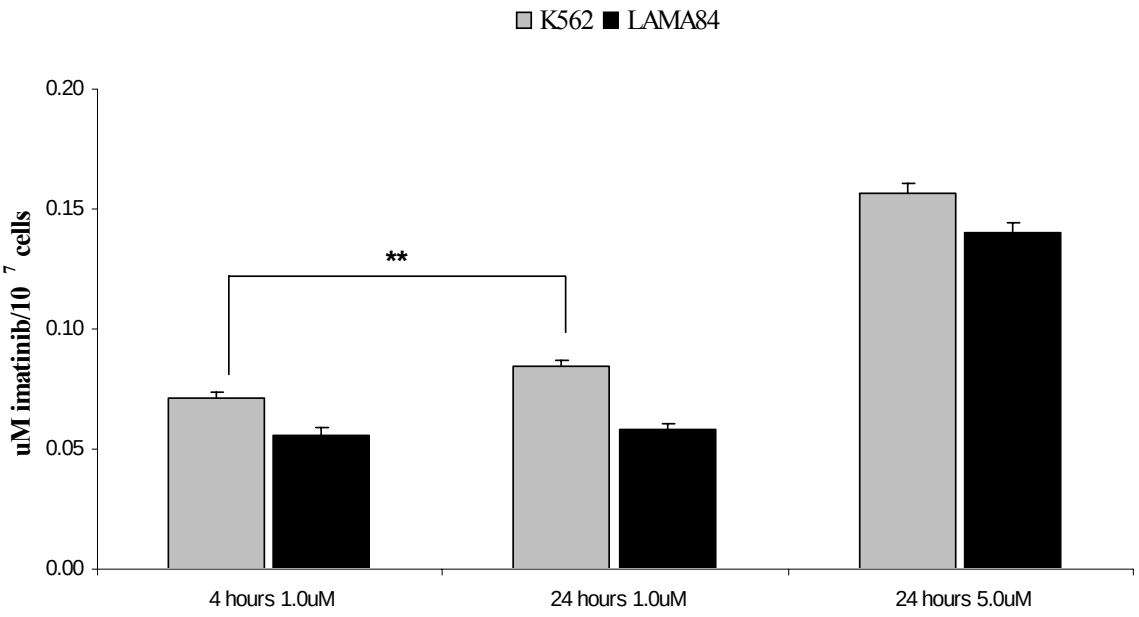

*Figure 3.25: Intracellular imatinib concentrations as calculated from HPLC/MS/MS data of with 1μM imatinib treated K562 and LAMA84 cells. The values were calculated as μM imatinib per 10^7 cells and represent means ± SD of 4 independent experiments; significance between 4 and 24 hours values **p<0.005 determined by TTest.*

3.3. Imatinib-resistant cell lines: Metabolic profiling

Drug therapy can cure many human cancers, but drug resistance, intrinsic or acquired, is a major problem for many patients. Imatinib has the potential to be a curative drug; unfortunately there is well-documented proof of primary or secondary resistance of leukemic cells to imatinib. Development of resistance to imatinib in advanced phase CML is frequent. Over 70% of patients with acute leukemia develop resistance within the first 6 months of treatment (Ottmann et al., 2002).

Although the correlation between the molecular mechanisms and imatinib efficacy in clinical trials is well established, there is no precise information about the changes in cell metabolism during exposure to the drug or in imatinib resistance. However, it has been suggested that the control of glucose-substrate flux is an important mechanism of the antiproliferative action of imatinib since Bcr-Abl positive cells express high-affinity GLUT-1 glucose transporters and have increased glucose uptake. Unlike solid-tumor patients, CML patients cannot undergo clinical PET evaluations on glucose metabolism.

For the evaluation of changes in glucose metabolism, three imatinib-resistant cell lines were used: K562-r (resistant to 1μM imatinib), K562-R (resistant to 5μM) and LAMA84-r (resistant to 1μM imatinib) cells. Their sensitive counterpart K562-s and LAMA84-s cells were used as controls.

3.3.1. Imatinib resistant cell lines: proliferation and viability

The compare growth kinetics, cells were counted using the Trypan-blue exclusion method. When in culture, all three resistant cell lines had proliferation rates and doubling times comparable to their sensitive counterparts (after 48 hours). Their membrane integrity was not changed as well.

YOPRO-1/PI flow cytometry apoptosis assays were performed on resistant cells. No significant changes in apoptosis/necrosis were detected in resistant cell lines compared to their sensitive counterparts. In addition, resistant cell lines themselves were treated with imatinib. In K562-r (1 μM) cells, addition of 5 μM imatinib led to an increase in apoptotic cells (111%, $p<0.07$, $n=4$), when compared to untreated resistant cells. Furthermore, a significant increase in the number of early apoptotic cells was observed when K562-r cells were treated with 1 and 5 μM imatinib for 24 hours. The increase was

at 150% and 153% of K562-r untreated cells ($p<0.005$, n=4). When treated with additional 1 μM or 5 μM imatinib, LAMA84-r showed results similar to K562-r cells in terms of apoptosis/necrosis development. In K562-R cells, addition of 1 or 5 μM imatinib for 24 hours did not cause significant changes (at 5 μM the number of apoptotic cells increased to 121% of untreated K562-R cells, $p<0.06$, n=4).

3.2.2. Glucose and energy metabolism in imatinib-resistant K562 and LAMA84 cells

Glucose metabolism. Resistant cells were compared to their sensitive counterparts.

In LAMA84-r cells, intracellular glucose concentration as calculated from the ^{1}H- and ^{13}C-MRS spectra was lower than in LAMA84-s cells. Their mitochondrial and especially glycolytical activities were highly increased (C4-glutamate and C3-lactate concentrations, Table 3.26), resulting in more glucose being needed for metabolism and therefore transported from extra- to intracellular space.

In contrast, in K562-r (1μM) cells the intracellular glucose concentration was increased (at 215.5% of control, $p<0.005$, n=6). At the same time, the C4-glutamate concentration decreased to 69.8% (not significant, n=6) (Table 3.26) and so did the intracellular concentration of ^{13}C-lactate (Table 3.26). The percentage of ^{13}C-enrichment in lactate dropped from control's 31.3±3.9 to 19.8±4.4 ($p<0.005$, n=6). But the extracellular glucose and ^{13}C-lactate concentrations were highly increased as they were in two other resistant cell lines (see 3.3.6.).

In K562-R (5μM) cells, intracellular glucose concentrations were more than 3-fold higher than in K562-s cells (Table 3.26). But although the cells had been "importing" more and even accumulating glucose molecules, their mitochondrial activity did not significantly change (slightly lower compared to K562-s cells, Table 3.26). Their intracellular lactate concentrations (^{13}C- as well as the unlabeled lactate) were even significantly reduced to 42% of K562-s (Table 3.26). On the other hand, the extracellular lactate concentration as measured in the cell media was significantly increased (see 3.3.6.) suggesting that the cells, in order to keep their intracellular pH stable, exported lactate. Furthermore, the PC/PDH-ratio [glutamate (C2+C3)/C4)] was decreased in K562-R cells, suggesting that a change in enzyme activities (anaplerotic *vs*. oxidative) occurred. Since the concentration of C4-glutamate was not significantly changed, the decrease in the PC/PDH-ratio could

be caused by a decreased PC activity compared to PDH. Both enzymes are located at the entrance into the Krebs-cycle and their down-regulation would result in an increased intracellular glucose concentration (as observed), a decrease of mitochondrial activity and lower cell energy balance / charge (*vide infra*).

	K562-s	K562-r 1μM	K562-R 5μM
$glucose_{intracellular}$ ANOVA: p<0.001	47.3±7.4	111.0±31.2**	180.6±26.3***
C3-lactate ANOVA: p<0.001	1086±200.5	377.5±69.4***	442.4±40.3***
C4-glutamate	329.6±63.4	230.2±82.0	257.4±13.4
PC/PDH ratio ANOVA: p<0.001	0.50±0.03	0.66±0.09	0.41±0.03**

	LAMA84-s	LAMA84-r 1μM
$glucose_{intracellular}$	228.8±48.9	93.1±13.0*
C3-lactate	515.0±143.8	892.9±218.8**
C4-glutamate	253.7±49.8	362.8±7*
PC/PDH ratio	0.59±0.11	0.52±0.09

*Table 3.26: The absolute amounts of ^{13}C (nmol/g cell wet weight) in individual carbon positions of amino acids calculated by integration of signals in ^{13}C-MRS spectra of K562 (top) and LAMA84 (bottom) cell extracts after 4 hours of incubation with 5 mM [1-^{13}C] glucose. The values are given as means ± SD of 6 independent experiments (n=3 for K562-r cells); significance *p<0.05; **p<0.005; ***p<0.001. Data for K562 cells was compared using ANOVA (with post-hoc pairwise multiple comparison Tukey-test).*

Interestingly, in K562-r (1μM) cells the total alanine concentration was highly elevated and almost 10-fold higher than in K562-s cells. In addition, the concentrations of labeled

[3-^{13}C]alanine (319.8±73.6 nmol/g) was greatly increased as well and even higher than the concentration of ^{13}C-lactate. In comparison, the concentration of [3-^{13}C]alanine in K562-s cells was only 43.0±24.4 nmol/g. During anaerobic stress, pyruvate must be metabolized to either lactate (via lactate dehydrogenase, LDH) and/or ethanol (via pyruvate decarboxylase, PDC and alcohol dehydrogenase, ADH) to regenerate NAD^+ required to sustain glycolysis and associated ATP production (Davies, 1980). Accumulation of pyruvate may shift the equilibrium of alanine aminotransferase, ALT (pyruvate + amino acid ↔ alanine + 2-keto acid) towards alanine accumulation, while controlling pyruvate flux trough LDH to lactate (Green et al., 1945). This is what possibly happened in the case of K562-r (1μM) cells: the shift in alanine aminotransferase enzyme activity towards alanine production and/or an inhibition of LDH activity. But, when the concentrations of both glycolysis products, intracellular [3-^{13}C]alanine and [3-^{13}C]lactate were added up, K562-r cells still showed a lower value then the K562-s cells (698 *vs.* 1216 nmol/g).

Energy state. High-energy phosphate concentrations followed the changes in mitochondrial activities. In K562-R (5μM) cells, lower Krebs cycle activities caused a decrease in the NTP concentrations as well as a decrease in the NTP/NDP ratios (5.11±0.45 vs. 7.15±1.19 in K562-s, $p<0.05$, n=6). In K562-r (1μM) cells the NTP/NDP ratio was at 5.07±0.34 ($p<0.05$, n=3) and almost the same as in K562-R cells. On the other hand, in LAMA84-r cells the energy balance changed in the opposite direction due to increased mitochondrial activity. The NTP/NDP ratios increased to 126% of that of LAMA84-s cells (3.98±0.40 *vs*. 3.17±0.86, $p<0.05$, n=6).

In addition to ^{31}P-MRS, HPLC-MS experiments were also performed on resistant cells. Energy charge was calculated as previously described: [(ATP+0.5*ADP)/(ATP+ADP+AMP)]. The data on energy charges changes confirmed the results from ^{31}P-NMR studies on energy balance and showed that the three resistant cell lines revealed various modifications in their high-energy phosphate metabolism when compared to controls. Treatment of resistant cells with additional 1μM imatinib for 24 hours caused a slight drop in the energy balances. In K562-R (5μM) cells the energy balance was at 77% ($p<0.05$, n=4) of K562-s cells and slightly decreased when cells were treated with additional 1 or 5 μM imatinib for 24 hours.

An HPLC/MS method was also used for the quantification of other nucleotide tri- and diphosphates as well as for quantification of NAD^+. In LAMA84-r cells (Figure 3.27) not only ATP, but also the concentrations of other investigated nucleotide triphosphates e.g. CTP were increased compared to the sensitive cells. The NAD^+ concentration did not significantly change in any of the three examined resistant cell lines. The changes started to become more evident when K562-r and LAMA84-r cells were treated with 5 μM imatinib for 24 hours and when apoptotic cells started to become detectable (3.3.1.). The NAD^+ concentrations decreased thereby to 63% ($p<0.05$, n=4) and 83% (not significant, n=4) to those of LAMA84-r and K562-r cells, respectively.

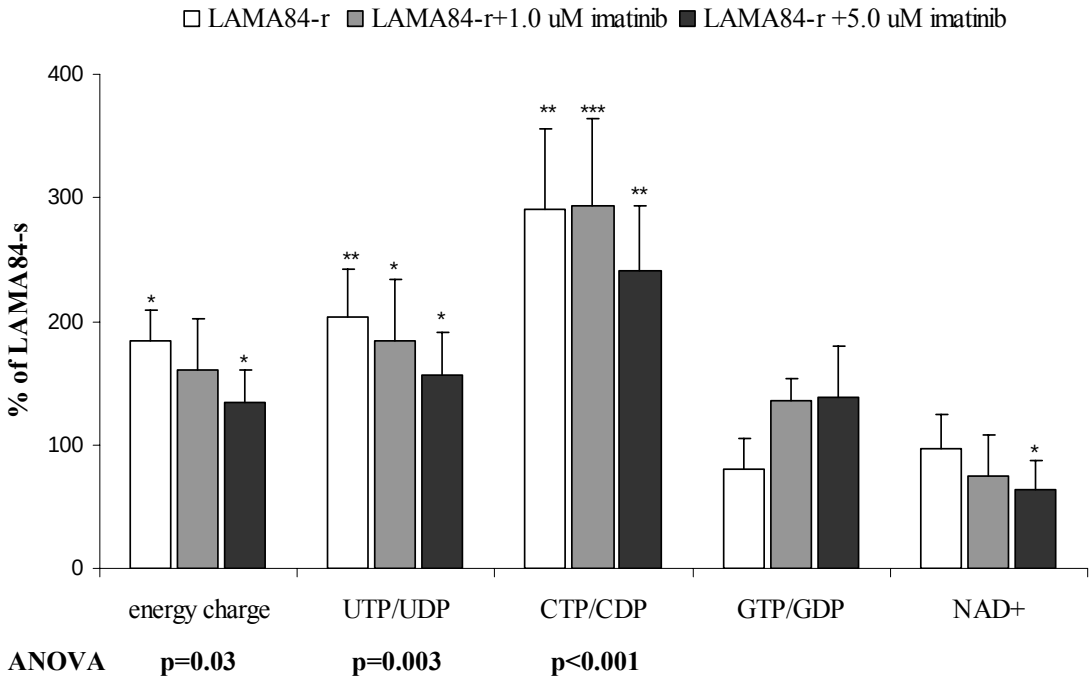

*Figure 3.27: NAD^+ concentration and ratios of high-energy phosphates as calculated from the HPLC/MS data of LAMA84-r cell extracts. LAMA84-r cells (1μM) were treated with 1 and 5 μM imatinib for 24 hours and compared to untreated sensitive cells (% of LAMA84-s). Energy charge was calculated as [(ATP+0.5*ADP)/(AMP+ADP+ATP)]. Values were calculated per number of cells (x 10^7). Relative concentrations are presented as means + SD of 4 independent experiments. Significance levels: *p<0.05; **p<0.005; ***p<0.001 were determined by ANOVA (with post-hoc pairwise multiple comparison Tukey-test).*

3.3.3. Lipid metabolism changes in imatinib-resistant K562 and LAMA84 cells

Changes in phospholipids metabolism. Major differences in phospholipids turnover

between sensitive and resistant cells were observed. In LAMA84-r cells increased phosphocholine and phosphoethanolamine (262% ($p<0.0005$) and 147% ($p<0.05$) of control, n=6) concentrations were observed (Figure 3.22), followed by a higher phosphatidylcholine concentration (137% of controls, $p<0.05$, n=6). K562-R (5μM) cells showed an increase in phosphatidylcholine signal as well (not significant at 117% of K562-s) and furthermore, substantially decreased GPE and GPC concentrations (23% and 54% of the control, $p<0.05$ and $p<0.001$, n=6). In K562-r (1μM) cells, concentration of phosphodiesters, such as GPE and GPC, was significantly lower as well with 116.7±24.7 *vs*. 507.5±165.2 nmol/g ($p<0.005$) and 506.4±105.6 *vs*. 944.7±195.9 nmol/g ($p<0.05$) than in K562-s cells. No significant changes in PC concentrations were observed, but the PE concentration was reduced to 32% of control ($p<0.005$, n=6). When the two resistant cell lines, K562-r and K562-R cells, were compared with each other, they showed almost no differences in PC, PE, GPE or GPC concentrations, suggesting that lower PE / GPE and GPC concentrations may be a common signature of K562 imatinib resistant cell lines.

Changes in neutral lipids and fatty acids. K562-r (1μM) cells had higher cholesterol signals then their sensitive counterparts (the increase reached 243% of control ($p<0.05$, n=3)). No significant changes in lipids were observed in LAMA84-r cells.

3.3.4. Amino acids concentration changes in imatinib-resistant cell lines

The K562-r (1μM) cell line showed significant differences in osmolytes distributions when compared to K562-s and K562-R cells. In both latter cell lines the taurine signal could not be integrated, while the signal of myo-inositol was present at a concentration of ca. 1500 nmol/g. In contrast, in K562-r cells the two metabolites have changed their positions revealing a very low concentration of myo-inositol (at 250 nmol/g), but a high taurine signal (with ca. 2000 nmol/g).

In K562-R (5μM) cells, concentrations of α-ketoglutarate were significantly decreased (at 63% of K562-s, $p<0.05$, n=6), indicating, as aforementioned, a lower mitochondrial turnover rate. In LAMA84-r cells, a decrease in alanine concentrations was observed (with 50% of LAMA84-s, $p<0.05$, n=6).

3.3.5. Changes in Bcr-Abl protein expression and protein phosphorylation

Resistant K562-r (1μM) clones were examined by flow cytometry and showed no significant overexpression of Bcr proteins (as previously reported by Mahon et al., 2000). In K562-R (5μM) cells, on the other hand, Bcr-Abl expression decreased (as reported by Donato et al., 2003). In LAMA84-r cells, the level of expression was 10-fold higher compared to LAMA84-s ($p<0.0005$, $n=4$). Mahon et al. (2000) reported a 12-fold increase of Bcr-Abl expression.

The same group also reported that the imatinib doses necessary to inhibit overall tyrosine phosphorylation were higher for resistant clones then for the corresponding parent clones.

3.3.6. Glucose uptake studies and Glut-1 transporter expression levels in imatinib-resistant cells

Glucose uptake / Lactate release. Regarding their glucose uptake, resistant cells behaved differently then their long- or short-term treated parental clones. Extracellular glucose concentrations decreased and were followed by an increase in ^{13}C-lactate release. The lactate concentration in the media reached 167% ($p<0.005$, $n=6$) in K562-R (5μM), 148% ($p<0.05$, $n=6$) in K562-r (1μM) and 171% in LAMA84-r cells ($p<0.005$, $n=6$) compared to their sensitive counterparts. Consequently extracellular glucose/lactate ratios were reduced to 65% and 61% ($p<0.006$, $n=6$). Comparable results were obtained when cell media were measured enzymatically.

Deoxyglucose uptake. In MS spectra, K562-r and LAMA84-r cell lines showed a significantly increased deoxyglucose uptake compared to their sensitive counterparts. In the case of sensitive K562 *vs.* K562-r cells the uptake was 1.99 *vs.* 2.47 $[(nmol/l)/min]/10^6$ cells. In LAMA84 cells the uptake rates were lower at 1.26 vs. 1.45 $[(nmol/l)/min]/10^6$ cells, respectively.

Glut-1 transporter total protein and m-RNA expression. While no significant changes were seen in K562-r (1μM) and LAMA84-r cells, the protein expression of Glut-1 was increased in K562-R (5μM) cells (140% of K562-s, $p<0.005$, $n=4$) (Figure 3.28).

Additionally, RT-PCR experiments on resistant cells showed no significant changes in Glut-1 mRNA levels.

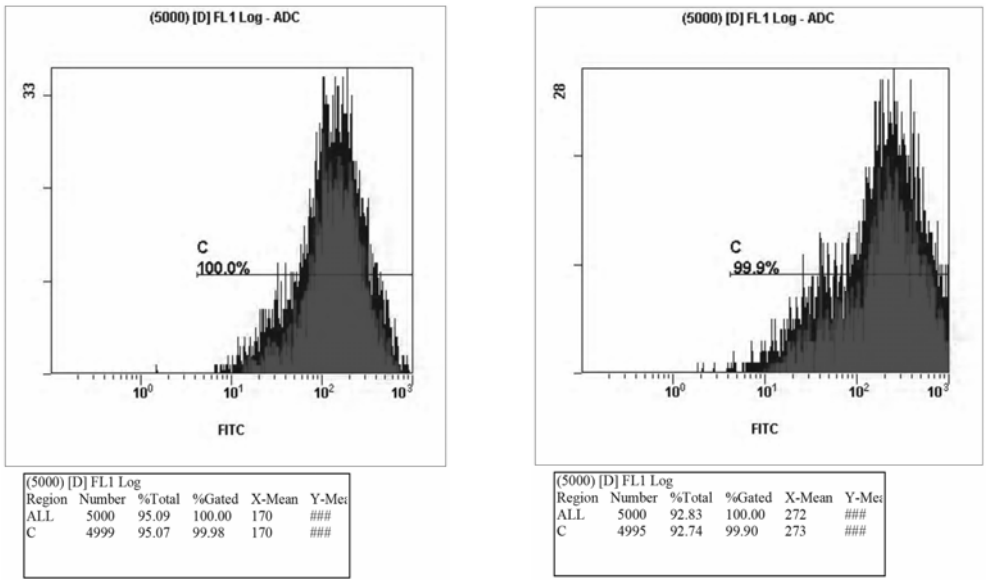

(5000) [D] FL1 Log					
Region	Number	%Total	%Gated	X-Mean	Y-Mea
ALL	5000	95.09	100.00	170	###
C	4999	95.07	99.98	170	###

(5000) [D] FL1 Log					
Region	Number	%Total	%Gated	X-Mean	Y-Mea
ALL	5000	92.83	100.00	272	###
C	4995	92.74	99.90	273	###

Figure 3.28: Flow cytometry plots of untreated K562-s (left) and imatinib-resistant K562-R (5μM cells (right). The cells had been fixated and permeabilized before staining with Glut-1. The mean fluorescence intensity (x-Mean ALL) was used to calculate Glut-1 protein expression.

3.3.7. Changes in intracellular imatinib concentrations and p-glycoprotein expression

While K562-r 5μM cells were shown not to overexpress pgp (Donato et al., 2003), both to 1μM imatinib resistant cell lines, K562-r and LAMA84-r, overexpress this multidrug resistance protein (Mahon et al, 2000). These findings were once again confirmed in our cells using flow cytometry and Western blot analysis of pgp protein expression.

When cells were treated with 1μM imatinib, the intracellular final drug concentration was still significantly higher than in their resistant partners. Imatinib-treated LAMA84 cells had mean intracellular drug concentrations 38% higher than their resistant counterparts ($p<0.005$, n=5). In imatinib-treated K562 cells there was an average 45% more drug than in K562-r ($p<0.005$, n=5). Both resistant cell lines showed a higher amount of pgp expression compared to their parental cell lines as well as when compared to their counterparts that had been treated with 1 μM imatinib (for 2, 4 or 24 hours). The drug-transporter is exporting imatinib out of the cells explaining the lower intracellular drug concentrations in the resistant than in the sensitive cell lines.

In case of K562 cells treated with 5 μM imatinib for 2, 4 or 24 hours, there were no

significant changes regarding their intracellular imatinib concentration when compared to K562-R (5μM) cells.

An interesting finding was that the intracellular imatinib concentration was only two-fold higher in cells treated with 5 μM as in those treated with 1 μM (e.g. in K562 cells 0.157±0.004 μmol/l per 10^7 cells *vs.* 0.085±0.003 μmol/l per 10^7 cells). A similar observation was made in K562-R (5μM) compared to K562-r (1μM) cells, in which the intracellular imatinib concentration was almost the same (Figure 3.29). The final concentration calculated as a sum of intracellular and extracellular (media) concentrations was as expected (1μM or 5μM, Figure 3.29), so that an analytical error could be excluded. Perhaps cells, in order to protect themselves from drug damage, possess or activate a different kind of transporter (not pgp) when being exposed to high imatinib concentrations (e.g. 5 μM). Imatinib has been shown to be a substrate of A1-acid glycoprotein (AGP) at high plasma drug concentrations (Gambacorti-Passerini et al., 2000).

A

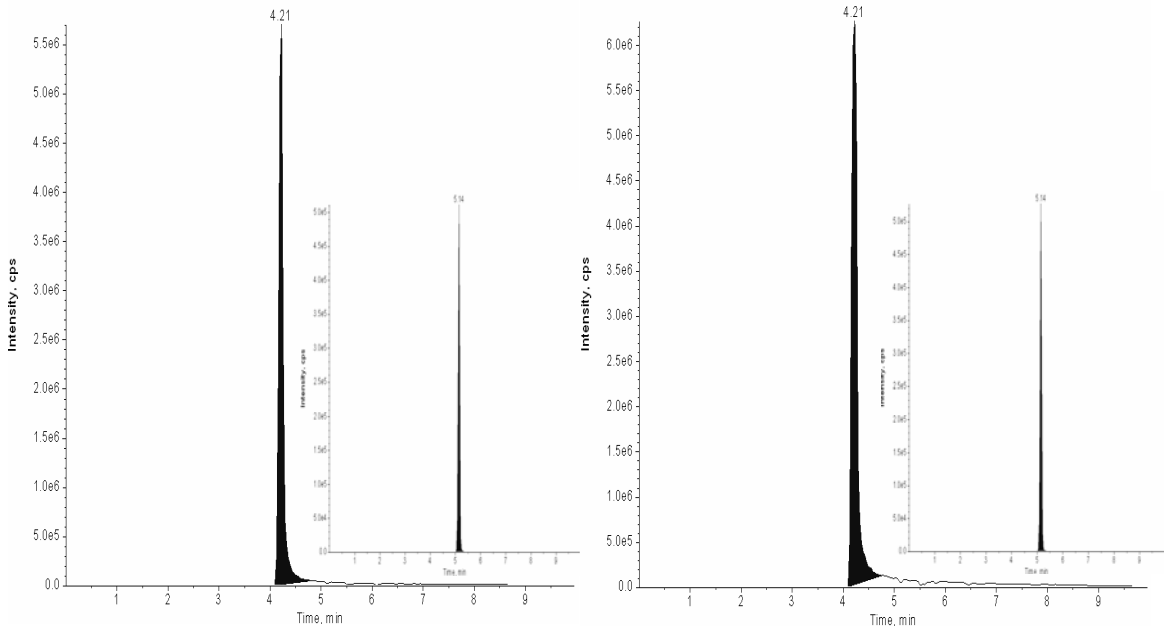

Figure 3.29 A: For figure description see bellow.

B

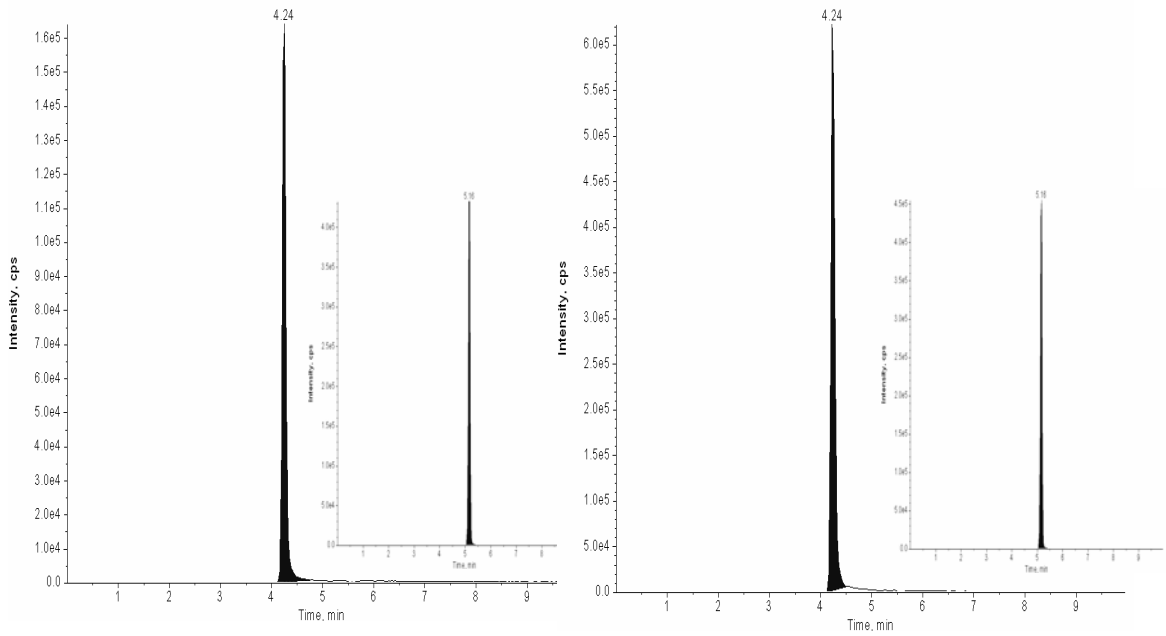

*Figure 3.29: Representative ion chromatograms of extracted human leukemia cells (**A**) and corresponding cell culture media (**B**).Left hand side: ion chromatograms of K562-r (1μM;) and right hand side: ion chromatograms of K562-R (5μM) cells. The areas under the imatinib peaks with the retention time of 4.2 min (m/z=494.5→394.2 amu) were compared to the peak of the internal standard trazodone hydrochloride (Sigma-Aldrich, St Louis, MO, see inserts) at 5.1 min (m/z= 372.6→176.4 amu). Calculated intracellular concentrations were almost the same in both resistant cell lines while the extracellular imatinib concentration was 4.5-fold higher in K562-R vs. K562-r cell media.*

3.4. Imatinib withdrawal from imatinib-resistant cell lines: Metabolic profiling

Previous studies have shown that imatinib removal led to apoptosis in Bcr-Abl-expressing leukemic cells, a phenomenon that could be exploited to sensitize imatinib-resistant cells to the cytotoxic effect of other drugs (Tipping et al., 2001; Desplat et al., 2005). Desplat et al. (2005) showed that imatinib removal induced a decrease in BCR-ABL expression in resistant cell lines and induced increased apoptotic cell death.

Therefore in this study, LAMA84-r cells (used from the study group above in Tipping et al., 2001) as well as K562-R (5μM) cells were withdrawn from imatinib after treatment for 1 week and changes in metabolic profiles were studied by MRS.

3.4.1. Imatinib influence on cell viability

When K562-r (1μM) cells were washed free from imatinib and grown in its absence for shorter (7-15 days) or longer (4-6 months) periods, no changes in their behavior were observed (Tipping et al., 2001) indicating that resistance mechanisms are stable in the absence of imatinib.

The metabolic profiles of LAMA84-r cells were markedly different. When washed thoroughly and replated in media without imatinib, LAMA84-r cells showed a significant reduction in proliferation that peaked at days 5-9 but recovered thereafter (Tipping et al., 2001). The same study showed, that 7 days after imatinib was removed from LAMA84-r cells, Bcr-Abl protein expression was reduced 5-fold and was followed by an increase in Bcr-Abl autophosphorylation and total phosphotyrosine content. Studying the same cell line, Desplat et al., 2005 showed that 3 and 5 days of imatinib removal, 17% and 41% apoptotic cells were found in the LAMA84-r cell line.

In our study, the Trypan-Blue exclusion method was used to follow the changes in cell viability. In LAMA84-r cells imatinib removal from the media resulted in an increase of dead cells, however, to a lesser extent than described by Tipping et al., 2001. Although the "same" cell line was used, the effects of imatinib removal on resistant cell viability were less pronounced and seemed to develop slower. While after 2 days no changes in cell viability were seen, an increase in dead-cells population started to become detectable after 4 days and reached 22±11% (n=4) after 7 days of imatinib withdrawal.

In K562-R (5μM) cells the changes were more obvious. After 5 days, 22% of dead cells were observed whereas their number increased to 35±8% after 7 days of imatinib removal.

3.4.2. Glucose and energy metabolism in imatinib-depleted cell lines

Glucose metabolism. After 7 days of imatinib removal, intracellular glucose content in LAMA84 resistant cells was significantly lower at 40.6% ($p<0.005$, n=4) when compared to LAMA84-s, but did not significantly change in comparison to LAMA84-r cells still grown in 1 μM imatinib. Their glycolytical activity was still significantly increased (C3-lactate concentration, Table 3.29), but their mitochondrial activity was significantly reduced (calculated from ^{13}C-MRS spectra, Table 3.30 and Figure 3.31).

	LAMA84-s *K562-s*	LAMA84-r 1μM *K562-R 5μM*	LAMA84-r and *K562-R* without imatinib for 1 week
glucose$_{intracellular}$ ANOVA: p=0.005; *p<0.005*	**228.8±48.9** ***47.3±7.4***	**93.1±13.0**** ***180.6±26.3******	**86.6±26.7**** ***127.6±31.1***
C3-lactate ANOVA: p=0.02; *p=0.05*	**515.0±143.8** ***1086±200.5***	**892.9±218.8**** ***230.2±82.0***	**748.5±77.1**** ***590.4±306.8****
C4-glutamate ANOVA: p=0.003; *p=0.05*	**253.7±49.8** ***329.6±63.4***	**362.8±87.7*** ***257.4±13.4***	**163.4±34.0*** ***187.1±12.0****
PC/PDH ratio ANOVA: p=0.03; *p=0.003*	**0.59±0.11** ***0.50±0.03***	**0.52±0.09** ***0.41±0.03*****	**0.45±0.08*** ***0.50±0.04***

*Table 3.30: The absolute amounts of ^{13}C (nmol/g cell wet weight) in individual carbon positions of amino acids as calculated by integration of signals in ^{13}C-MRS spectra of LAMA84 and K562 (italic) cell extracts after 4 hours incubation with 5 mM [1-^{13}C] glucose. The values are given as means ± SD of 6 independent experiments for sensitive and resistant LAMA84 and K562 cells and n=4 for LAMA8-r (1μM) and K562-R (5μM) resistant cells without imatinib. Significance was determined by ANOVA (with post-hoc pairwise multiple comparison Tukey-test): *p<0.05; **p<0.005; ***p<0.001.*

In imatinib-depleted K562-R (5μM) cells, intracellular glucose concentration was still significantly higher than in K562-s cells, but started to decrease after withdrawal compared to cells still exposed to imatinib (at 71%, n.s., n=4). Mitochondrial activity of K562-R cells after imatinib withdrawal decreased to 57% of K562-s ($p<0.05$, n=4) and/or to 73% of K562-R cells (n.s., n=4). Their intracellular lactate concentrations (^{13}C- as well as the unlabeled lactate) remained lower then in K562-s, but was increased compared to the resistant K562-R cells still grown in 5μM imatinib (256%, $p<0.05$, n=4). The cells accumulated glucose molecules, and showed reduced mitochondrial activity on one side and increased glycolytical activity on the other. Measurements of extracellular lactate concentrations revealed that there were no significant changes between K562-s and cells after imatinib withdrawal. The export of excessive lactate, highly elevated in K562-R cells, was down-regulated after imatinib withdrawal.

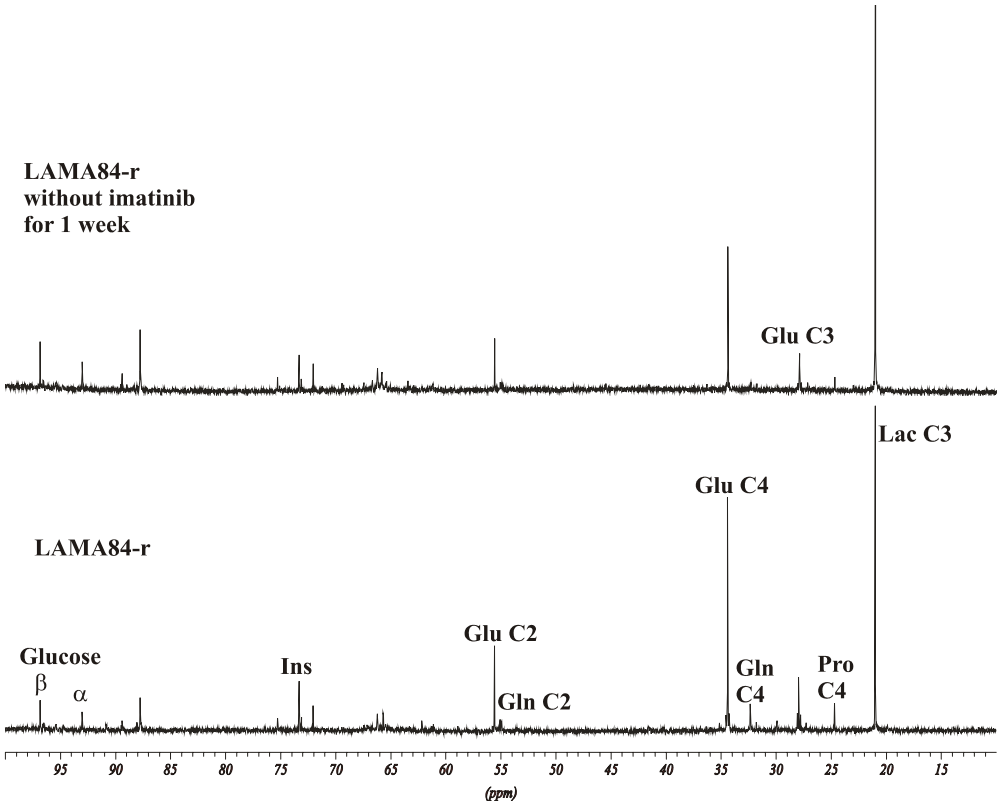

Figure 3.31: Representative ^{13}C-MRS spectra of LAMA84-r cell extracts. Cells were either grown in the presence of 1μM imatinib (LAMA84-r, bottom) or imatinib had been removed from the culture media for 1 week (top). LAMA84-r cells were incubated with 5 mM [1-^{13}C] glucose for 4 hours. Peak assignments: Glu: glutamate, Gln: glutamine, Pro: proline, Lac: lactate.

Energy state. High-energy phosphates did not follow the decrease in TCA-cycle activity, after imatinib had been removed from the LAMA84-r cell culture media. The NTP/NDP ratios remained unchanged compared to either LAMA84-r or LAMA84-s cell lines. It was slightly lower compared to LAMA84-r (3.77±0.24 *vs.* 3.98±0.40). Those cells had been shown to exhibit a better energy balance compared to the corresponding sensitive LAMA84-s cells. Imatinib withdrawal showed an impact on another energy releasing molecule, PCr, the signal of which decreased to 67% of LAMA84-r ($p<0.05$, n=4).

In K562-R (5μM) cells, imatinib removal lowered the Krebs cycle activity and, furthermore, caused a decrease in the NTP concentrations as well as a decrease in the NTP/NDP ratios (4.15±0.63 *vs*. 5.11±0.45 in K562-R ($p<0.05$, n=4) and *vs*. 7.15±1.19 in K562-s, ($p<0.005$, n=4)). And not only did the NTP concentration decrease, but also did the concentrations of PCr decrease to 47% of the K562-s cells ($p<0.005$, n=4). In addition

to a decrease in high-energy substrates, a reduced concentration in NAD(H) was observed. NAD(H) signal intensity was reduced to 49% of K562-s ($p<0.005$, n=4) and/or to 66% of K562-R ($p<0.05$, n=4).

3.4.3. Changes in lipid metabolism after imatinib withdrawal in resistant cell lines

Changes in phospholipid metabolism. Imatinib removal brought the metabolic profiles of LAMA84-r cells closer to those of their sensitive counterparts. Phosphocholine concentrations decreased to 39% of the LAMA84-r cells ($p<0.005$, n=4), but still remained higher than in LAMA84-s cells (137%, $p<0.05$, n=4). Phosphoethanolamine concentrations did not significantly changes in comparism to either the resistant or to the sensitive clone. The same observations were made for phosphatidylcholine, the signal of which revealed a tendency to lower concentrations (77% of LAMA84-r, $p<0.07$, n=4).

In K562-R (5μM) cells, an increase in GPE and GPC concentrations was found when the cells were washed free of imatinib compared to cells growing in the presence of imatinib. The increase (140% and 147% of corresponding controls) was statistically significant ($p<0.05$, n=4 in both cases). However, this did not change the fact that both signals were still significantly lower than in the parental K562-s cell line. Furthermore, a decrease of phosphatidylcholine signals was noticed. It reached 58% of the concentrations found in K562-s and 70% of the concentrations found in K562-R cells (both $p<0.05$, n=4).

Changes in neutral lipids and fatty acids. Two different observations regarding the cholesterol contents were made when imatinib was removed from LAMA84-r and K562-R cells. In the first cell line (LAMA84-r), the removal caused a decrease in cholesterol C18 and C19 signals, while in K562-R cells an even higher concentration of these lipid metabolites was found. The increase reached 152% of the concentrations found in K562-R ($p<0.005$, n=4) (or 272% of the concentrations found in K562-s cells, $p<0.001$, n=4)). Unfortunately, if the assumption is correct that the apoptosis is related to the increase of cholesterol content as seen in our long-term imatinib studies, the changes observed here (decrease of C18 and C19 signals in LAMA84-r cells undergoing apoptosis) did not support the previous observation.

3.4.4. Changes in amino acid concentrations after imatinib depletion

While imatinib withdrawal caused the concentrations of myo-inositol to increase in

LAMA84-r cells, in K562-R cells its concentration moved into an opposite direction. This data may be indicating differences in osmoregulation. LAMA84-r cells may be shrinking and K562-R cells swelling. Based on these and especially glucose metabolism data, it can be hypothesized that those two resistant cells lines were either undergoing two different "death-processes", apoptosis in the case of LAMA84-r (Nicotera and Lesia, 1997) and necrosis or that the apoptosis was already in the stage of "secondary necrosis" in case of K562-R cells (Robertson and Orrenius, 2000).

3.4.5. Intracellular imatinib concentration in LAMA84-r cell line after imatinib withdrawal

After LAMA84-r resistant cells were washed free of imatinib and cultured in imatinib-free media for 1 week, imatinib traces were still detectable in cellular extracts (Figure 3.32). Interestingly, re-exposure to 1μM imatinib for one additional week did not bring the intracellular drug-concentration back to the same levels that had been maintained before imatinib was withdrawn. The concentration was two-fold lower than before imatinib withdrawal (Figure 3.32).

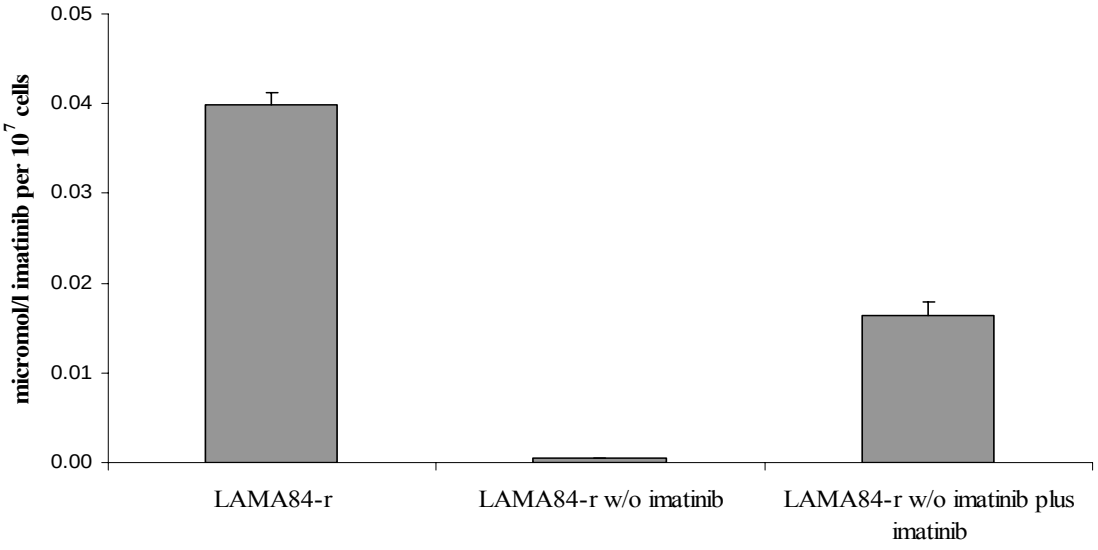

Figure 3.32: Intracellular imatinib concentrations as measured in LAMA84-r cells using HPLC/MS/MS data. LAMA84-r cells were withdrawn from imatinib for 1 week (w/o imatinib), and then re-exposed to 1μM imatinib (w/o imatinib plus imatinib).Concentrations were calculated as μM imatinib per 10^7 cells and means +SD of 4 independent experiments are shown. All concentrations were significantly different from each other ($p<0.001$, ANOVA (with post-hoc pairwise multiple comparison Tukey-test).

3.4.6. Discussion and Conclusions: Short-term imatinib treatment and Imatinib Resistance

In the absence of the appropriate cytokines, such as IL-2, IL-3, IF-α or TGF-β, haemopoietic cells normally die *via* apoptosis. However, the requirement for growth factors appears to be partially abrogated in some malignancies, including CML. Although Bcr-Abl expression is not sufficient for full transformation, expression of this oncoprotein is an important initial step in leukaemogenesis. The discovery of the specific Bcr-Abl tyrosine kinase inhibitors, imatinib (formerly STI571, Gleevec), has started a new era of targeted cancer therapy. Despite its highly specific mechanism of action, resistance development to imatinib treatment occurs in patients with diverse origins of CML (Druker et al., 2001).

Previously, Barnes et al. (2005) and Gottschalk et al. (2004) showed that inhibition of Bcr-Abl activity by imatinib in K562 cells caused significant changes in cellular glucose metabolism. Bcr-Abl positive cells express high affinity Glut-1 glucose transporter and demonstrate high glucose uptake, therefore effects of imatinib on glucose flux and metabolism are important in understanding resulting cell changes, from apoptosis to the occurrence of resistance. It was also proposed that imatinib treatment may restrict *de novo* nucleic acid synthesis by inducing a significant decrease in hexokinase and glucose-6-phosphate-1-dehydrogenase activity and altering carbon fluxes of the pentose cycle (Boren et al., 2001).

In our study, we used MRS to assess changes in cell glucose metabolism (mitochondrial activity, energy production, membrane synthesis, and degradation) in human Bcr-Abl-positive cells after exposure to imatinib as well as in imatinib-resistant cells. The concentration of imatinib chosen for our experiments was demonstrated to reduce cell proliferation and induce apoptosis.

The extracellular glucose concentrations in media were increased and as expected, induction of apoptosis led to a decrease in glucose uptake in both cell lines during treatment with imatinib. The decrease of glucose uptake was even significant only after a short incubation time (one to two hours) and became more evident after longer incubation periods. Time-dependency was almost linear. The expression of Glut-1 transporter

proteins was slightly down-regulated, but more interestingly, translocation of the transporter from the cell surface to the inner cell occurred (Miljus et al., 2005; manuscript in preparation). As revealed by immunofluorescence microscopy and cell surface photoaffinity labeling, the transmembrane Glut-1 distributes from the cell surface into the cytoplasm, resulting in a reduction of glucose uptake. Assessment of the time-dependency of glucose uptake indicated that the translocation and mobility of Glut-1 transporters may be a function of time. Imatinib regulates glucose fluxes through down-regulation and translocation of Glut-1 in leukemia cells, inducing apoptosis and making the treatment effective. The maintenance of glucose uptake is a key component for the suppression of apoptosis (Kan et al., 1994).

Besides inducing apoptosis and lowering the glucose uptake, imatinib strongly suppressed glycolytical activity (C3-lactate production from [1-^{13}C]-glucose through glycolysis) by reversing the Warburg effect. Simultaneously, the decrease in C4-glutamate production from [1-^{13}C]-glucose indicated suppression of the mitochondrial Krebs cycle by imatinib.

Interestingly, the energy state in both imatinib-treated cell lines did not change. An increase in mitochondrial activity and energy balance was observed, when cells were treated with lower concentrations of imatinib (0.1μM for 96 hours or 1 week, see 3.1. Long-term imatinib treatment). These different metabolic responses from decrease of mitochondrial activity at higher imatinib concentrations to an increase of energy charge at lower concentrations suggested a cut off between sub-therapeutic effects and therapy success resulting in cancer cells destruction. As previously mentioned, most studies demonstrated that apoptotic stimulation reduced, to a certain extent, the total cellular ATP level. The fact that the cells can show the same or even better energy status was also reported (Zamaraeva et al., 2005; Leist et al., 1997; Budd et al., 2000). With an increasing number of apoptotic cells, the energy steady-state collapses: the concentration of ATP and PCr drops significantly (as observed after 48 hours with 5μM imatinib).

Clinical studies of patients with imatinib-resistant c-KIT-positive tumors have demonstrated increased glucose uptake using PET scan (Van den Abbeele and Balawi, 2002). Similar observations were made in all three tested resistant cell lines: extracellular glucose concentrations were decreased, revealing an increased glucose uptake rate

compared to the corresponding sensitive cell lines. While in both cell lines that were to resistant 1μM imatinib no changes in cellular contents or mRNA level of Glut-1 were observed, the cell line resistant to the highest amount of imatinib, 5μM, showed even an overexpression of the transporter protein.

When resistant cell lines were compared with each other, they showed slightly different profiles regarding their glucose utilization patterns. While the LAMA84-r cells showed increased glycolytic activity, improved mitochondrial status and elevated levels of high- energy phosphates, glycolytic and Krebs cycle activities of K562-resistant cell lines did not change. All three cell lines had an increased glucose uptake rate compared to the corresponding sensitive cell lines. The glucose utilization rate in LAMA84-r cells was extremely fast. Despite their increased glucose uptake, intracellular glucose concentrations were still lower compared to untreated cells.

The major difference between the K562 and LAMA84 resistant cell lines certainly lies in their different origins: both K562-resistant cell lines were derived from the same sensitive cell line, the K562-s cells. They are resistant to different imatinib concentrations (1 and 5 μM) and show some variance on the molecular and protein expression basis, such as the Glut-1, pgp or Bcr-Abl expression. Nonetheless their metabolic profiles are very similar indicating that both cell lines have gone through the same metabolic changes on their way to become resistant.

Another reason for the metabolic changes observed in resistant cells may be their MDR1 phenotype. Many changes are associated with multidrug resistance (MDR) of tumor cells (Lehnert, 1994; Zgurskaya and Nikaido, 2000). There are several efflux pumps, such as p-glycoprotein (pgp), which can decrease drug accumulation in cells and render therapy ineffective (Clynes et al., 1998). LAMA84-r cells over-express pgp and that seems to be one of the main reasons for this cell line's resistance to imatinib. In contrast, K562-r 5μM cells do not show changes in pgp expression. Until now, a number of wild and drug-resistant cell lines have been studied. The resistant cells overexpressing pgp included cells selected with various drugs e.g. Adriamycin. Those cells showed striking ^{31}P-MRS spectral changes resulting in elevated levels of NTP and increased levels of phospholipids metabolites (Cohen et al., 1986; Kaplan et al., 1990). The resistance was furthermore accompanied by an increase in glycolysis rates (Lyon et al.,

1990). The same changes as above were observed in the pgp overexpressing cell line, LAMA84-r. This suggests that the metabolic changes observed in this imatinib-resistant cell line have a common ground with other MDR1 expressing resistant cell lines. Unfortunately, K562-r (1μM) cells, which also overexpress pgp, showed slightly lower NTP levels as well as a decrease in PC and GPC concentrations. Therefore the reason for this cell line's resistance to imatinib may relay in their pgp overexpression, but the metabolic changes are a result of other changes on a protein expression and activity level.

Another significant difference between sensitive, imatinib treated and resistant cells was their lipid metabolism. The decreased concentrations of phosphomonoester and phosphatidylcholine in imatinib-treated cells, as well as the increased total lipid synthesis rates were likely related to the induction of apoptosis and inhibition of cell proliferation and differentiation processes (J Henke, 1998). Phosphocholine, the major precursor for membrane synthesis, is known to be increased in all rapidly proliferating malignant cells including leukemia cells (Ackerstaff et al., 2001, 2003; Franks et al., 2002). An increase in glycerophoshocholine, a membrane catabolism product, is related to apoptotic processes and membrane dysfunctions (Evelhoch et al., 2000).

Major differences in phospholipids turnover between sensitive and resistant cells were observed. While in LAMA84-r cells, the concentrations of phosphocholine and subsequently phosphatidylcholine were increased, K562-r and K562-R cells showed a decrease in PE, GPE and GPC contents. In conclusion, both K562-resistant cell lines showed almost no differences in either phosphomonoester (PE/PC), or phosphodiester (GPE/GPC) concentrations, suggesting that these metabolic changes may be a common signature of K562 imatinib resistant cell lines.

Remarkably, in tumor cells, the development of drug resistance has been associated with changes in their plasma membrane lipids. Pgp has been reported to localize in low-density, decreased membrane fluidity, cholesterol-enriched membranes (Lavie et al., 1996; Kok et al., 2000; J Ferte, 2000). In case of K562-r an increase of cholesterol concentration was observed compared to the corresponding sensitive cells. And the drug concentrations were significantly lower in to 1μM imatinib resistant, pgp overexpressing cells than in the corresponding sensitive cell lines (when treated with the same imatinib concentration for 24 hours). The finding that the intracellular imatinib

concentrations did not increase linearely with the increasing treatment dose (from 1 to 5 μM) could indicate that cells, in order to protect themselves from drug damage, possess or activate a different kind of transporter when being exposed to high imatinib concentrations (e.g. 5 μM). Imatinib has been shown to be a substrate of A1-acid glycoprotein (AGP) at high drug plasma levels (Gambacorti-Passerini et al., 2000).

Results from studies after imatinib withdrawal showed that resistant cells underwent metabolic changes, mainly based on effects resulting from apoptosis or necrosis / ”secondary necrosis” induction. It furthermore seemed that the cells were regaining some of the properties of their parental clones (e.g. lactate production, phosphodiester concentration). In contrast, the observation was made that the intracellular imatinib concentration was much lower in cells being withdrawn from imatinib and re-exposed to the drug. If the assumption is correct that this observation resulted from an increase in drug-transporter activity, a combination therapy with agents inhibiting p-glycoprotein or A1-acid glycoprotein could be useful to overcome imatinib resistance.

In conclusion, two different metabolic profile types were correlated to imatinib resistance. In the first, increase of cytosolic glycolysis, improvement of mitochondrial metabolism, increased phosphocholine and phosphatidylcholine concentrations together with an overexpression of pgp could serve as a metabolic signature for the development of imatinib resistance (as in LAMA84-r cells). On the other hand, regardless of the pgp involvement, enhanced cytosolic glycolysis as well as a significant decrease in phospholipids synthesis constitute a second set of metabolic markers for the development of imatinib resistance (as seen in case of both K562 resistant cell lines). Elevated glucose uptake and lactate production were common markers for both groups. Furthermore, the fact that imatinib-resistant cells will undergo apoptosis or necrosis / “secondary necrosis” after imatinib withdrawal can be used as a helpful tool to treat the phenomenon of imatinib-resistance. After resistant cells have been sensitized, they can either be exposed to and respond to other drugs or to imatinib itself.

These observation and findings may be important in the evaluation, identification and prediction of patients developing resistance. Based on our results, metabolic profiling of blood from imatinib-treated patients has the potential to be developed into a diagnostic

tool to detect the development of resistant leukaemia cells at an early stage. If this hypothesis is correct, metabolic profiling as a diagnostic tool may significantly improve the treatment of imatinib resistance.

Imatinib resistance			
	LAMA84-r	***K562-r (1μM)***	***K562-R (5μM)***
p-glycoprotein	+	+	−
Bcr-Abl expression	−	↑↑	↓
intracellular lactate	↓	↑	↓
TCA-cycle activity	−	↑	−
energy balance	−	↑	↓
Glut-1 protein	−	−	↑
$glucose_{extra}$ / $lactate_{extra}$	↓ / ↑	↓ / ↑	↓ / ↑
phosphocholine	↓	↑	↓
phosphatidylcholine	−	↑	−
cholesterol	↑	−	−
imatinib $concentration_{intra}$	↓	↓	−
imatinib withdrawal (1 week)	apoptosis induction		necrosis induction or "secondary necrosis"

Figure 3.33: Summary of metabolic effects in imatinib-resistant leukemia cells. The cells were divided into 2 groups: p-glycoprotein overexpressing (K562-r (1μM) and LAMA84-r) and pgp not overexpressing cells (K562-R (5μM) cells. Both K562 resistant cell lines showed similar metabolic profiles.

3.5. Metabolic signatures of a novel EGFR inhibitor gefitinib in human colon cancer cells: Comparison with 5-FU and Celecoxib

Many tumor types, including colon cancer cells, overexpress the epidermal growth factor receptor (EGFR) and its ligands (Van der Geer et al., 1994). The up-regulation of these factors is involved in tumorgenesis and presumably allows cancer cells to sustain their uncontrolled growth (Johnston et al., 1999). Compounds targeting the EGFR family of receptors and their signal transduction pathways, such as the quinazoline-based ZD1839 (Iressa™, Astra Zeneca, Sweden), have been in development over the past years. Since gefitinib has been relatively well tolerated as a single agent, several studies are looking at gefitinib in combination with other chemotherapeutic agents, such as capecitabine (prodrug of 5-Fluorouracil (5-FU)) or anti-inflammatory agents.

Evidence for the involvement of COX proteins in cancer was suggested from pharmacologic analysis of prostaglandins. Various animal and human tumor tissues, including colon cancer, have been reported to contain high concentrations of prostaglandins (Bennet and del Tacca, 1975; Bennet et al., 1977; Jaffe BM, 1974). The increased levels of prostaglandins in tumors provided the rationale for the use of non-steroidal anti-inflammatory drugs (NSAIDs) as potential chemoprevention agents. Celecoxib (Celebrex™, Pfizer, USA) is an effective COX-2 inhibitor and chemopreventive agent (Steinbach et al., 2000). Moreover, there is data that shows that COX-2 inhibitors can inhibit angiogenesis perhaps through down-regulation of VEGF (Jones et al., 1999).

In this study, two human colorectal cancer cell lines, HCT-116 and HT-29, were used to evaluate metabolic effects of gefitinib (15 μM), 5-FU (1.5 μM) and Celecoxib (3.5 μM) after 96 hours of incubation. Both cell lines are widely used for experimental studies. HT-29 cells e.g. retain many biochemical and physiological features of normal colorectal epithelial cells (von Kleist et al., 1975). The major difference between the two cell lines, and highly relevant for our studies, was the discrepancy in the expression of COX-2. While HCT-116 cells are COX-2 deficient, HT-29 cells express COX-2 (Elder et al., 1997; Groesch et al., 2001; Liu et al., 2003). Therefore changes in cell metabolism and especially differences between the COX-2 expressing and the not expressing cell line

were expected to be seen when Celecoxib was co-administrated to 5-FU and gefitinib.

Cells were assigned to seven different treatment groups:

1) 5-FU;

2) Gefitinib;

3) Celecoxib;

4) 5-FU + gefitinib = ***Comb*** (together in combination for 96 hours);

5) 5-FU (96 hours) + gefitinib = ***5-FU + gefitinib*** (given for the last 48 hours);

6) Gefitinib (96 hours) + 5-FU = ***gefitinib + 5-FU*** (given for the last 48 hours) and

7) 5-FU + gefitinib + Celecoxib = ***TRI*** (all three together for 96 hours) (Figure 3.34).

The different sequences of drug administration in 4), 5) and 6) were investigated due to results of Magne et al., who discovered that when gefitinib was administrated prior to 5-FU, synergetic drug effects were observed while its administration during or after treatment with 5-FU caused antagonism (Magne at al., 2001). The drug concentrations were based on dose-finding studies using inhibition of proliferation as outcome marker (MTT-assays were performed in the group of Prof. Dr. G. Eckhardt according to 4.2.1.).

The goal of this study was to distinguish the differences in metabolic pathways during different treatment types in colon cancer cells and to use these *in vitro* results as predictors for future clinical trials.

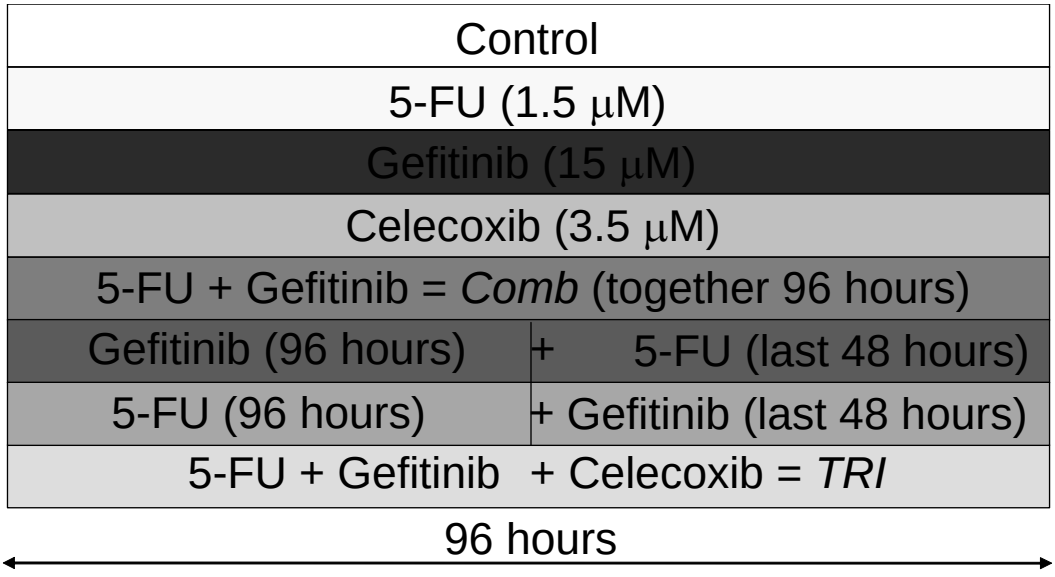

Figure 3.34: Treatment plan for HCT-116 and HT-29 colon cancer cells. Metabolic profiles of seven different treatment groups were assessed and subsequently compared to untreated controls.

3.5.1. Effects of 5-FU, gefitinib and Celecoxib on proliferation and cell viability of colon cancer cells

In order to examine the influence of 5-FU and gefitinib on cell viability, both cell lines were exposed to increasing drug concentrations over the period of 96 hours. Subsequently, corresponding cytotoxicity MTT-assays were performed. All MTT-assays were mainly performed and analyzed by our collaborators (group of Prof. Dr. G. Eckhardt) and the results are presented in the following. While the IC_{50} values for 5-FU were almost the same in both cell lines (ca. 2 μM), HT-29 cells were more affected by addition of gefitinib than HCT-116 cells (Figure 3.35). The IC_{50} values were at 12.5 μM in HT-29 compared to 15 μM in HCT-116 cells (Figure 3.35). IC_{50} values for Celecoxib were adapted from previous studies (which showed 2-5 μM concentration range in different cell lines; group of Prof. Dr. Eckhardt).

For future MRS experiments on both colon cell lines, gefitinib concentrations were set to 15 μM, 5-FU at 1.5 μM and Celecoxib concentrations to 3.5 μM.

Combination treatments with different 5-FU and gefitinib concentrations, different exposure periods, and different treatment regimens (in combination together or a single drug prior to the addition of the second drug) were investigated as well. The nature of the interaction between gefitinib and 5-FU was determined by calculating the combination index (CI) according to the method of Chou and Talalay, 1984. CI values of <1, 1, and >1 indicate synergistic, additive, and antagonistic effects, respectively. In all cases the combination indices were above 1, indicating an antagonistic effect when both drugs were present.

In addition, cell proliferation experiments were performed (cell counting of viable cells using the Cell Counter). While both cell lines showed similar doubling times, their response to the above-mentioned treatment groups was different. In HCT-116 cells the treatment with 5-FU was the controlling and decisive part for cell proliferation. Therefore all cells that were treated with 5-FU for 96 hours showed the highest inhibition of cell proliferation (Figure 3.36). In HT-29 cells, 5-FU itself did not show a high impact on the inhibition of cell proliferation. But its combination with gefitinib resulted in a decrease of proliferation rates (cells treated with drug combinations grew approximately twice as

slow as untreated control cells, Figure 3.36), suggesting that gefitinib was the determining compound in this particular cell line.

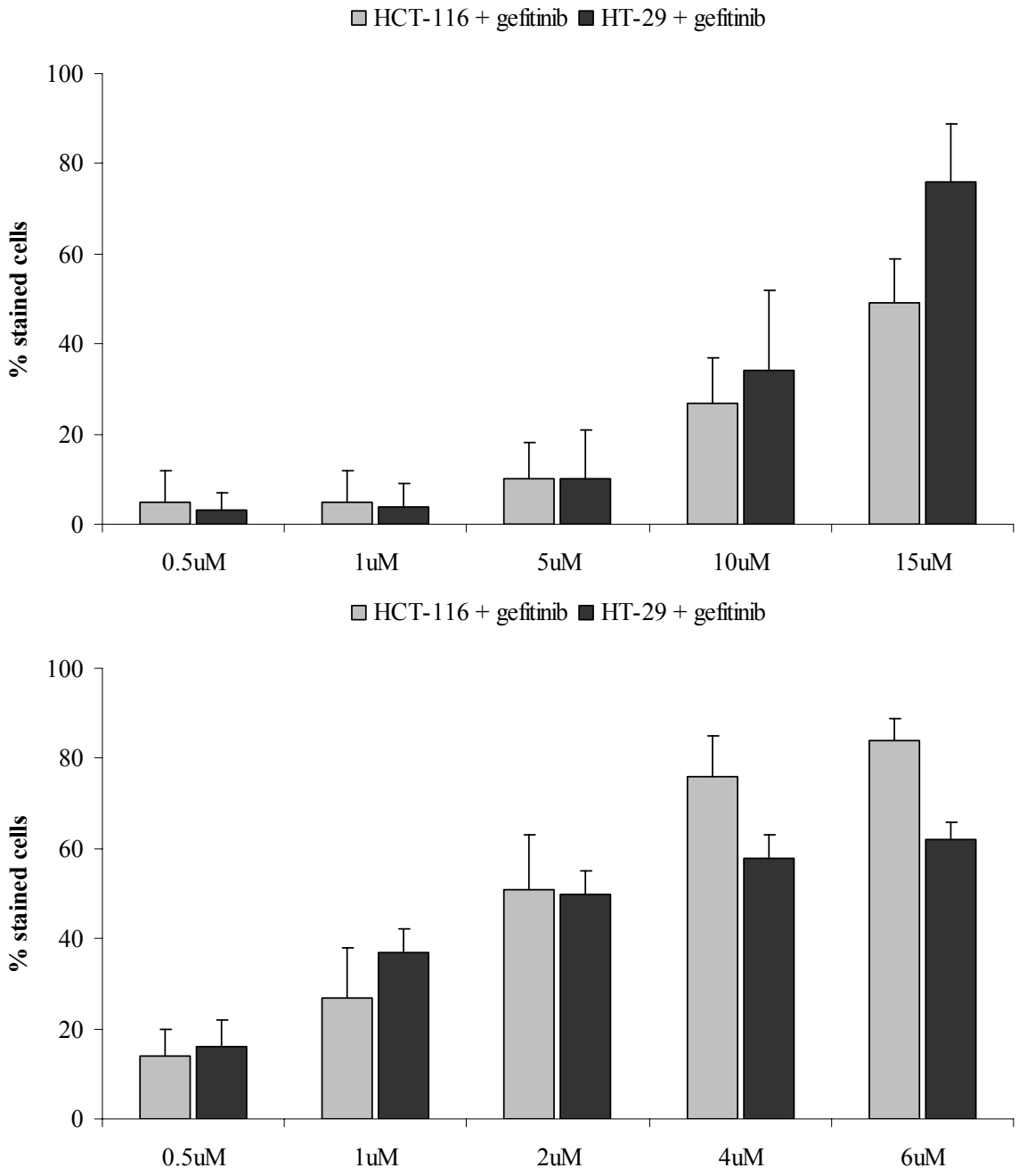

Figure 3.35: Data used for the calculation of IC_{50} values based on MTT-assays in HCT-116 and HT-29 colon cancer cells after incubation with increasing concentrations of gefitinib (top) and 5-FU (bottom) for 96 hours. The data are presented as means + SD of six independent experiments. All treatment groups were significantly different compared to untreated controls ($p<0.001$, ANOVA (with post-hoc pairwise multiple comparison Tukey-test)).

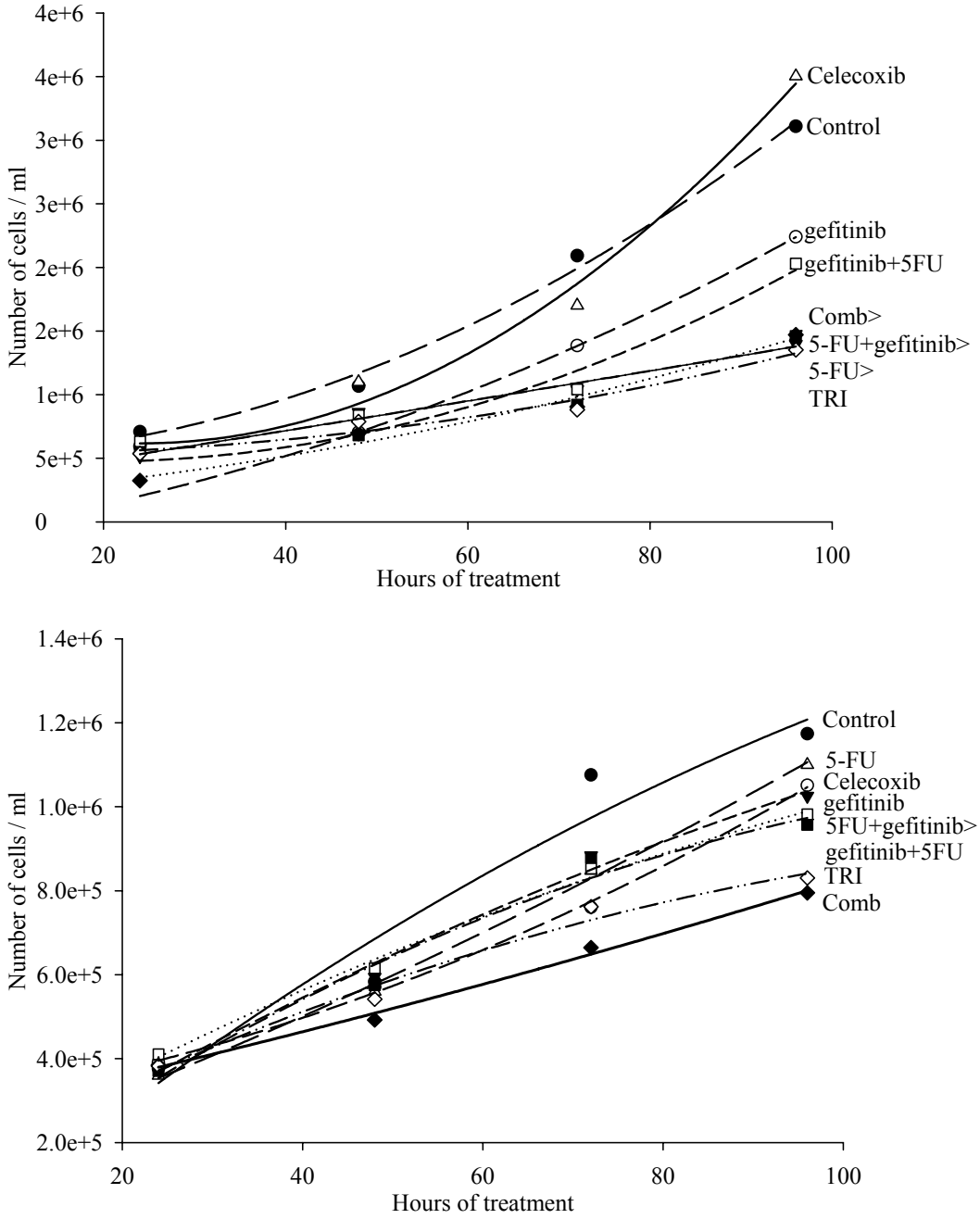

Figure 3.36: Proliferation of HCT-116 (top) and HT-29 (bottom) colon cells. Comparison between untreated control cells and cells treated with 5-FU, gefitinib and Celecoxib and their combinations (mean of n=3 experiments). Standard deviations are not shown to facilitate visual comparison.

3.5.2. Glucose and energy metabolism in HCT-116 and HT-29 colon cells / Changes after 5-FU, gefitinib and Celecoxib treatments

Glucose and energy metabolism in HCT-116 cells. After 96 hours of treatment and 4

hours of incubation with 5 mM [1-^{13}C]glucose, intracellular concentration of labeled glucose was increased in all treatment groups (Table 3.37). The anaerobic glycolysis branch of the glucose metabolism pathway did not significantly change in any of the single treatments, but was significantly decreased in all combination treatments. The cancer drugs alone do not have the potential to inhibit the glycolytic pathways, but act synergistically when combined. The most significant decrease in glycolysis resulting in the lowest concentration of ^{13}C-lactate was seen in the gefitinib + 5-FU (last 48 hours) group (Table 3.37).

Another significant difference between the untreated and treated cells were the concentrations of C3-alanine, which decreased mainly due to 5-FU. 5-FU reduced the alanine signal not only during treatment with this drug alone but also when combined with gefitinib and Celecoxib (349.0±162.9 in control *vs*. 272.2±28.0 in 5-FU and 191.5±81.6 nmol/g in 5-FU + gefitinib (last 48 hours) treated cells; ANOVA: $p<0.03$, $n=7$). The reduction of [3-^{13}C]alanine concentrations corresponded to the observed decrease of [3-^{13}C]-lactate production and therefore indicated inhibition of glycolysis.

The decreased glycolysis rates as well as the inhibition of mitochondrial glucose utilization (*vide infra*) had an impact on the extracellular glucose and lactate concentrations as well. [1-^{13}C]Glucose concentrations were elevated in the combination treatments, especially in the media of the TRI-combination, in which the average concentration reached 2.10±0.63 (mmol/l)/g compared to 0.83±0.26 (mmol/l)/g in untreated control ($p<0.005$, $n=6$). At the same time the concentrations of ^{13}C-lactate in this and only in this particular treatment group was significantly higher at 1.76±0.05 (mmol/l)/g *vs.* 1.45±0.23 (mmol/l)/g in control cells ($p<0.05$, $n=6$). In the case of other drug regimens, for example when 5-FU and gefitinib were combined (together for 96 hours), extracellular ^{13}C-lactate concentrations showed a decrease (to 0.95±0.02 (mmol/l)/g ($p<0.005$, $n=6$)).

The mitochondrial Krebs cycle, on the other hand, was mostly influenced by the addition of gefitinib. Treatment with 5-FU resulted in strong inhibition of cell proliferation (Figure 3.36), but did not cause a significant change in mitochondrial activity of HCT-116 cells. The energy state of the cells as calculated from the NTP/NDP-ratios did not significantly change as well. Gefitinib decreased the concentrations of labeled glutamine

and glutamate. This turned out to be characteristic for the combination treatments that all showed a reduced Krebs cycle activity (Table 3.37). Although the concentration of Krebs cycle metabolites after treatment with gefitinib alone was reduced to 67% (the sum of glutamine, glutamate and aspartate concentrations; $p<0.005$, $n=7$), the decrease did not influence the energy state of the cells. The NTP/NDP ratios were even rather increased than reduced (110% of controls, not significant, $p<0.08$, $n=7$). Exposure to a combination of 5-FU + gefitinib surprisingly showed a significant improvement of the cells' NTP/NDP-ratios. The combination treatment 5-FU + gefitinib (last 48 hours) resulted in an NTP/NDP ratio of 8.81±0.66 ($p<0.05$, $n=6$) compared to 6.69±1.21 in control cells. The NTP/NDP ratio was even higher with 9.77±1.63 in gefitinib + 5-FU (last 48 hours) treated cells ($p<0.05$, $n=6$). Treatment with Celecoxib showed no significant changes in either cell proliferation, glucose metabolization (Table 3.37) or in the energy state. When Celecoxib was combined with gefitinib and 5-FU, no significant changes in neither glycolysis rates nor Krebs cycle activities were seen. Interestingly, the NTP/NDP-ratios improved to 131% of control ($p<0.05$, $n=6$), indicating that the addition of Celecoxib improved not only glycolysis but also mitochondrial activities without affecting the energy state of the cell.

During the same time, in which the NTP/NDP-ratio remained unchanged or even increased, the concentration of phosphocreatine significantly diminished. In the case of treatment with gefitinib alone, PCr signals decreased to 59.9% of the controls ($p<0.05$, $n=7$) and to 54.8% of the controls after 5-FU + gefitinib (last 48 hours) treatment ($p<0.05$, $n=6$). Addition of Celecoxib to 5-FU and gefitinib once again reversed their "negative" combinatory effects and increased PCr concentrations (to approximately 80% of the normal control values).

The percentages of ^{13}C-enrichments in individual carbons, i.e. in the C2-, C3- or C4-glutamate positions after addition of [1-^{13}C] glucose, depended on the relative fluxes through Krebs cycle enzymes. The ratios [glutamate (C2+C3)/C4] changed only in the case of gefitinib treatment (0.53±0.08 *vs.* 0.65±0.03 in control cells, $p<0.05$, $n=7$), indicating a change in the relative distribution of the anaplerotic/oxidative pathways.

	$glucose_{intracellular}$ [nmol/g]	C2-glutamate [nmol/g] C3-glutamate	C4-glutamate [nmol/g]	C3-lactate [nmol/g]
Control	**282.5±44.4**	**277.6±119.1** **238.7±100.7**	**794.8±202.4**	**961.3±178.8**
5-Fluorouracil	**471.5±60.4*****	**247.2±23.2** **221.0±15.1**	**694.3±48.4**	**814.9±272.3**
gefitinib	**379.4±94.4***	**149.4±27.9**** **133.5±18.7***	**529.8±47.9***	**869.7±333.4**
5-FU + gefitinib (together 96h)	**419.6±101.1***	**189.2±23.5*** **158.7±18.6***	**536.2±69.8***	**668.5±221.1****
5-FU + gefitinib (last 48h)	**426.8±33.6*****	**230.1±43.4** **172.4±41.7**	**602.8±112.1**	**787.7±138.5***
gefitinib + 5-FU (last 48h)	**385.5±118.4***	**160.9±49.2*** **133.9±51.5***	**441.5±130.1****	**733.0±135.8***
Celecoxib	**284.0±116.3**	**216.6±34.1** **197.1±42.9**	**663.8±119.8**	**833.1±248.1**
5-FU + gefitinib + Celecoxib	**569.9±112.9****	**201.9±50.1** **195.7±86.3**	**660.9±193.8**	**673.4±305.5***
ANOVA:	**p<0.001**	**p=0.009** **p<0.05**	**p=0.003**	**p=0.004**

*Table 3.37: The absolute amounts of ^{13}C (nmol/g cell wet weight) in individual carbon positions of amino acids as calculated by integration of signals in ^{13}C-MRS spectra of HCT-116 cell extracts after 4 hours incubation with 5 mM [1-^{13}C] glucose. The values are given as means ± SD of 7 independent experiments. Significance was determined by ANOVA (with post-hoc pairwise multiple comparison Tukey-test): *p<0.05; **p<0.005; ***p<0.001.*

Glucose and energy metabolism in HT-29 cells. Compared to HCT-116 cells, in which the intracellular [1-^{13}C]glucose concentration was highly elevated in all treated cells, HT-29 cells showed a similar profile. A significant increase in glucose signals was observed when cells were treated with gefitinib. The only exception was the TRI-combination.

Here glucose signals did not significantly change most likely due to an antagonistic effect of Celecoxib. Celecoxib alone decreased the glucose concentrations to 68% of the controls ($p<0.05$, n=6).

The increase in intracellular glucose concentrations may have been the result of decreased glycolytic and/or more mitochondrial activity. The ^{13}C-enrichment and the concentration of labeled glutamine and glutamate (C2-, C3- and C4-) were decreased after gefitinib treatment, including the combination treatments (Figure 3.38). The total Krebs cycle metabolite concentrations changed from 838.5±144.4 nmol/g in the controls to 567.2±76.6 nmol/g in gefitinib treated ($p<0.005$, n=7) or to 532.8±170.8 nmol/g in gefitinib + 5-FU (last 48 hours) treated cells ($p<0.05$, n=6). No changes were observed after 5-FU or Celecoxib alone

Parallel with the decrease in mitochondrial activity, NTP/NDP-ratios were reduced after almost all treatment types. After treatment with 5-FU or gefitinib alone, NTP/NDP ratios decreased to 61% of the controls in both cases ($p<0.05$, n=7), and decreased even further to 56% of the controls when 5-FU and gefitinib were co-administered for 96 hours ($p<0.005$, n=7). The maximal reduction of NTP/NDP-ratios was achieved by 5-FU + gefitinib (last 48 hours) exposure. Here, NTP/NDP ratios dropped to 44.5% of the controls ($p<0.05$, n=6). Interestingly, as seen in HCT-116 cells, the administration of Celecoxib alone did not influence the energy state and moreover, it even improved the NTP/NDP-ratios when co-administered with 5-FU and gefitinib (although the ratios remained significantly lower then in untreated controls).

The concentrations of PCr, another high-energy phosphate compound, was influenced by the drug regimens as well and showed even more significant changes than the NTP/NTP-ratios (2-3-fold decrease). For example, in case of the TRI-combination group, the decrease was statistically significant (49% of the controls, $p<0.05$, n=6). Celecoxib had the ability to antagonize the decrease of NTP/NDP-ratios (*vide supra*), but had no influence on the concentrations of PCr, a "shorter-life" energy storage compound, which presumably is the first resource during the cells' attempt to regain required energy. The observation that the cells were using PCr as their first line of energy supply prior to the use of ATP was already made in long- and short-term imatinib treated leukemia cells (during apoptosis inducing processes).

While no changes in NAD(H) concentrations were observed in HCT-116 cells, a significant increase occurred in gefitinib treated HT-29 cells. The maximal increase to 221% of control ($p<0.005$, $n=6$) was found after gefitinib + 5-FU (last 48 hours) co-administration.

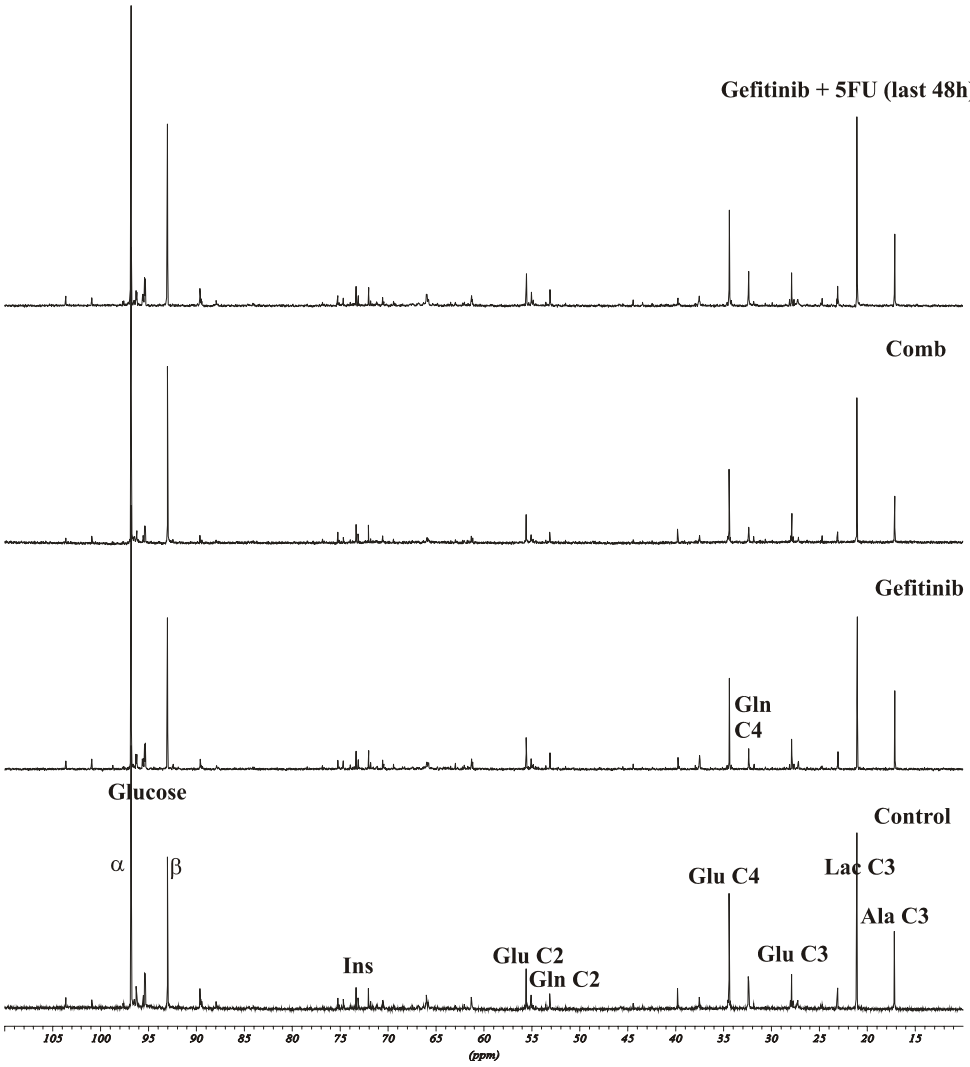

Figure 3.38: Representative ^{13}C-MRS spectra of HT-29 cell extracts. Cells were incubated with either gefitinib alone or in combination with 5-FU. In the last 4 hours of incubation 5 mM [1-^{13}C] glucose was added. Peak assignments: Glu: glutamate, Gln: glutamine, Lac: lactate.

3.5.3. Changes in lipid metabolism after 5-FU, gefitinib and Celecoxib treatments

Changes in phospholipid metabolism in HCT-116 cells. The most pronounced change, which clearly distinguished gefitinib-treated from untreated HCT-116 cells, was the concentration of phosphocholine (PC). The PC signal, as calculated from the ^{31}P-MRS

spectra, significantly decreased to 37.5% of the controls ($p<0.001$, n=7) after administration of gefitinib alone, and it moved into the opposite direction to 163.2% of the controls ($p<0.05$, n=7) when 5-FU was added to the cells. In the case of simultaneous administration for 96 hours, their antagonistic effects were abrogated, resulting in a slightly reduced PC concentration (76.5% of control, $p<0.05$, n=7). Analogous, neither did the addition of gefitinib to 5-FU during the last 48 hours of incubation result in a reduction of the PC signal nor did the combination with Celecoxib. Celecoxib alone, like 5-FU, led to an increase of PC concentrations to 159.8% of the controls ($p<0.005$, n=6).

Parallel to the decrease of phosphomonoester concentrations, concentrations of the phosphodiesters GPE and GPC decreased as well and reached their minimums of 43.6% and 66.8% of the controls ($p<0.05$, n=7, respectively) after treatment with gefitinib alone. On the other hand, GPE concentrations increased in the TRI-combination group to 164.8% ($p<0.05$, n=6) and GPC concentrations to 135% of the controls (statistically not significant), primarily due to the effects of Celecoxib that caused a highly significant ($p<0.001$) increase of GPE and GPC when administered alone.

Changes in phospholipid metabolism in HT-29 cells. Changes in phosphocholine concentrations followed the same trends as observed in HCT-116 cells: the signal decreased after gefitinib treatment, but stayed unchanged after Celecoxib and TRI-combination treatments.

However, in contrast to HCT-116 cells, the reduction of PC was accompanied by raising GPE and GPC signals, which reached their maxima of 147.8% ($p<0.05$, n=6) and 177.5% of the controls ($p<0.005$, n=6) after exposure to gefitinib + 5-FU (last 48 hours). No significant changes were observed after Celecoxib administration and a slight, but significant increase after its co-administration with 5-FU and gefitinib.

Changes in neutral lipids and fatty acids. In the HCT-116 cell line, both single drug treatments, 5-FU and gefitinib, caused an increase in cholesterol C18 and C19 signals. Their effects were synergistic when combined, leading to an increase of C18 and C19 signals to 162% and 154% of the controls ($p<0.005$, n=7) after 5-FU + gefitinib (simultaneous incubation for 96 hours) co-administration. Furthermore, an increase in fatty acids concentrations compared to untreated controls was observed as well, such as $F\alpha$ (to 146%), $F\beta$ (to 138%) and F_{mix} (to 141% of control) ($p<0.05$, n=6, respectively).

Compared to HCT-116 cells, HT-29 cells showed changes in the opposite direction in regards to accumulation of fatty acids. Cholesterol as well as the free fatty acids concentration was decreased, but due to a high standard deviation the differences did not reach statistical significance. PtdCho concentrations showed a decrease as well. The difference reached statistical significance only in cells treated with gefitinib + 5-FU (last 4 hours). Here, the PtdCho signal decreased from 10.23 to 7.38 nmol/g of the controls ($p<0.05$, $n=6$).

3.5.4. Changes in concentration of osmoregulators after 5-FU, gefitinib and Celecoxib treatments in colon cancer cells

Changes in concentration of osmoregulators, such as taurine, myo-inositol, glycine or GPC, can be detected and quantified using MRS. Their increase or decrease results from the adaptive volume regulation upon cell swelling or shrinkage and is responsible for a variety of cellular processes.

In HCT-116 cells, treatment with gefitinib alone as well as in combination with 5-FU resulted an increase of myo-inositol (Ins) and taurine (Tau) concentrations. In all combination treatments, both signals were increased to 150-160% of controls ($p<0.05$), with the exception of 5-FU + gefitinib (last 48 hours) and TRI-combination, which did not show a significant change in taurine concentrations.

3.5.5. Changes in EGFR, p-EGFR and VEGF protein expressions after 5-FU, gefitinib and Celecoxib treatments

As aforementioned, gefitinib inhibits EGF-stimulated EGFR autophosphorylation in a broad range of EGFR-expressing human cancer cell lines (Hirata et al., 2003).

In order to confirm the gefitinib-mediated EGFR/p-EGFR inhibition in our cell models, flow cytrometric expression analysis of both proteins was performed. As expected, addition of gefitinib decreased the level of EGFR and EGFR phosphorylation in both cell lines. Thereby HT-29 cells showed more distinctive changes than HCT-116 cells. p-EGFR expression decreased to 45% of the controls after treatment with gefitinib alone and to 43.2% of the controls after treatment with the TRI-combination ($p<0.0001$, $n=4$, respectively, Figure 3.39). Administration of either 5-FU or Celecoxib alone did not

cause changes in EGFR/p-EGFR expression; neither did they affect the changes of protein expression as caused by administration of gefitinib (Figure 3.39).

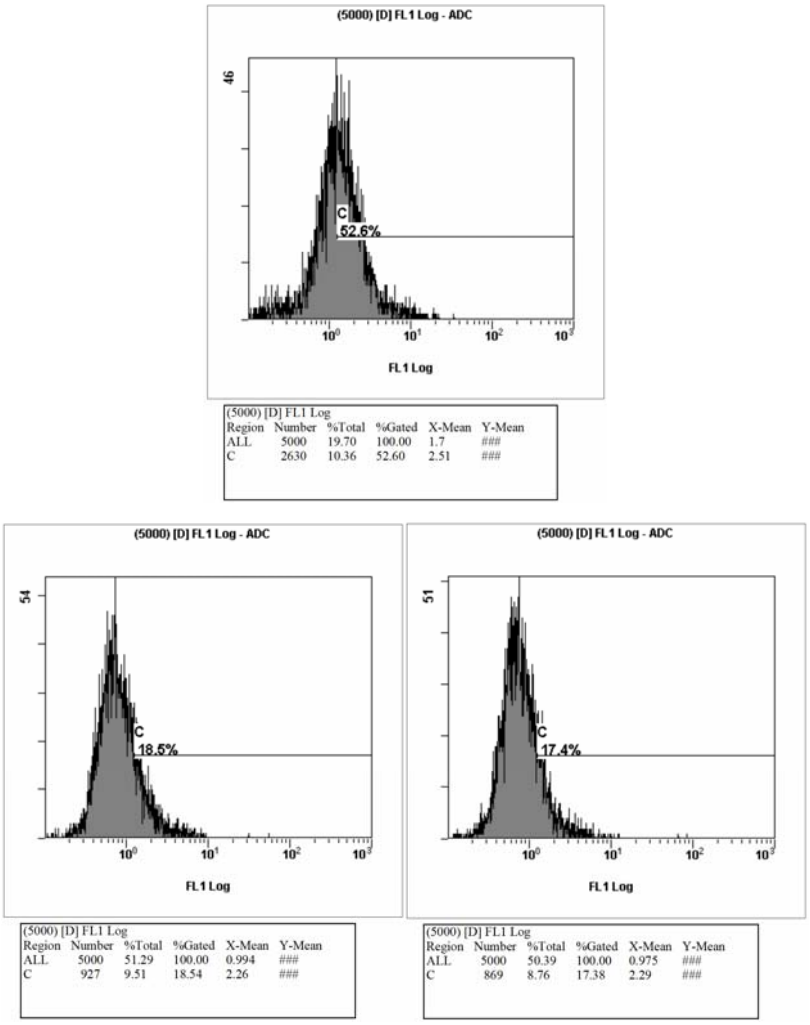

Figure 3.39: Flow cytometry plots of controls (top) and gefitinib (bottom left) and TRI-combination (bottom right) treated HT-29 cells (96 hours). All cells were fixated and permeabilized before staining with phospho-EGFR antibody. The mean fluorescence intensity (x-Mean ALL) was used to calculate p-EGFR protein expression.

Expression of EGF, VEGF, or their respective receptors has been shown to correlate with angiogenesis and progressive growth of human colon carcinoma (Iqbal and Lenz, 2004).
In order to investigate if the VEGF expression had an influence on the metabolic response / metabolic changes after treatment with 5-FU, gefitinib and/or Celecoxib, VEGF-excretion was measured (ELISA-based intra- and extracellular VEGF concentration analysis) and revealed different trends. While gefitinib treatment generated

an increase in VEGF production in HCT-116 cells (intracellular concentration increased to 154% ($p<0.001$, n=6 + n=3) and increased extracellular concentrations to 119% of the controls ($p<0.001$, n=3)), HT-29 cells were not influenced.

Another difference between the cell lines was their behavior in response to the combined treatment regimens. The combination treatment groups showed similar patterns of changes in the HCT-116 cell line as treatment with gefitinib alone. Significant increases of VEGF concentrations were achieved by treatment with gefitinib + 5-FU (last 48 hours) as well as with the TRI-combination (slightly higher VEGF excretion into the surrounding cell media (at 109% of control, $p<0.05$, n=3)). Furthermore, COX-2 deficient HCT-116 and COX-2 expressing HT-29 cell line showed no changes in VEGF after Celecoxib addition. Interestingly, in HT-29 cells the TRI-combination succeeded in reducing the VEGF excretion to 79% of the controls (1567 *vs.* 1982 pg/mg protein, $p<0.05$, n=3). Even more effective was the addition of 5-FU + gefitinib (last 48 hours) without Celecoxib (reduction to 25% of untreated controls, $p<0.005$, n=3), suggesting that the process of VEGF reduction was not related to COX-2 expression and/or its inhibition.

3.6. Metabolic effects of 5-FU and gefitinib in non-small lung cancer cells: An MRS-based study.

Lung cancer is the leading cause of cancer death in the United States and the world. In the United States, it is the leading cause of cancer death in both males and females and kills more individuals than breast, colorectal, and prostate cancers combined (Greenlee et al., 2000). The cure rate remains <15% despite advances in chemotherapeutic agents (Bunn and Kelly, 1998) and recent developments in tyrosine kinases inhibitor research.

In order to investigate the effects of gefitinib on non-small cell lung cancer (NSCLC, for which it was approved by FDA in 2004), two cell lines were chosen: NCI-H1334 (referred to as H1334) and NCI-H322 (referred to as H322). H1334 cell line belongs to the group of large cells, H322 to the broncheo-bronchoalveolar cells. Both cell lines express EGFR.

In this model we used the same 5-FU and gefitinib concentrations as before in colon cancer cells. Three treatment groups were investigated:

1. ***5-FU*** (1.5 μM, 96 hours)
2. ***gefitinib*** (15 μM, 96 hours) and
3. 5-FU + gefitinib = ***Comb*** (1.5 μM + 15 μM, together for 96 hours). The observation time of 96 hours was the same as used before.

The goal of the study was the attempt to distinguish the differences in metabolic pathways between the 2 NSCLC cell lines and to compare these with the colon cancer cells treated the same way. The results answered the important question as to whether the two investigated cancer agents were causing the same metabolic changes in cell lines of different origins and if those were mainly correlated with the inhibition of cell proliferation and apoptosis/necrosis induction or if unrelated metabolic effects were involved.

3.6.1. Glucose and energy metabolism in non-small lung cancer cells / Changes after 5-FU and gefitinib treatment

Glucose and energy metabolism of H1334 cells. Experiments with [1-^{13}C]glucose revealed an increase of intracellular glucose concentrations in gefitinib-treated *vs*. untreated cells (4223 nmol/g *vs.* 2844 nmol/g, $p<0.05$, n=6). Incubation with 5-FU on the other hand rather decreased (by 30%, not significant) the glucose signals and antagonized the effect of gefitinib when both agents were combined. In this case, gefitinib effects were reversed and no significant differences were seen.

Treatment with 5-FU reduced the concentrations of C3-alanine (19.64±9.37 nmol/g in control *vs*. 47.76±26.92 nmol/g in treated cells, $p<0.05$, n=5). This observation was similar to the effect of 5-FU in HCT-116 cells. 5-FU reduced the alanine signal not only when administered alone but also when combined with gefitinib (decrease to 15.26±11.25 nmol/g, $p<0.05$, n=5). The reduction of glycolysis detected in colon cancer cells was not found in H1334 cells after exposure to 5-FU or gefitinib alone. However, the combination of the two agents markedly reduced glycolytic activity. The % ^{13}C-enrichment of lactate decreased from 22.87±3.58 to 18.91±1.0 ($p<0.05$, n=5) and was followed by a decrease of ^{13}C-lactate concentrations from 729.8±158.3 nmol/g to 376.2±103.8 nmol/g ($p<0.001$, n=5).

The mitochondrial Krebs cycle was notably affected and inhibited in all treatment groups.

While there was still some mitochondrial activity left in 5-FU treated cells, addition of gefitinib almost completely blocked the Krebs cycle. There was no ^{13}C-enrichment in glutamine or glutamate. The peaks observed in ^{13}C-MRS spectra of cell extracts equaled their 1.1% ^{13}C-natural abundance (Figure 3.40) indicating that there was no flux of ^{13}C-glucose metabolites through the Krebs cycle.

Surprisingly, almost complete inhibition of the Krebs cycle did not affect the NTP/NDP ratios of gefitinib-treated cells (Figure 3.40). But, a significant decrease was observed when 5-FU was added to the cells (alone and combination treatment). The fact that cells treated gefitinib alone maintained "normal levels" of NTP/NDP could be partially explained by the observation that the glycolytic activity was not diminished in this group as it was in cells treated with a combination of gefitinib and 5-FU. In addition, gefitinib-treated cells again used phosphocreatine as their first-line energy source. Thus, the phosphocreatine signal was not detectable after either of the treatments; it disappeared from 167±16 nmol/g in control H1334 cells to undetectable concentrations.

The high intensity of UDP-amino sugars in ^{31}P-MRS spectra of H1334 cells was noteworthy. UDP-amino sugars were present at remarkably high concentrations in control cells. Their signals were only slightly decreased after treatment with gefitinib alone, but almost completely disappeared after 5-FU + gefitinib treatment ("UDPG" signal; Figure 3.40). Since different UDP-sugars have been shown to have different effects on cell metabolism e.g. cell differentiation or intracellular signaling, a complete analysis of peaks under the "UDPG" signal will be required in order to gain more insights into the remarkable metabolism of H1334 cells.

Glucose and energy metabolism of H322 cells. The fact that cells will limit their glucose uptake and slow the metabolism of this energy source when exposed to proliferation inhibitors, has been seen in almost all cell lines investigated in this study. The same observation was made in this bronchoalveolar cell line, in which the intracellular glucose concentration increased 2-3.5-fold compared to the control values.

The glycolytic activity of this cancer cell line was not affected and remained the same before and after 96 hours of treatment. The cells continued to utilize glucose *via* the glycolytical anaerobic pathway, but their Krebs cycle activity was very low (*vide infra*), which caused the observed raise in intracellular glucose concentrations.

As in H1334 cells, treatment with 5-FU alone decreased the signals of most metabolites detected in the ^{13}C-spectra metabolites (glutamine, glutamate, aspartate etc.), but still showed positive % ^{13}C-enrichment. Treatment with gefitinib, on the other hand, almost completely inhibited Krebs cycle activity (for example, the %^{13}C-enrichment factors of labeled glutamate were almost zero).

As expected, 5-FU treated H322 cells maintained their energy status. However in contrast to H1334 cells, H322 showed decreased NTP/NDP ratios after treatment with gefitinib alone or in combination with 5-FU (60% of the controls, $p<0.05$, $n=4$). Unfortunately, the PCr signal in the ^{31}P-MRS spectra of H322 cells was too low to allow for reliable integration and quantification and therefore no conclusions regarding the effects of the different treatment regimens could be drawn.

3.6.2. Changes in phospholipid metabolism after 5-FU and gefitinib treatments

As discussed above, treatment with 5-FU significantly affected H1334 cells, while H322 cells were inert. However, one similarity between both cell lines was found: 5-FU treatment led to increased phosphocholine and glycerophosphocholine concentrations. In H322 cells PC concentrations increased to 265% of the controls ($p<0.05$, $n=4$) and GPC concentrations to 331% of the controls ($p<0.005$, $n=4$). Almost identical percent changes were seen in H1334 cells where PC concentrations changed from 804 nmol/g to 1776 nmol/g ($p<0.05$, $n=4$) and GPC concentrations from 1160 nmol/g to 3898 nmol/g ($p<0.05$, $n=4$). Addition of gefitinib, on the other hand, resulted in a decrease of PC signals in cells treated either with gefitinib alone or in combination with 5-FU (Figure 3.41). Parallel to the decrease of phosphomonoester concentrations, concentrations of phosphodiesters GPE and GPC decreased in H1334 cells, but were markedly augmented in H322 cells (Figure 3.41).

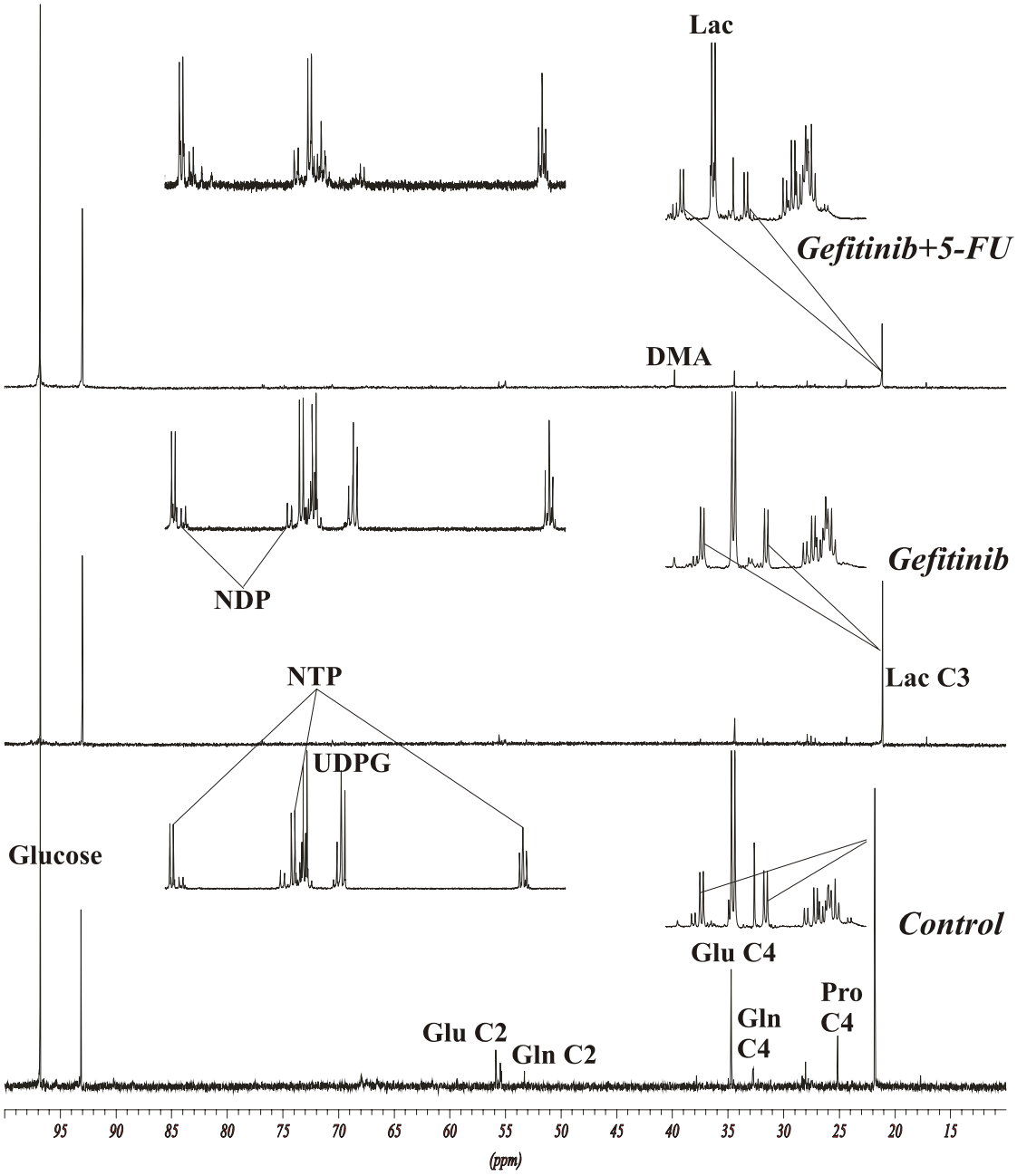

Figure 3.40: Representative ^{13}C-MRS spectra of H1334 cell extracts. Corresponding ^{1}H-MRS spectra (right, showing lactate signals) and ^{31}P-MRS spectra (left, showing NTP and NDP signals) are inserted. Cells were incubated with either gefitinib alone or in combination with 5-FU for 96 hours. In the last 4 hours of incubation, 5 mM [1-^{13}C]glucose was added. Peak assignments: DMA: dimethylamine, Glu: glutamate, Gln: glutamine, Lac: lactate, Pro: proline, NTP: nucleoside triphosphates, NDP: nucleoside diphosphates.

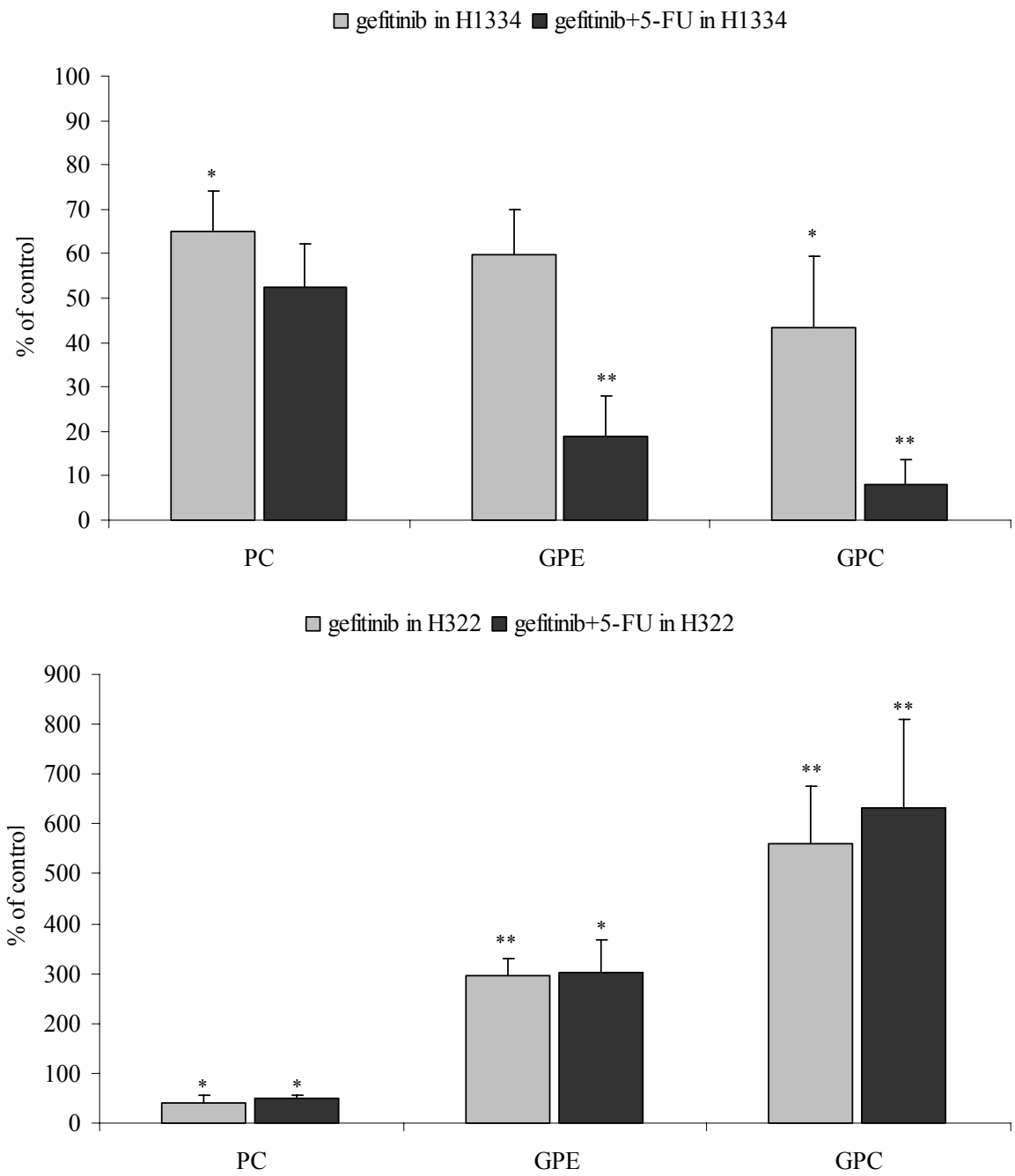

*Figure 3.41: Changes in phosphomonoester (PC) and phosphodiester (GPE and GPC) concentrations as calculated from the ^{31}P-MRS spectra of H1334 (top) and H322 cells (bottom). The values are presented as % of control (set at 100%) and represent means + SD of 4 independent experiments. Significance levels: *p<0.05; **p<0.005 were determined by ANOVA (with post-hoc pairwise multiple comparison Tukey-test).*

3.6.3. Discussion and Conclusions: Metabolic signatures of 5-FU, gefitinib and Celecoxib treatment in colon and non-small lung cancer cells

Growth factors and their receptors play a pivotal role in the regulation of cancer progression and neovascularization (Suhardja and Hoffman, 2003). Epidermal growth factor (EGF) and transforming growth factor α (TGF-α) can bind to EGF receptor (EGFR) and stimulate downstream signaling cascades involved in cell proliferation [Ras/mitogen-activated protein kinase (MAPK)] and antiapoptosis (phosphatidylinositol 3-kinase, PI3K/Akt) (Janmaat and Giaccone, 2003). Overexpression of EGF, TGF-α, and EGFR by many carcinomas has been shown to correlate with the development of cancer metastasis, resistance to chemotherapy and hence poor prognosis (Mendelsohn, 2001; Herbst, 2004). Inhibiting signaling pathways through EGFR represents a good strategy for therapeutic intervention. Gefitinib (Iressa^{TM}, AstraZeneca, Sweden), which was approved by the FDA for treatment of non–small cell lung cancer, inhibits EGF-stimulated EGFR autophosphorylation in a broad range of EGFR-expressing human cancer cell lines (Hirata et al., 2003).

Tumor cell proliferation and survival depend on vasculature to supply adequate oxygen and nutrients (Harris, 2002). Vascular endothelial growth factor/vascular permeability factor (VEGF/VPF) production is substantially increased in most cancers and leads to increased microvascular density (Ferrara and Alitalo, 1999). VEGF acts not only as a mitogenic and permeability factor but also as an antiapoptotic survival factor by activating intracellular signaling, such as MAPK and PI3K/Akt pathways (Gerber et al., 1998; Huang et al., 2004). Therefore, the VEGF and VEGFR signaling pathways have been targeted for treatment of solid tumors.

In vivo and *in vitro* studies showed that prostaglandins, which are being produced by stimulation of cyclooxygenase-2 (COX-2), can up-regulate VEGF expression (Cheng et al., 1998). Recently, levels of COX-2 were found to correlate with both VEGF expression and tumor vascularization in HNSCC cells (Gallo et al., 2002; Lim et al., 2003). This finding in human tissues is consistent with prior evidence that overexpression of COX-2 in epithelial cells led to enhanced production of VEGF and the formation of capillary-like networks (Liu et al., 2003).

We therefore hypothesized that the dual inhibition of EGFR (*gefitinib*) and COX-

2 (*Celecoxib*) / VEGF signaling pathways in colon cancer cells combined with chemo-therapy (*5-FU*) could increase their efficiency in tumor treatment. The hypothesis was tested in HCT-116 and HT-29 colon cancer cells, often used as *in vitro* models for protein research and pathways identification.

In ***HCT-116*** cells, 5-FU and gefitinib led to inhibition of cell proliferation when administered alone or when combined, whereas the addition of Celecoxib did not influence cell growth. Probably due to their lower proliferation rates, treated cells were not requiring and metabolizing as much glucose as the untreated cells, which caused a decrease in their intracellular glucose concentrations. In addition, gefitinib-treated cells decreased glucose metabolite fluxes through their Krebs cycle resulting in the reduced synthesis of labeled amino acids (primarly glutamine and glutamate). A clear trend between the groups was obvious. The dominant biochemical effect of gefitinib was inhibition of the Krebs cycle. The greatest impact had the combination of gefitinib + 5-FU (last 48 hours), while 5-FU or Celecoxib alone did not have any detectable effect. In contrast, glucose metabolism by anaerobic glycolysis was decreased in all combination treatment groups, indicating synergetic interactions between 5-FU and gefitinib in lowering lactate and alanine *de novo* production. The NTP/NDP-ratios remained unchanged and even improved during combination treatments, especially when all three investigated drugs were co-administered. A possible explanation could be that, as seen in the case of imatinib-treated leukemia cells, induction of apoptosis resulted in a higher energy charge of the cells, before taking its toll and switching over to the "secondary necrosis". The concentration of phosphocreatine, which has been shown to reduce prior to changes in NTP/NDP ratios during apoptotic processes, was significantly decreased in all treatment groups, except after a treatment with Celecoxib alone or after administration of the TRI-combination. Another feature of apoptotic cell death is cell shrinkage as indicated by an enlargement in osmolytes concentration. Myo-inositol and taurine concentrations were indeed increased in all treatment groups, except again after Celecoxib and the TRI-combination. Phosphatidylcholine had been identified as a marker of ongoing apoptosis progression (in imatinib treated leukemia cells, see 3.1.3. and 3.2.3. and by Henke, 1996 etc.). The decreased concentrations of PC and PtdCho in gefitinib alone and 5-FU + gefitinib combination treatments (except when combined with

Celecoxib) constituted an additional indicator for a potentially successful treatment option of invading tumor cells.

In the ***HT-29*** cell line, similar proliferation rates of drug-treated cells and an even higher degree of EGFR-phosphorylation inhibition were observed than in HCT-116 cells. The intracellular glucose concentration was increased as well, suggesting a lower metabolic rate. The exception was treatment with Celecoxib alone, which showed lower intracellular glucose concentrations and affected and partially reversed the effects of 5-FU and gefitinib in the TRI-combination. Gefitinib alone and in its combination groups, including the TRI-combination, reduced mitochondrial Krebs cycle activity. In parallel, the energy balance as calculated from the NTP/NDP ratios and, even more pronounced, the PCr concentration dropped (approximately by 2-fold). Treatment with Celecoxib alone did not affect TCA and, moreover, it improved the NTP/NDP-ratios of the cells. This improvement was also visible when Celecoxib was combined with 5-FU and gefitinib, resulting in a higher energy balance in the TRI- than in DUO-combinations. In contrast to the HCT-116 cells, phosphatidylcholine concentrations rather decreased in HT-29 cells treated with gefitinib and 5-FU combinations.

In conclusion, in the HCT-116 cell line, gefitinib itself was successful in inhibiting mitochondrial as well as the glycolytical activity, which is highly elevated in tumor cells (Warburg effect; Warburg, 1956). It successfully induced apoptosis, while keeping the energy state of the cells high enough to provide sufficient amounts of energy necessary for apoptotic cell death progression (Leist et al., 1997; Budd et al., 2000; Zamaraeva et al., 2005). The metabolic effects of gefitinib were even more pronounced when it was combined with 5-FU. The most promising combination sequences were the 5-FU + gefitinib (simultaneous incubation for 96 hours) and gefitinib + 5-FU (last 48 hours), in which gefitinib had enough time to establish its effect and to synergistically interact with 5-FU. Celecoxib did not cause changes in either cell proliferation or glucose metabolism. Its combination with 5-FU and gefitinib on the other hand seemed to reverse the “positive” effects of gefitinib + 5-FU combination regarding the death induction in tumor cells. Although the cell proliferation rates were markedly decreased, as well as anaerobic glycolysis, the TRI-combination failed to inhibit mitochondrial activity or the energy balance of the cell. Moreover, phosphocreatine and phosphatidylcholine

concentrations remained unchanged as well as the cell volume, indicating that the cells were not in an advanced apoptotic stage yet (Zeisel and Blusztajn, 1994; J. Henke, 1997). Therefore, in HCT-116 cells, the TRI-combination treatment (5-FU + gefitinib + Celecoxib) disrupted tumor progression / proliferation, but seemed to be less cytotoxic. The involvement of possible mechanisms including the production of reactive oxygen species will be discussed below. If the hypothesis that Celecoxib prevented the cells from oxidative stress damage without reducing the anti-proliferative action of gefitinib and 5-FU is correct this will be a promising "adjuvant" feature that could help to develop less toxic combination chemotherapies.

In HT-29 cells, gefitinib and the combination treatments (DUO-combinations more then the TRI-) reduced Krebs cycle activity. However, in contrast, the reduction of mitochondrial activity was followed by a decrease in high-energy phosphates (phosphocreatine concentrations and NTP/NDP-ratios; Leist et al., 1997). Phosphatidylcholine concentrations were reduced as well, suggesting that HT-29 cells had already reached the stage of apoptotic "secondary necrosis" or were directly undergoing necrotic changes (Arias-Diaz et al., 1994). Decreased PC and increased GPC concentrations can be considered surrogate markers for cell membrane degradation (Evelhoch et al., 2000) and fit well into the pool of previous observations. Celecoxib did not change mitochondrial activities and slightly improved the energy balance. Its combination with 5-FU and gefitinib resulted in similar trends. Since PtdCho concentrations tended to decrease and myo-inositol concentrations were slightly decreased as well, a likely explanation was that the cells were swelling (Robertson and Orrenius, 2000; Nicotera and Lesia, 1997). It can be speculated that the TRI-combination was inducing the same metabolic changes, but at a slower rate and to a lesser extent than the DUO-combination therapies (due to partially antagonistic effects of Celecoxib on cells). Like in HCT-116 cells, the TRI-Combination treatment seemed to keep the cells in a stage, in which they responded well to the antiproliferative therapy, but without implying negative effects on the cells metabolism (no decrease of TCA cycle activity or NTP/NDP-ratio).

As reported by Sheng et al. (1997), HCT-116 cells lack COX-2 protein. Furthermore, these cell "produced no detectable PGE_2, 6K-$PGF_{1\alpha}$, $PGF_{2\alpha}$, PGD_2, or

TXB_2, indicating a total absence of COX activity" (Sheng et al., 1997). Thus, any responses to Celecoxib in these cells are quite unlikely to be due to the inhibition of COX-2. Similarly, COX-2 activity in HT-29 cells is problematic as well. Although expressed at high levels, COX-2 has been shown to be enzymatically inactive in these cells (His et al., 2000). But the finding may seem to be in conflict with a report by Yamazaki et al. (2002), who reported that 0.001 μM Celecoxib reduced the elevated PGE_2 levels induced by the ionophore A23187 by >50% in HT-29 cells. This same group further demonstrated that 50 μM Celecoxib potently induced apoptosis in these cells and that, at higher concentrations (e.g. 100 μM) some necrosis occurred as well (Yamazaki et al., 2002). In light of our results and the literature, it seems reasonable to conclude that the effects of Celecoxib observed in our studies were likely independent of COX-2.

Recently, levels of COX-2 were found to correlate with both VEGF expression and tumor vascularization in HNSCC cells (Gallo et al., 2002; Lim et al., 2003). In our cells, gefitinib lead to an increase of VEGF expression and excretion in all treatments groups (single and combination administration). Celecoxib, on the other hand, did not influence VEGF expression in either of the cell lines. But interestingly it succeeded in reducing the VEGF expression in HT-29 when treated with the TRI-combination.

In our experiments, Celecoxib was influencing and, more importantly, reversing the apoptosis/necrosis-induced metabolic changes. Interestingly, those effects were more distinct in COX-2 deficient HCT-116 then in HT-29 cells. Our study design did not allow for further evaluation of the nature of the observed partial gefitinib and Celecoxib antagonism. Possible explanations may range from interaction during cell uptake, gene expression, toxicodynamic interactions to direct competition for target proteins. Further studies that specifically address the potential interaction mechanisms will be required to gain further insight. The correlation between PGE_2 levels and VEGF expression would also need to be evaluated. Since gefitinib treatment resulted in increased VEGF expression, it is possible that the prostaglandin levels were increased as well and may have provided the opportunity for Celecoxib to reduce those and to down-regulate VEGF expression (as reported by Yamazaki et al., 2002).

When Celecoxib was administered alone, it failed to significantly change or modify cell metabolism, indicating that the chosen concentration (adapted from

collaborators) was too low to induce metabolic and morphologic changes itself. However, the Celecoxib concentration used in our studies was efficacious when co-administered with 5-FU and gefitinib. In light of our results, systematic studies assessing dose- and time-dependency of potential COX-2 independent metabolic effects of Celecoxib are warranted. This should include testing of the hypothesis that Celecoxib influences the production of reactive oxygen species and that this is a possible mechanism for the slow-down and reversion of the induced cell-death processes (as discussed by Figueiredo-Pereira et al., 2002). As of today, published findings regarding Celecoxib and regulation of oxidative stress have been controversial and ranged from a complete lack of effect (Huang et al., 2005) to Celecoxib's ability to up-regulate ROS (Hou et al., 2005). Most reports correlate Celecoxib's ability to reduce COX-2 activity with its pro-/anti-ROS effects. However, the cell lines used in our studies either had inactive or a lack of COX-2 enzymes. Thus, a potential effect on ROS in our study may have been different from reports in the literature.

In colon cancer cell lines treated with gefitinib alone or its combination with 5-FU and/or Celecoxib, total glutathione concentrations were glutathione in its reduced form (GSH) is the most abundant thiol antioxidant in mammalian cells. It directly reacts with reactive oxygen species (ROS), functions as a cofactor of antioxidant enzymes, maintains thiol redox potential in cells and regulates cell signaling pathway in apoptosis (Hayes and McLellan, 1999; Chandra et al., 2000; Dringen et al., 2000; Engel and Evens, 2006).

In lung cancer cells, treatment with gefitinib and its combination with 5-FU showed effects on cell metabolism that were unexpected based on the drugs' effect on the other cell lines studied. In NCI-H1334 large cells and NCI-H322 bronchoalveolar cells, treatment with the EGFR-TK inhibitor resulted in an almost complete inhibition of Krebs cycle activity. While the reduced energy state of H322 cells was associated with the inhibition of mitochondrial activity, H1334 cells which maintained an NTP/NDP-ratio not different from untreated controls during treatment with gefitinib alone. However, the ratio changed when 5-FU was added. One of the possible explanations for these different patterns includes the observation that cells treated with gefitinib alone maintained a high level of anaerobic glycolysis, while in the cells treated with a combination of gefitinib and 5-FU the glycolysis was inhibited.

Another difference between the cell lines was the effect of gefitinib on the concentration of phosphodiester, markers for membrane degradation processes (Evelhoch et al., 2000). An enhancement in PDE concentrations (GPE and GPC) was found in H322, while their concentrations were reduced in H1334 cells. A possible explanation is that the process of cell death was more advanced in H322 than in H1334 cells, which was also evidenced by their poorer baseline energy state. At the end of this "blinded" study, collaborators provided us with IC_{50} values for gefitinib and as predicted by the MRS results, the H322 cells proved to be more sensitive to gefitinib than H1334 cells.

Consequently, gefitinib and its combination with 5-FU were successful in inhibiting proliferation and inducing cell death of non-small lung cancer cells.

	gefitinib	**5-FU + gefitinib**	**5-FU + gefitinib + Celecoxib**
glycolysis	− (↓) ↓	↓ ↓	↓ ↓
TCA-cycle activity	↓ ↓	↓ ↓	− ↓
energy balance	− ↓	↑ ↓	↑ ↓ **(−)**
phosphocreatine	↓ ↓	↓ ↓	↓ (−) ↓
phosphocholine	↓ ↓	↓ ↓	− (↓) **− (↓)**
phosphatidyl-choline	↓ ↓	↓ ↓	− (↓) ↓
lipids biosynthesis	↑ **− (↓)**	↑ **− (↓)**	↑ **− (↓)**
VEGF expression	↑ −	↑ ↓	↑ ↓

*Figure 3.42: Summary of metabolic effects in colon cancer cells (HCT-116 are presented in normal and HT-29 in **bold** fonts). Investigated lung cancer cells showed very similar patterns in their metabolic response (H1334 closer to HCT-116 cells and H322 closer to HT-29 cells).*

In summary, the rationale for targeting EGFR and COX-2 in a clinical trial is as follows:

- Preclinical *in vitro* models of human colon cancer, have demonstrated the anti-tumor effects when combined targeting EGFR and COX-2.
- Chemotherapeutics (5-FU) combined with EGFR-TK (gefitinib) and COX-2 (Celecoxib) inhibitors showed a promising therapy model for treating colon and non-small cells lung cancer.
- Preclinical models of human colon cancer suggest the potential benefit of combined targeting of COX-2 and EGFR for cancer prevention: inhibition of cell growth and cell death induction (reduced glucose utilization rate, inhibited mitochondrial and glycolytical activity, diminished energy state of the cell and/or cell swelling followed by the cell membrane degradation), which can easily be accessed by MRS-based approaches.

3.7. Perspectives

Our results gave new insights into the potential benefits of MRS-based metabolic profiling for *in vitro* feasibility studies of cancer therapeutics and their combinations. Although this work was primarly based in the field of cancer research, the metabolic profiling as a tool for early prediction of either treatment failure or success is also relevant strategy in other areas of pharmacological and medical research.

Some questions still remain unanswered such as:

- Comparison of profiles between cultured leukemia cells *vs*. freshly isolated healthy human leukocytes (as partly described in Miljus et al., 2005 (abstract)) *vs*. freshly isolated leukocytes from leukemia patients. Not only will it be necessary to study changes in metabolic profiles but also the changes in biochemical pathways *per se* (e.g. enzyme activity, protein expression, and drug-transporter activity). Furthermore, effects of imatinib mesylate on cells directly isolated from patients needs to be evaluated.
- Another important aspect is the translation of our results into the clinic. Is it possible to implement the results on imatinib resistance development into clinical trials? Do the metabolic profiles of imatinib resistant cell lines correspond and reveal the same changes as the blood cells of leukemia patients?

- Will the imatinib withdrawal and re-exposure (under restoration of sensitivity) succeed in the treatment of patients?

Imatinib mesylate inhibits not only Bcr-Abl activity, but also c-kit and PDGFR (platelet derived growth factor receptor) expression. Therefore it will be interesting to investigate

- The effects of imatinib in c-kit and PDGFR expressing tumors. (Preliminary studies were conducted in C6 rat glioma cell line, which expresses great number of genes to those reported for human brain tumors, such as EGFR, PDGF or PDGFR).

Furthermore, the LC-LS/MS-MS method developed as part of our studies can be used in the clinical practice for monitoring of effective imatinib concentrations not only in blood but more importantly in leucocytes themselves.

The same questions regarding the translation of the results from our cell models into clinical practice will need to be studied regarding the effects of gefitinib in lung and colon cancer. Important questions that should be addressed in such clinical trials include:

- Does Celecoxib affect gefitinib's ability to inhibit tumor cell proliferation?
- Is the protective effect of Celecoxib on cell metabolism of clinical relevance?
- Does a potential effect of Celecoxib on ROS play a clinically significant role?
- Are there other chemotherapeutic drugs that can benefit from the combination with Celecoxib as observed in our studies?

The answers to the above questions could result in a new platform for the development of chemotherapeutic drug regimens. As demonstrated in our studies, metabolic profiling is an important strategy for systematic evaluation of the effects of chemotherapeutic drugs on cancer cells from different tumors, to monitor and to predict the development of resistance in cancer cells, and to study the additive, synergistic and antagonistic effects of combinations of chemotherapeutic agents. Based on our results, it is also reasonable to expect that MRS-based metabolic profiling is a valid strategy for guiding clinical trials in terms of efficacy and toxicity of drugs, for guiding dose finding studies, for fine tuning drug combinations, and for therapeutic monitoring of cancer patients to predict individual responses.

Chapter 4

4. MATERIALS AND METHODS

4.1. Cell culture and incubation conditions

Cell cultures are used as *in vitro* models for cell metabolism specific studies under physiological and pathological condition. Rapid improvement in biotechnology techniques led to an enormous number of cell lines being developed, cloned or isolated directly from patients in an attempt to develop easily accessible clinically relevant *in vitro* models for studying human disease under controlled conditions.

4.1.1. Cell lines

In this study three different types of cells were used: leukemia (for imatinib-related studies), colon and non-small lung cancer cell (for gefitinib studies).

K562 cell line were purchased from the American Type Culture Collection (ATCC, Manassas, VA: http://www.atcc.org); ***HC-1*** and ***LAMA84*** from the German Collection of Microorganisms and Cell Cultures (DSMZ, Braunschweig, Germany: http://www.dsmz.de). K562 (Drexler HG, 1994) and LAMA84 are Bcr-Abl positive CML cell lines, in which the Bcr-Abl transcript is abundant and the amplification is robust. HC-1 cells lack the Philadelphia chromosome and belong to the hairy leukemia cell type.

Imatinib resistant ***K562-r (1μM)*** and ***LAMA84-r (1μM)*** cells were a generous gift from Dr. J. Melo (Imperial College London, UK) (described in Mahon et al., 2000), while the ***K562-R (5 μM)*** cells were obtained from Dr. M. Talpaz (MD Anderson Cancer Center, Texas, USA) (described in Donato et al., 2003).

Lung cancer non-small cells ***NCI-H322*** (bronchoalveolar) and ***NCI-H1334*** (large cell) were a generous gift from Dr. P. Bunn (UCHSC Cancer Center, Colorado, USA).

HCT-116 and ***HT-29*** are colon cancer cells purchased from ATCC as well (*vide infra*).

Leukemia cells were grown in suspension and maintained at approx. 1.0×10^6 cells

per mL medium in 240-mL culture flasks. Imatinib resistant cell lines were maintained in 1μM or 5μM imatinib containing media (depending on the cell line) at all times. The culture medium used was RPMI 1640 containing 10% FBS (fetal bovine serum) (20% FBS for HC-1 cells) (Gibco^{TM}, Invitrogen, USA) and 1% penicillin/streptomycin (Invitrogen, USA). The same media was also used for the culture of the adherent colon and lung cancer cells. All cells were incubated at 37°C with 95% air/ 5% CO_2 (v/v) for the time of experiments and subcultured every 48-72 hours or after they have reached confluency.

4.1.2. Assessment of metabolic fluxes with labeled compounds using MRS

For MRS experiments, cells were washed with PBS in order to remove cell debris and remaining media. Hereafter, cells were incubation with 5 mmol/l [1-^{13}C]-labeled glucose (Cambridge Isotope Laboratories, MA) for the last 4 hours of treatment prior to perchloric acid (PCA) extraction.

4.1.3. Drug treatment

Imatinib mesylate was a generous gift of Dr. E. Buchdunger (Novartis, Basel, Switzerland). 5-Fluorouracil was purchased from Sigma (St. Louis, MO, USA). Gefitinib and Celecoxib were generous gifts from Prof. Dr. G. Eckhardt (UCHSC, Denver, USA).

Imatinib treatment. *Long-term imatinib* incubations of K562 and HC-1 cells were carried out for 4 weeks. Then, cell extracts, lipids and media fractions were analyzed by MRS. The idea behind the dosing schedule was the attempt to make the K562 cells resistant to 1.0 μM imatinib (according to the treatment scheme on page 19), while evaluating time-dependant changes in metabolic and cytogenetic parameters. After 5 weeks (concentration increase reached 0.5 μM imatinib) more than 70% of treated K562 cells were dead, while HC-1 cells were not affected in terms of their growth or differentiation. Due to the insufficiency of cell material further MRS analysis was not performed, but the process of resistant cells generation ("small-scale") was continued. *For short-term imatinib* experiments, K562 and LAMA84 cells were treated with 1.0 μM or 5.0μM imatinib for 24-48 hours. For *imatinib-withdrawal* experiments, LAMA84-r and K562-R cells were washed with PBS (phosphate buffered saline) and transferred into

fresh flasks with imatinib-free medium.

For ***removal of dead cells*** the Hystopaque™-1077 (Sigma-Aldrich, USA) gradient density sedimentation method, a one-step centrifugation technique, was used. The sterile separation medium contains 9.6% of the aggregation agent sodium metriozoate and 5.6% Ficoll resulting in a density of 1.077 g/mL and an osmolarity of 280 mOsm/kg. The separation of dead cells was performed weekly according to the product information sheet (www.sigmaaldrich.com/sigma/product%20information%20sheet/h8889pis.pdf). After re-suspension in media, cells were layered on top of the separating medium in the ratio 1:2 (vol/vol). After the viable cells had been harvested at the sample/medium interface and repeatedly washed off with PBS, they were transferred into new flasks with fresh media and the treatment with imatinib was continued.

Treatment with gefitinib, 5-FU and Celecoxib was performed as previously described on page 78 (and Figure 3.34) and pages 90-91.

4.2. Biochemical methods

4.2.1. Cell proliferation and Cell viability

Rapid and accurate assessment of viable cell number and cell proliferation is an important requirement for *in* vitro studies, including determination of cytostatic potential of anti-cancer compounds in toxicology testing.

Cell viability was measured as the number of healthy cells in percent of the total number of cells. For studying how fast the cells were dividing in a culture, aliquots were taken from the cell suspensions and measured (on a daily or weekly basis depending on the experiment). In case of leukemia suspensions, cell aliquots were taken directly from the culture flasks, whereas adherent cells underwent trypsination prior to analysis. Cell numbers were determined using a ***Cell Counter*** (Beckman Coulter Z2), and the results were calculated as the number of cells x 10^6/mL and corrected for the number of dead cells. To assess the number of dead cells, cells were stained with ***Trypan blue*** and counted in a hemacytometer. Viable cells with uncompromised membrane integrity excluded the dye while dead cells showed a blue color (as described on page 22). Metabolic activity and IC_{50} values were assayed by ***MTT***, a standard colorimetric cellular

proliferation assay. The amount of yellow MTT (3-(4,5-dimethylthiazol-2-yl)-2,5-diphenyl-tetrazolium bromide) oxidized to purple formazan is measured spectrophotometrically at 570nm (NADH → NAD^+ conversion). The oxidation takes place only when mitochondrial reductase enzymes are active, and thus conversion is directly related to the number of viable cells (Mosmann T, 1983). For this reason, cells were incubated with 0.02% MTT for 1 hour at 37˚C. Hereafter, the media were removed and the cells were covered with isopropanol / 5% acetic acid over night. The production of purple formazan in treated cells was measured relative to the production in untreated (control) cells, and dose-response curves were generated (MTT-assays were performed in collaboration with Prof. Dr. G. Eckhardt).

4.2.2. Protein determination

The principle of the ***bicinchoninic acid (BCA) assay*** is similar to the Lowry procedure. Both rely on the formation of a Cu^{2+}-protein complex under alkaline conditions, followed by reduction of the Cu^{2+} to Cu^{1+}. The amount of reduction is proportional to the protein present. BCA forms a purple-blue complex with Cu^{1+} in alkaline environments, thus providing a basis to monitor the reduction of alkaline Cu^{2+} by proteins with an absorbance maximum of 562 nm. A standard curve using purified BSA (bovine serum albumin) was used to estimate the protein concentration of an unknown sample. A linear regression was calculated from the absorbance values of 6-8 different concentrations of the protein standard and was used to estimate the protein concentration from the absorbance of the unknown sample.

The protein assay was performed following the manufacturer's instructions (Pierce Biotechnology, USA; http://www.piercenet.com/files/1296dh4.pdf). Briefly, 25µL of each standard or unknown sample were pipetted into a microplate well and 200µL of working solution (50 parts "A" + 1 part "B") were added. The plate was incubated for 30 minutes at 37˚C and the absorbance was measured at 560nm. BSA and solutions A and B were supplied with the kit.

4.2.3. Extraction methods

4.2.3.1. Cell extraction for MRS

All cell extractions for MRS were performed using an established PCA (perchloric acid)

extraction protocol (Serkova et al., 1996). Samples were kept on ice at all times. In brief: For each extract, approximately 10^{10} cells were pooled. The cells were washed with isotonic NaCl, centrifuged (5min at 400g) and immediately frozen in liquid nitrogen. The extraction was performed using 8mL of ice-cold 12% PCA followed by the same amount of water. Extracted samples were sonicated 5 minutes, centrifuged (10 min at 1300g), weighted (to determine wet weight) and the aqueous phase was removed and neutralized using KOH. The samples were centrifuged again and lyophilized overnight. The remaining protein precipitates containing lipids and acid insoluble compounds were resuspended in water, neutralized and lyophilized as well. In addition to the cells, incubation media containing labeled glucose and metabolites were collected, a pH of 7.0 was adjusted, and the samples were lyophilized overnight.

4.2.3.2. Cell extraction for HPLC/MS

For the HPLC/MS determination of intracellular imatinib concentrations, cells were counted and washed thoroughly with ice-cold PBS in order to remove any traces of imatinib. After centrifugation the cell pellets were frozen in liquid nitrogen, followed by re-suspension in 800 µL methanol / 0.2 M zinc sulfate (7:3 v/v) solution. The methanol/$ZnSO_4$ solution was already spiked with 2 ng/mL trazodone (Sigma-Aldrich, USA), which was used as internal standard in all samples. After vortexing and ultrasonic treatment for 10 minutes, the samples were centrifuged (13000g, 10 minutes, 4˚C) and the supernatants were transferred into HPLC vials. Samples were injected into the HPLC system and extracted online (for further details, please see paragraph 4.3.8).

For the measurement of nucleotide concentrations (ATP, ADP, AMP, UTP, CTP, NAD^+), cells were counted and extracted using the same PCA extraction method as described for the MRS experiments (4.2.3.1., for details regarding the HPLC/MS assay see 4.3.8. and 4.3.9.l).

4.2.3.3. Cell extraction for RT-PCR

The RNA extraction required careful handling in order to avoid contamination or degeneration. Therefore all steps were performed on ice using RNA-free materials.

For RNA extraction from the leukemia cell suspensions, the RNeasy™ Mini Kit (Qiagen,

Chatworth, CA) was used and the manufacturer's instructions were followed:

- Cells (ca. 10^7) were centrifuged (at 400g and 4°C for 10 minutes) and were washed with 20 mL ice-cold PBS for media removal.
- *Cell lysis and homogenization*: For the cell membrane disruption 600 µL buffer RLT (RNeasy lysis buffer containing β-mercaptoethanol) were added to the cell pellet. Pellet and buffer were mixed by repeated drawing the solution into and expelling from a pipette. Subsequently the lysate was transferred on top of a QIAshredder spin column (Qiagen, USA) that had been placed into a 2 mL collection tube and centrifuged for 2 minutes at 13000g (4°C).
- *Genomic DNA (gDNA) removal*: After homogenization, the cell lysate was transferred to a gDNA eliminator spin column that had been placed into a fresh 2 mL collection tube and centrifuged at 10000g for 30 seconds (4°C).
- *Add ethanol*: the same volume (600 µL) of 70% ethanol was added to the elute and both were mixed again by repeated drawing into and expelling from a pipette.
- *Bind total RNA*: 700-800 µL of sample was transferred on top of an RNeasy spin column that had been placed in a 2 mL collection tube and samples and column were centrifuged for 15 seconds at 10000g (4°C).
- For *DNase digestion during RNA purification* 100 µL of RNase-free DNase set solution (DNase I in RDD buffer) were added directly to the column and incubated for 15 minutes at room temperature.
- *Wash RNA*: 700 µL buffer RW1 (RNeasy wash buffer) was added to the RNeasy spin column and centrifuged for 15 seconds at 10000g (4°C). In addition, the same procedure was followed with 500 µL buffer RPE (RNeasy phosphate elution buffer). In the last membrane washing and drying step, 500 µL buffer RPE was added to the RNeasy column and centrifuged for 2 minutes at 10000g (4°C).
- *Elute RNA:* For RNA elution, an RNeasy spin column was placed into a fresh 1.5 mL collection tube. 50 µL RNase-free water were added directly to the spin column membrane and centrifuged for 1 minute at 10000g (4°C).

The RNA isolated from the cells using this procedure was aliquoted for spectrophotometric quantitation (5 µL in 95 µL RNase-free water; 4.3.6.1.) and for RNA

integrity control (2 μL; 4.3.6.2.), whereas the remaining RNA was frozen at -80˚C until RT-PCR was carried out.

4.2.3.4. Cell extraction for ELISA / Western blots

Approximately 10^8 cells were lysed in 1.0 mL of ice cold cell lysis buffer (formulation provided at the end). This buffer, a modified RIPA (RadioImmunoPrecipitation) buffer, is suitable for recovery of most proteins, including membrane receptors, cytoskeleton-associated proteins, and soluble proteins. After resuspending the cells by pipetting, the suspension was transferred into an insulin syringe with a 28-gauge needle for mechanical disruption by pushing trough and re-aspirating (ca. 10 times). The cellular debris was subsequently removed by centrifuging the lysates at 13000g for 10 minutes (4°C). The clear cell lysates were transferred into clean tubes and protein concentrations were determined.

Formulation of the cell lysis buffer: 200 mM Tris-HCl (pH 7.5), 1.5M NaCl, 10 mM EDTA, 10% Triton, 25 mM sodium pyrophosphate, 10 mM β-glycerophosphate, 1 complete protease inhibitors cocktail tablet (Roche Applied Biosciences, USA; 1 tablet used per 50 mL buffer).

4.3. Analytical Methods

4.3.1. Flow cytometry analysis of apoptosis/necrosis

All flow cytrometric analyses were performed at the UCHSC Cancer Center Flow Cytometry Core with help of Dr. K. Helm and Mr. M. Ashton.

In order to observe the induction and to follow up the process of apoptosis in K562 and LAMA84 cells after imatinib treatment, DNA-intercalating dye YO-PRO-1 (Molecular Probes, USA) was used as an assay for membrane permeability changes. YO-PRO-1 stain selectively passes through the plasma membranes of apoptotic cells and labels them with moderate green fluorescence. Necrotic cells are stained red-fluorescent with propidium iodide, while live cells show low or no fluorescence.

The assay was performed following the manufacturer's instructions. Cells were centrifuged at 300g for 10 minutes, washed in PBS, and resuspended in RPMI media without Phenol red at a concentration of 10^6 cells/mL (Gibco^{TM}, Invitrogen, USA).

Following staining with 0.1 μM YO-PRO-1 and 1 μg of propidium iodide (PI) per mL, the cells were incubated for 30 minutes on ice and subsequently analyzed by flow cytometry with FL1@530 nm- and FL2@575 nm-compensated emission readings on a FACSCaliur and/or a Beckman Coulter FC500 (both Becton Dickinson, Franklin Lakes, NJ, USA). The apoptotic index (AI) excluded the necrotic cell population and was calculated as (number of viable apoptotic cells/total number of viable cells) × 100.

Prior to flow cytometry analysis, ***fluorescence microscopy*** experiments with imatinib long-term treated cells using ***Annexin V***–fluorescein isothiocyanate / propidium iodide (Annexin-FITC; Sigma, USA) had been carried out. This was for the periodical assessment of apoptosis progression, and not for quantification.

Cell cycle distribution. Cell cycle distribution was also performed at the beginning of the long-term imatinib treatments. In the first 96 hours of K562 cells incubation with 0.1μM imatinib, no differences in the cell cycle distribution were observed (n=3) with ca. 35% cells in G1, 60% in S and 5% cells in G2M cell cycle-phases. Approximately 10^6 cells were washed with PBS, centrifuged at 400g for 10 minutes (4°C) and the PBS supernatant was removed. One mL of saponin/PI stain (0.3% saponin / 50mg/mL PI in RNase (125 Worthington U/mL) containing PBS) was added to the pellet, vortexed and let stand for 6-24 hours before analysis at 4˚C.

4.3.2. Western Blot analysis

Bcr-Abl expression and p-tyrosine kinase activities were assessed by Western blot analysis. Protein lysates (diluted in sample buffer containing 0.006% bromophenol blue and 1.8% β-mercaptoethanol) were boiled for 3–5 minutes. 5-20 μg total protein was applied per lane of 7-14% SDS-PAGE precast gels (BioRad, USA). Molecular weight standards (BioRad, USA) were run in each gel. After successful electrophoresis, the gels were blotted onto polyvinylidene difluoride membrane (Millipore Immobion-P, USA) by semi-dry electrophoretic transfer. The membrane was blocked with 3% dry milk and 0.1% Tween 20 in PBS and incubated with primary antibodies (4G10 anti-phosphotyrosine and β-actin (Santa Cruz Biotechnology, Santa Cruz, CA, USA) as well as anti-Bcr (Cell Signaling Technology, Inc., Beverly, MA, USA)). The membranes were washed and incubated with secondary horseradish peroxidase-conjugated donkey anti-rabbit or anti-

mouse antibody (both HRP-antibodies from Cell Signaling Technology, MA, USA). After development (using Pierce SuperSignal™ detection set, components A+B in 1:1 dilution) and visualization using the UVP EpiChemi system (UVP, USA), the quantities of proteins relative to β-actin were determined by densiometry (LabWorks Software, UVP, USA).

4.3.3. Flow cytometry on protein expression

In order to compare protein expression levels, the cells were prepared for flow cytometry analysis according to the following protocol:

- *Fixation*: ca. 10^7 cells were collected and washed in PBS. After centrifugation the cells were resuspended in 5 mL freshly prepared methanol-free formaldehyde (2% in PBS). The fixation was carried out at 37˚C for 15 minutes. Hereafter, the cells were centrifuged, the supernatant was aspirated and the cells were washed once again in 5 mL ice cold PBS.
- *Permeabilization*: Cells were permeabilized by adding ice-cold 90% methanol while gently vortexing and were kept on ice for 30 minutes. The samples were either stored at -20˚C in 90% methanol at a concentration of $1x10^6$ cell/mL or were directly processed by intracellular protein staining.

- *Intracellular staining with unlabeled primary and conjugated secondary antibodies.* One mL of cell suspension ($1x10^6$ cells) was aliquoted into a fresh tube and rinsed twice by centrifugation with FACS buffer (0.5% BSA in PBS). In the second washing step the cells were soaked in the FACS buffer for 20 minutes and were then resuspended in 100 µL primary antibody and were transferred into 96-well plates. The list of antibodies, their dilutions and incubation time are listed at the end of this paragraph. After removal of the primary antibody, the cells were rinsed off and soaked in FACS buffer for 30 minutes at room temperature. The secondary FITC-conjugated antibody was diluted in FACS buffer according to the manufacturer's recommendations. 100 µL were added to the cell pellet, resuspended and incubated in the dark for 45 minutes (under light shaking). Another washing step and soaking in FACS buffer followed. At the end, the cell pellets were resuspended in 500 µL FACS buffer, transferred into the FACS tubes, capped and stored in the dark at 4˚C until

flow cytometry analysis.

For the quantification of protein expression the mean fluorescence intensity (x-mean ALL) of treated and control cells was used. The protein expression was calculated as % of control.

Since the LAMA84 cell line does not contain a normal ABL gene, the level of Bcr-Abl overexpression in LAMA84 cells was examined by flow cytometry of permeabilized cells with an anti-Abl mAb in 1:50 dilution and after an incubation time of 45 minutes (Cell Signaling Technology, Beverly, MA USA). Other primary antibodies used were: anti-Bcr in 1:50 dilution in combination with an incubation time of 45 minutes (Cell Signaling Technology, Beverly, MA, USA), anti-p-gp in 1:25 dilution in combination with an incubation time of 120 minutes (MRK16, Alexis Biochemicals, San Diego, CA, USA), anti-Glut-1 in 1:50 dilution in combination with an incubation time of 120 minutes (Dako Cytomation, Carpinteria, CA, USA) and anti-phosphotyrosine 4G10 in 1:50 dilution in combination with an incubation time of 30 minutes (Santa Cruz Biotechnology, Santa Cruz, CA, USA). For assessment of EGFR and p-EGFR expression, both antibodies were purchased from Cell Signaling Technology (Beverly, MA, USA) and were used in 1:50 (p-EGFR) and 1:200 (EGFR) dilutions for 30 minutes. Secondary antibodies used were: goat anti-mouse and anti-rabbit FITC-conjugated IgG (Amersham Biosciences, Piscataway, NJ, USA) in 1: 50 dilution.

4.3.4. Enzymatic analysis of glucose and lactate concentrations

D-Glucose and L-lactate concentrations in cell extract and media were determined using the respective Megazyme Assay Kits. The assays were run according to the manufacturer's protocols (hyperlinks: http://secure.megazyme.com/downloads/en/data/K-GLUHKR.pdf and http://secure.megazyme.com/downloads/en/data/K-LATE.pdf). The experiments were performed in 96well plates and absorbances were measured at 340 nm.

Briefly, for glucose studies 170 µL water (for media or 68 µL for cell extracts), 10 µL solution 1 (imidazole buffer), 10 µL solution 2 ($NADP^+$/ATP) and 8 µL sample (for media or 100 µL cell extract solution) were mixed together and the absorbance read after 2-3 minutes. The reaction was started by addition of 2 µL suspension 3 (Hexokinase (HK, 425 U/mL) plus glucose-6-phosphate dehydrogenase (G6P-DH, 212 U/mL)):

$$\text{glucose} + \text{ATP} \xrightarrow{HK} \text{Glucose-6-phosphate} + \text{ADP},$$

$$\text{glucose-6-phosphate} + \text{NADP}^+ \xrightarrow{G6P-DH} \text{gluconate-6-phosphate} + \text{NADPH} + \text{H}^+.$$

The absorbances were read again after 5-20 minutes and the concentration of glucose was calculated as follows:

$$c = (V * M_w) / (\varepsilon * d * v) * \Delta A_{Glucose}$$

where: V: final volume [mL]; Mw: molecular weight of glucose [g/mol]; ε: extinction coefficient of NADPH at 340 nm [6300 l mol^{-1} cm^{-1}]; d: light path [cm] and v: sample volume [mL].

For lactate studies 128 µL water (for media or 36 µL for cell extracts), 50 µL solution 1 (glycylglycine buffer), 10 µL solution 2 (NAD^+), 2 µL suspension 3 (D-glutamate-pyruvate transaminase (D-GPT, 1000 U/mL) and 8 µL sample (for media or 100 µL cell extract solution) were mixed together and the absorbance read after 2-3 minutes. The reaction was started by addition of 2 µL suspension 4 (L-Lactate Dehydrogenase, L-LDH, 2000 U/mL):

$$\text{lactate} + \text{NAD}^+ \xrightarrow{L-LDH} \text{pyruvate} + \text{NADH} + \text{H}^+,$$

$$\text{pyruvate} + \text{glutamate} \xrightarrow{D-GPT} \text{alanine} + \text{2-oxoglutarate}.$$

The absorbances were read again after 10-30 minutes and the concentrations of lactate were calculated based on the equation above for calculation of glucose concentration (where M_w: molecular weight of lactate [g/mol]).

4.3.5. ELISA analysis of VEGF excretion

The DuoSet ELISA development kit (R&D Systems, Minneapolis, MN, USA) was used to measure the intra- and extracellular concentrations of vascular endothelial growth factor in HCT-116 and HT-29 cells. The media from both cell lines after 96 hours of treatment was collected as well as the cells (cell extraction according to 4.2.3.). The assay was run following the manufacturer's protocol.

- *Plate preparation:* The *mouse anti-human capture antibody* was diluted to 1 µg/mL with PBS and 100 µL of the solution per well were used to coat the 96-well plate, which had been sealed and incubated overnight at room temperature (RT). In the morning, each well was washed with wash buffer (0.05% Tween™ in PBS) 2x3

times and the remaining fluid was removed by blotting the plate against paper towels. Subsequently, 300 µL of reagent diluent (1% BSA in PBS) were added to each well and incubated at RT for 1.5 hours. The washing step was repeated afterwards.

- 100 µL of *sample or standards* in reagent diluent were added per well and incubated for 2 hours at RT, after which the plate's washing step followed. The samples and standards were run in triplicates. The standard curve contained seven point 2-fold serial dilutions starting from 1000 pg/mL down to 15.6 pg/mL. 100 µL of *detection antibody* (biotinylated goat anti-human VEGF diluted to 50 ng/mL in reagent diluent) were added, the plate covered and incubated for 2 hours at RT. The washing step followed.
- 100 µL of *Streptavidin-HRP* solution was added to each well. The plate was covered and incubated for 20 minutes in the dark at RT, after which the washing step was performed.
- 100 µL of *substrate solution* (1:1 solution of H_2O_2 and tetramethylbenzidine) was added to each well and the plate was covered and was incubated for 20 minutes in the dark at RT.
- 50 µL of *stop solution* (2 M H_2SO_4) was added to each well. The optical density was determined at 450 nm (Multiscan Ascent, Thermo Lab Systems). The regression curve fit was used to calculate the intra- and extracellular VEGF concentrations of unknown samples (per mg protein).

4.3.6. RT-Polymerase Chain Reaction (RT-PCR)

4.3.6.1. Spectrophotometric quantitation of RNA

The concentration of RNA was determined by measuring the absorbance at 260 nm (A_{260}) in a spectrophotometer. To ensure significance, A_{260} readings should be greater then 0.15. An absorbance of 1 unit at 260 nm corresponds to 44 µg of RNA per mL. Considering dilution factors the total amount of RNA in sample can be calculated.

4.3.6.2. Integrity of RNA

The integrity and size distribution of total RNA was checked by using an Agilent 2100 Bioanalyzer (Palo Alto, CA, USA). The respective ribosomal RNAs should appear as sharp bands or peaks. The apparent ratio of 28S rRNA to 18S rRNA should be 2:1.

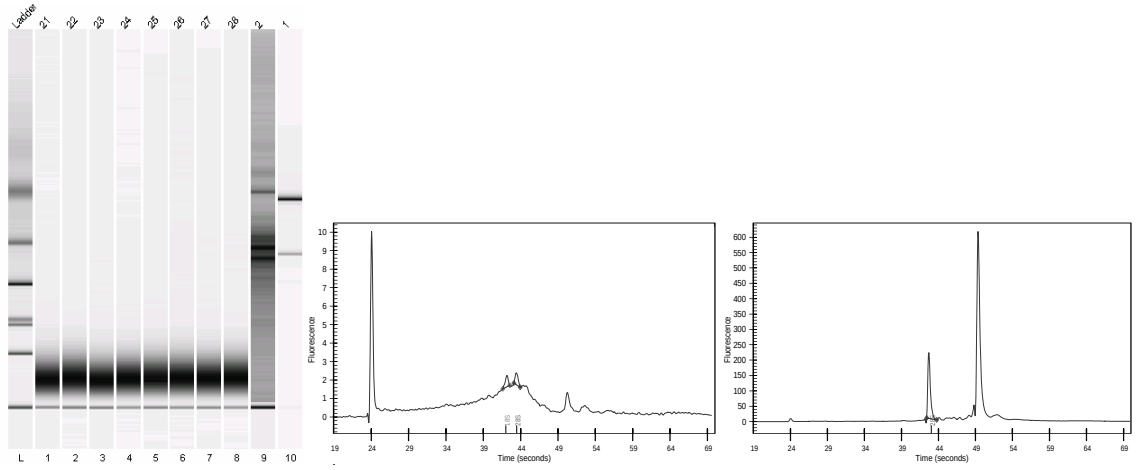

Figure 4.1: Representative Bioanalyzer results assessing RNA integrity. The sample 1 on the gel showed clear bands and 2:1 ratio of 28S to 18S rRNA (right electropherogram). The sample 2 on the other hand (left electropherogram) had suffered either a major degradation either before or during RNA purification.

4.3.6.3. RT-PCR performance

RT-PCR is the most sensitive method for mRNA detection and for quantitative analysis of gene expression. Semi-quantitative RT-PCR measures the band intensity of amplification products relative to an internal control such as glyceraldehyde-3-phosphate dehydrogenase (GAPDH).

All PCR reactions were performed using the QuantiTect SYBR Green PCR Kit (Qiagen, Valencia, CA, USA). The primers and templates were added to the ready-to-use PCR master mix (containing HotStarTaq DNA polymerase; QuantiTect SYBR Green PCR buffer (for highly specific primer annealing); SYBR Green I dye (yields a strong fluorescent signal upon binding double-stranded DNA); dNTP mix). The pipetting scheme and the real-time cycler program are presented in Table 4.2. The reactions were run in triplicate, and three independent experiments were run for each sample. Relative quantification of Glut-1 expression was determined by comparison of the amount of Glut-1 transcript to a housekeeping gene (GAPDH).

	GAPDH	Glut-1
QuantiTect SYBR Green master mix	12.5 µL	12.5 µL
Forward primer (10 µM)	0.5 µL	0.5 µL
Reverse primer (10 µM)	0.5 µL	0.5 µL
RNAse-free water	1.25 µL	1.25 µL
Sample	10 µL	10 µL
QuantiTect RT mix (add last)	0.25 µL	0.25 µL

30 min @ 50˚C
15 min @ 95˚C
15 sec @ 94˚C
30 sec @ 55˚C* x 40 cycles
30 sec @ 72˚C

* Annealing temperature approximately 5˚C below Tm (melting temperature).

Table 4.2: Pipetting scheme and RT-PCR program (on Glut-1/GAPDH) using the Qiagen QuantiTect SYBR Green PCR Kit.

The following primer sets were used:
Glut-1 forward sequence: ACC CTG GAT GTC CTA TCT GAG C;
Glut-1 reverse sequence: GCT GAA GAG TTC AGC CAC GAT;
GAPDH forward sequence: CAG CCT CAA GAT CAT CAG CAA;
GAPDH reverse sequence: GGT CAT GAG TCC TTC CAC GAT AC.

4.3.7. 2-Deoxyglucose uptake

The cells in their mid-log phase (1×10^7 cells/mL) were used for hexose uptake assays. The experiments were performed at the radioactivity core laboratory, University of California, San Diego, CA. After 24 hours of imatinib treatment, the cells were washed twice with PBS to remove glucose. The cells were re-suspended with 100 µL PBS, were supplemented with 5 mmol/L 2-deoxy-D-glucose (containing 2 µCi/mL 2-deoxy-[1-^{3}H]-glucose) and were incubated at 37°C for 5, 10, 20, 30, 40, 50 and 60 min. Uptake was stopped by addition of 100 µL ice-cold PBS with 100 µM phlorentin. The cells were

transferred to 1.5 mL reaction tubes and centrifuged at 20,000g for 30 seconds. Cell pellets were washed once and put into a scintillation vial containing 10 mL Optifluor (Perkin Elmer, Inc., Shelton, USA). The incorporated radioactivity was measured by a liquid scintillation counter (Perkin Elmer, Inc., USA) at the Radioactivity Core Laboratory, UC San Diego. The uptake of 2-deoxy-[1-^{3}H]-glucose was reported as nmol/10^{6} cells.

4.3.8. Development and validation of a high-throughput assay for quantification of imatinib using LC/LC-MS/MS in blood and cell culture samples

4.3.8.1. Calibrators and quality control samples

Stock solutions of imatinib were prepared in methanol / 0.1% formic acid (8:2 v/v) at a concentration of 1 mg/mL and stored at -80ºC. The working solutions to construct quality control and calibration curve samples were prepared by dilution of the stock solutions with methanol / 0.1% formic acid (8:2 v/v). Working solutions were always prepared fresh. The use of blood samples from healthy volunteers for assay development and validation purposes received "exempt" status from our institutional review board, the Colorado Multi-Institutional Review Board (COMIRB). For calibrators and quality controls in isolated, cultured leukemia cells and cell culture media, blank cell samples and media were extracted as described below and spiked with imatinib.

4.3.8.2. Calibrators and quality control samples

The only manual step during the extraction of blood samples was protein precipitation. The protein precipitation solution (methanol / 0.2 M $ZnSO_4$, 7:3, v/v) contained the internal standard trazodone (Sigma-Aldrich, USA) at a concentration of 2 ng/mL. 800 µL protein precipitation solution was added to 200 µL blood, leukemia cells or cell culture media. After vortexing (10 min) and centrifugation (4ºC, 13,000g, 10 min), the supernatant was transferred into an HPLC vial. The extraction of leukemia cells has been described in detail in 4.2.3.2.

4.3.8.3. Automated online extraction and HPLC conditions

The extracts were analyzed using an LC/LC-MS/MS system. The two HPLC systems consisted of the following components (all series 1100, Agilent Technologies, Palo Alto, USA): HPLC I: G1312A binary pump, G1379A degasser; HPLC II: G1312A binary

pump, and a G1316A column thermostat. A Sciex API 4000 triple-stage quadrupole mass spectrometer was used as detector (Applied Biosystems, Foster City, USA). The HPLC systems were connected *via* a 6-port column switching valve mounted on a step motor. Connection of the switching valve is shown in Figure 4.3. The HPLCs, switching valve and the mass spectrometer were controlled by the Analyst software (version 1.3.1., Applied Biosystems).

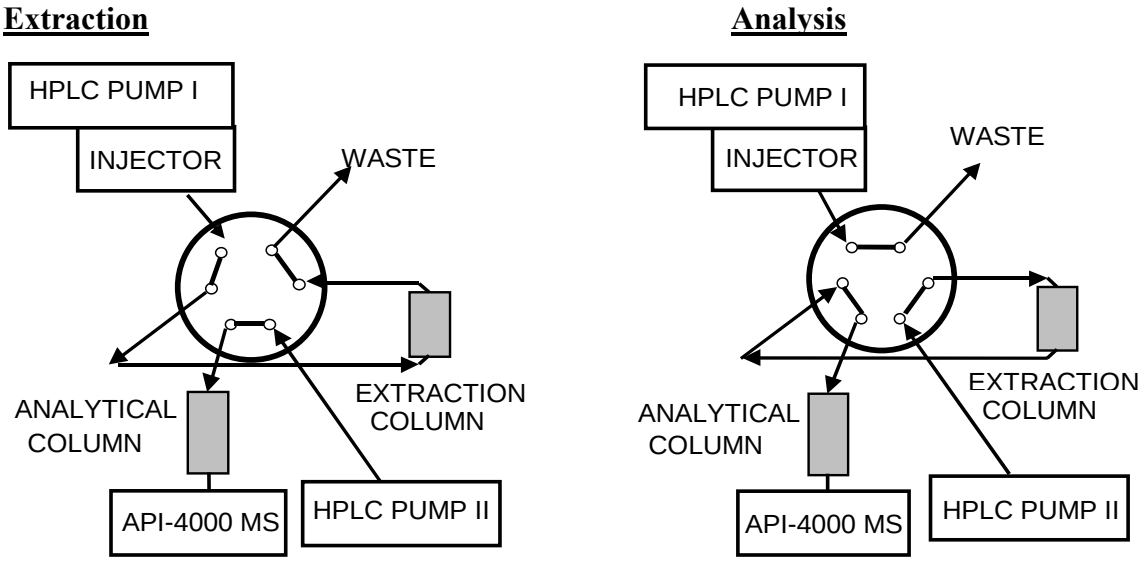

Figure 4.3: Connections and positions of the column switching valve.

Two hundred µL of the samples were injected onto a 4.6 × 12.5 mm extraction column filled with Eclipse XDB-C8 material of 5 µm particle size (Agilent Technologies, Palo Alto, USA). Samples were washed with a mobile phase of 10% methanol and 90% 0.1% formic acid. The flow was 5 mL/min. After 1 min, the switching valve was activated and the analytes were back-flushed from the extraction column onto a 4.6 × 50 mm column filled with Luna 5u C18 material of 5 µm particle size (analytical column). The mobile phase consisted of methanol and 5 mM ammonium acetate supplemented with 0.01% trifluoracetic acid (TFA). The flow rate was 1 mL/min. The following gradient was used:

Total Time(min)	Flow Rate(µl/min)	A (%)	B (%)
0.00	1000	30.0	70.0
1.00	1000	30.0	70.0
4.50	1000	98.0	2.0
9.00	1000	98.0	2.0
9.50	1000	30.0	70.0
10.00	1000	30.0	70.0

with A: methanol and B: 5 mM ammonium acetate supplemented with 0.01% trifluoracetic acid (TFA).

The extraction column was cleaned with 98% methanol (flow: 5 mL/min) between minutes 4 and 9. The column switching valve was switched back into the extraction position after 9 minutes and the analytical column was re-equilibrated to the starting conditions (minutes 9-10). Both columns were kept at 65ºC. Injection of the next sample was initiated 10.5 min after injection of the previous.

4.3.8.4. MS/MS analysis

The triple quadrupole mass spectrometer and HPLC system interfaced with a turbo-ion spray source. Nitrogen (purity: 99.999%) was used as Collision Activated Dissociation (CAD) gas. The mass spectrometer was run in the positive MRM (multiple reaction monitoring) mode. The declustering potential (DP) was set to -70 V. The interface was heated to 700ºC. The first quadrupole was set to select the $[M+H]^+$ adduct of imatinib (*m/z* 494.5) and trazodone (IS, *m/z* 372.5). The second quadrupole was used as collision chamber, and the third quadrupole to select the characteristic product ions of imatinib (*m/z* 394.2) and trazodone (IS, *m/z* 176.4). Peak area ratios obtained from MRM mode of the mass transitions for imatinib (*m/z* 494.5 → 394.2) and trazodone (IS, *m/z* 372.5 → 176.4) were used for quantification (Figure 4.4).

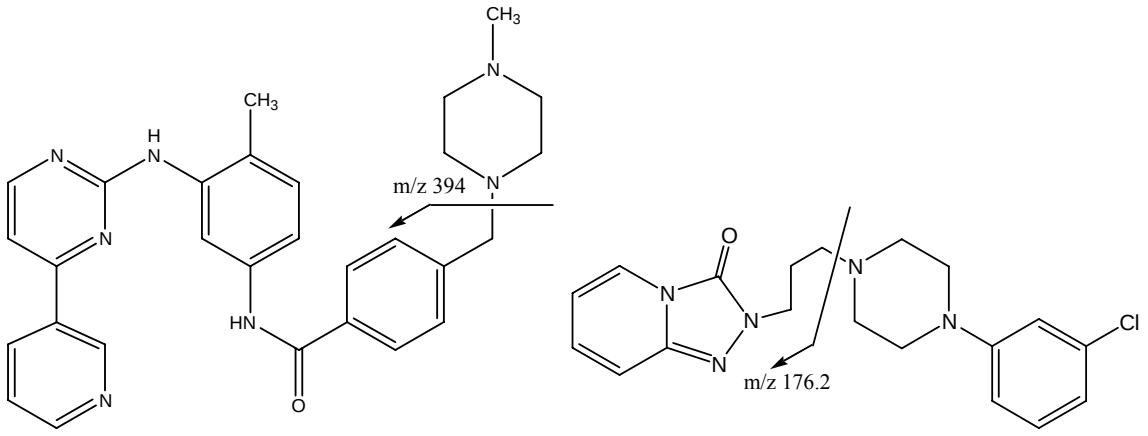

Figure 4.4: Chemical structure of imatinib (left) and trazodone (left). Arrows indicate the product ions selected for the multiple-reaction monitoring experiments.

4.3.8.5. Calibration

Calibration and quality control samples were prepared by spiking blank blood, pelleted

leukemia cells or cell culture media samples with imatinib. The calibration curves (0, 0.005, 0.01, 0.05, 0.1, 0.5, 1, 2.5, 5, 10, 25, 50 and 100 ng/mL, n=6 per concentration) were constructed using non-weighted linear regression. Quality control (QC) samples were prepared at following concentrations: lower limit of quantitation (0.03 ng/mL), 0.1 ng/mL, 1 ng/mL, 10 ng/mL and upper limit of quantitation (50 and 75 ng/mL). For stability studies, quality control samples were prepared in human blood at seven concentration levels: 0.03, 0.05, 0.1, 1, 10, 50 and 75 ng/mL.

4.3.8.6. Validation procedures

Validation strategy. The assay was completely validated using spiked blood samples, including inter-day performance and stability. Hereafter, the validation was extended to the cultured leukemia cells and cell culture media using an abbreviated validation strategy since the only change was the matrix. Parameters determined for abbreviated validation included lower limit of quantitation, upper limit of quantitation, linearity, intra-day accuracy and precision and 24 hour stability.

Predefined acceptance criteria. The assay was considered acceptable if precision (coefficient of variance, CV%) at each concentration was ≤ 15% for intra-day and day-to-day variability. The accuracy compared with the nominal value had to be within ± 15% for both intra- and day-to-day variability. The calibration curve had to have a correlation coefficient r of 0.99 or better. The absolute recovery had to exceed 60%.

Limit of detection (LOD) and lower limit of quantitation (LLOQ). The limit of detection (LOD) was defined as a signal-to-noise ratio of 3:1. The lower limit of quantitation (LLOQ) was determined as the lowest quantity consistently achieving accuracy ≤ ±20% of the nominal concentration, precision ≤ 20%, and a signal-to-noise ratio greater than 5:1.

Precision and accuracy. The method was validated using human blood, isolated leukemia cells and cell culture media. The intra-day precision and accuracy were determined by analysis of each of the six quality control samples containing imatinib (n= 6) on the same day. Determination of inter-day precision and accuracy was also based on quality control samples. Samples were extracted and analyzed on three different days over a one-week period (n= 6/concentration and day). Precision is reported as coefficient of variance in % and accuracy in % of the nominal concentration.

Recoveries. Absolute recoveries were determined by comparing the signal of imatinib obtained after extraction of the six quality control samples (n= 6) with the signal after injection of the respective nominal amount from standard solutions (in methanol / 0.1% formic acid (8:2 v/v)) directly onto the analytical column.

4.3.8.7. Validation results

As a first step, MS and MS/MS spectra were recorded after direct infusion of imatinib mesylate into the electrospray source *via* a syringe pump (KD Scientific, Holliston, USA). Imatinib mesylate was dissolved at a concentration of 10 µg/mL in methanol / 0.1% formic acid (80/20, v/v) and was delivered at a rate of 2 mL/h. The mass transitions for imatinib (*m/z* 494.5 → 394.2) and trazodone (IS, *m/z* 372.5 → 176.4) were selected for quantification (Figure 4.4).

To investigate the ion suppression effects on quantification of imatinib, blood samples from 10 different individuals were tested following the recommendations by Müller et al., 2002. No ion suppression at the times when imatinib or its internal standard eluted was observed.

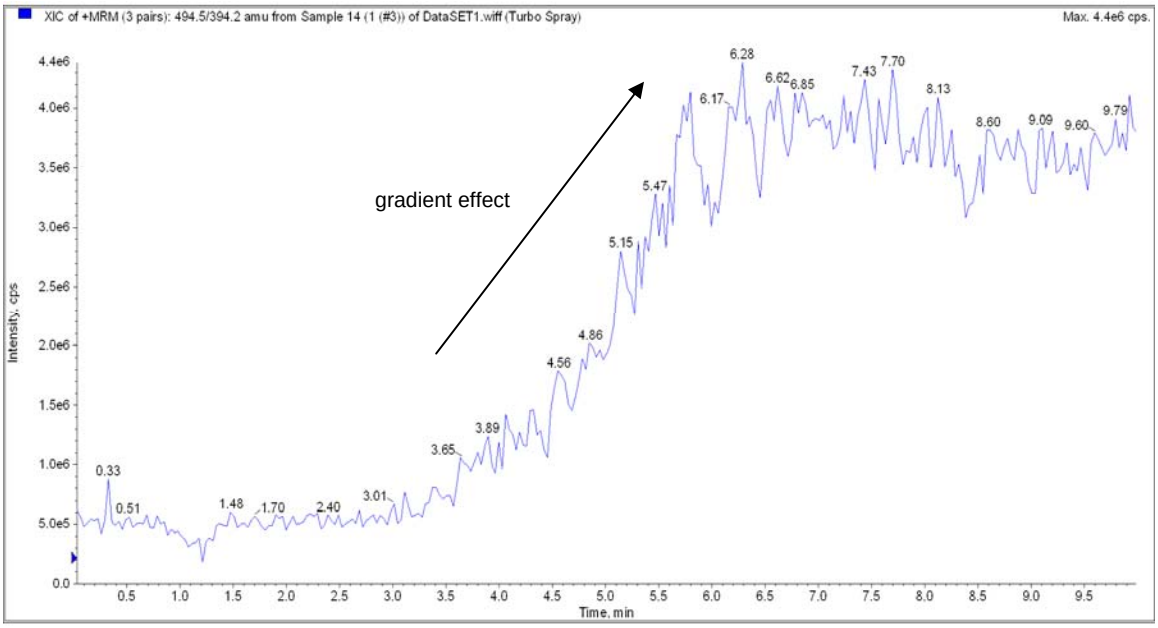

Figure 4.5: Ion suppression test (total ions were monitored). The slope in the chromatogram was caused by the increasing methanol concentration (gradient effect).

The absolute recovery of imatinib after protein precipitation of human blood and column switching was 92.5±8.6% (mean ± standard deviation). The recovery of the internal

standard trazodone was 100.7±2.0%.

Imatinib eluted with an average retention time of 4.19±0.10 min and the internal standard trazodone with a retention time of 5.11±0.11 min. The total chromatographic run time was 10 min. The analyses of blank blood and tissue samples did not detect any significant interferences with imatinib or trazodone.

In human blood, the lower limit of quantification was 0.03 ng/mL and the assay was linear from 0.03-75 ng/mL (y=0.0429x-0.0236, r=0.9994) (Figure 4.6; Table 4.7). In leukemia cell extracts the assay was linear from 0.03-75 ng/ml, in the cell culture media from 0.01–75 ng/mL.

Assay accuracy and precision were determined using following concentrations: lower limit of quantitation (0.01, 0.03 and 0.05 ng/mL), 0.1 ng/mL, 1 ng/mL, 10 ng/mL and upper limit of quantitation (50 and 75 ng/mL). The results for intra-day precision and accuracy are listed in the Table 4.7.

In human blood, inter-day accuracies were: 105.1% (0.03 ng/mL); 114.6% (0.1 ng/mL); 114.5% (1 ng/mL); 111.6 (10 ng/mL); and 99.0% (75 ng/mL). The inter-day precisions were: 8.4% (0.03 ng/mL); 7.2% (0.1 ng/mL); 6.5% (1 ng/mL); 8.2% (10 ng/mL); and 4.3% (75 ng/mL).

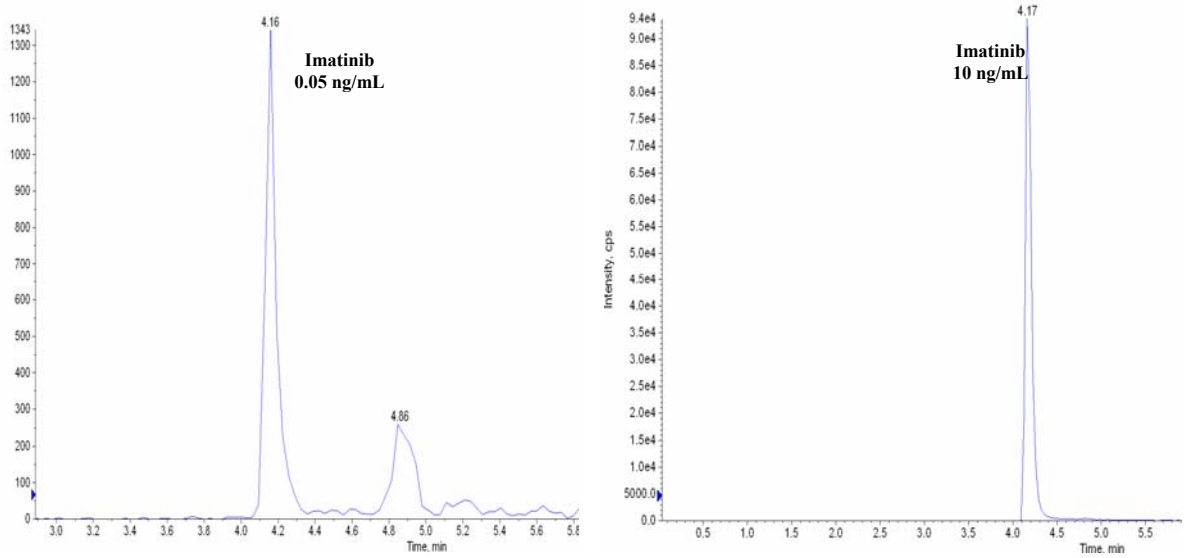

Figure 4.6: Representative ion chromatograms of imatinib at the lower limit of quantitation (left, 0.05 ng/mL) and 10 ng/mL (right).

		Human whole blood	Human leukemia cells	Cell culture media
INTRA-DAY ACCURACY	LLOQ	100.9%	98.1%	93.2%
	0.1 ng/mL	108.6%	100.1%	100.1%
	1 ng/mL	94.7%	100.0%	100.2%
	10 ng/mL	107.8%	107.6%	98.8%
	ULOQ 75 ng/mL	92.8%	86.5%	94.24%
INTRA-DAY PRECISION	LLOQ	8.8%	13.2%	14.9%
	0.1 ng/mL	7.2%	6.8%	6.8%
	1 ng/mL	6.7%	3.1%	7.3%
	10 ng/mL	8.2%	7.0%	2.4%
	ULOQ 75 ng/mL	4.3%	5.4%	11.0%
INTER-DAY STABILITY	LLOQ	114.1%	118.1%	107.4%
	0.1 ng/mL	97.3%	114.0%	113.3%
	1 ng/mL	93.1%	111.0%	113.7%
	10 ng/mL	102.0%	109.7%	115.9%
	ULOQ 75 ng/mL	99.6%	112.0%	105.4%

Table 4.7: Intra-day accuracy and intra-day precision of imatinib quantification in human blood, leukemia cells and cell culture media. Abbreviations: LLOQ: lower limit of quantitation, ULOQ: upper limit of quantitation. ***LLOQ for human whole blood and leukemia cells: 0.03 ng/mL and for cell culture media 0.01 ng/mL. Inter-day stability measured after 24 hours at 4˚C.***

After extraction, imatinib was stable in the autosampler at 4°C as well as at room temperature in all concentrations tested for at least 24 hours. After seven days at 4°C, no changes in imatinib concentrations were observed, indicating the compound's high stability. Furthermore imatinib was stable over at least 3 freeze-thaw cycles. The assay was successfully used for the quantification of intracellular and extracellular imatinib concentrations in leukemia cells and their growth media (see Results and Discussion section).

4.3.9. Quantification of nucleotide tri-, di- and monophosphates using LC/LC-MS in cell culture samples

The samples were extracted as described in 4.2.3.2. After dissolving the lyophilisates in 500µL water, 20-40 µL of sample were injected into an Agilent 1100 Series LC/LC system with an online desalting column (Agilent Zorbax C18) and an analytical column (250mm X 5mm Phenomenex Synergy Hydro C18) coupled to an 1946D Agilent mass detector (MSD). The Figure 4.3 shows the connections and positions of the column switching valve. In the desalting position, the extracts were pumped onto the C18 cartridge column with 95% 4mM dibutylammonium formate buffer (DBAF) with a flow of 2mL/min for 0.7 min using PUMP I. At 0.7 min the switching valve was activated to connect analytical PUMP II to the desalting column which was now in row with the analytical column. PUMP II back-flushed the analytes onto the analytical column that was connected to the mass selective detector. The negative charge on the phosphate groups of the nucleotides led to better ionization in the electrospray chamber in the negative compared to the positive ion mode. The following single negatively charged ions were monitored: AMP (m/z= 346), ADP (m/z= 426), ATP (m/z= 506), GDP (m/z= 442), GTP (m/z= 522), UDP (m/z= 403), UTP (m/z= 483), CDP (m/z= 402), CTP (m/z= 482), NAD^+ (m/z= 662) and FAD (m/z= 784). This assay also has the potential to measure NADH (m/z= 664), $NADP^+$ (m/z= 742), GMP (m/z= 362), UMP (m/z= 323), CMP (m/z= 322) and deoxyribonucleoside mono-, di- and triphosphates (Figure 4.8).

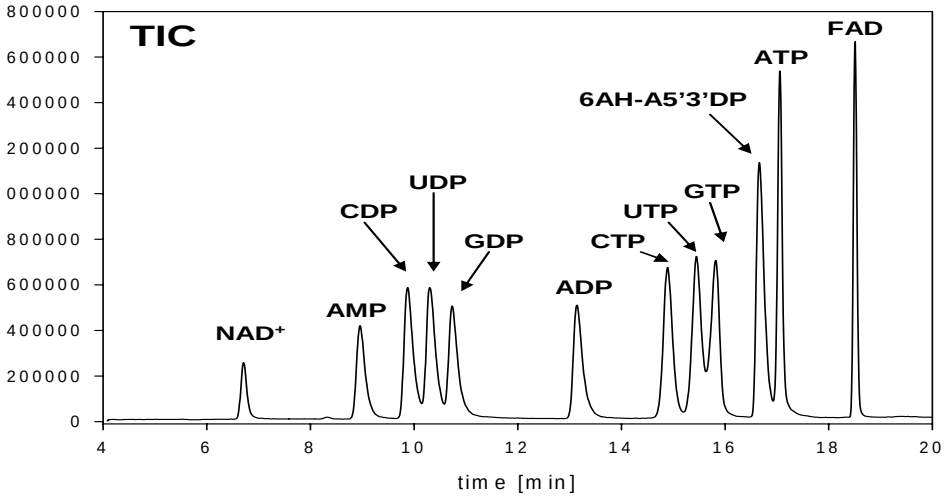

Figure 4.8: Representative total ion chromatogram. The chromatogram was acquired using the conditions shown in Table 4.9.

The method has been fully validated by Klawitter et al. 2005, according to the current US Federal Drug Administration (FDA) guidance for the industry "Guidance for Industry, Bioanalytical Method Validation" (May 2001). N6-(aminohexyl)-adenosine-5'3'-diphosphate was used as an internal standard. HPLC set-up (gradient program) and analytical parameters are shown in Table 4.9.

time [min]	% methanol	% 2mM DBAF pH6	description
0 → 1	8	92	isocratic
1 → 13	27	73	slow gradient
13 → 17	50	50	fast gradient
17 → 19	8	92	equilibration for next run

Source parameter	Value	Ion optics	Value
Ion source	electro spray	Fragmentor	162
Polarity	negative	Skim1	30
Detection mode	Single ion mode	Lens1	-4.7
Drying gas	9 L/min	Lens2DC	12.6
Nebulizer pressure	50 PSI	Iris	-5
Drying gas temp.	320°C	Energy	4.5
Capillary voltage	4000 V	Octopole Peak	297
		Octopole Knee	280
		Quadropole DC	2.2

Table 4.9: HPLC gradient programs (top) and optimal spray chamber and ion optics parameters (bottom). Nomenclature follows Agilent Chemstation software (version 09.03, Agilent Technologies, Palo Alto, CA). Abbreviation: DBAF: dibutylammonium formate.

4.3.10. NMR Spectroscopy

4.3.10.1. Sample preparation

Lyophilized PCA cell extracts were redissolved in 0.55 mL deuterium oxide (D_2O) and the media in 1 mL D_2O. The extracts were centrifuged and the clear supernatant transferred into NMR tubes and the pH to 7.2 adjusted (with DCl and NaOD) to allow for unique chemical shift assignments. The lipid-extracts were dissolved in 1.2 mL $CDCl_3$/MeOD (2:1, v/v). Before ^{31}P-MRS spectra were recorded, EDTA (100 mmol/L) was added to each PCA extract to complex divalent cations.

4.3.10.2. Analysis of ^{1}H-, ^{13}C- and ^{31}P-spectra

Trimethylsilyl propionic-2,2,3,3,-d_4 acid (TMSP) (0.5 mmol/L for cell PCA extracts and 1.1 mmol/L for media and lipids) in a sealed capillary was set at 0 ppm for chemical shift

reference and was used as an external standard for metabolite quantification. Absolute concentrations of major amino acids, fatty acids, phospholipids and their precursors, as well as lactate were calculated from ^{1}H-MRS spectra. The signals in ^{13}C-MRS spectra were referenced to the C3 carbon of lactate set at 21.3 ppm. Methylene diphosphonic acid (MDP, 3mmol/L) was used as an external standard for metabolite quantification in ^{31}P-MRS. The resonance of phosphocreatine at -2.33 was used as internal shift reference.

4.3.10.3. Acquisition- and processing parameters for NMR spectra

All high-resolution ^{1}H- and ^{13}C-MRS experiments were performed either on a 500 MHz Bruker DRX system equipped with an inverse TXI 5-mm probehead (UCHSC, Denver, USA) or on a Bruker Avance WB-360 system operating at 360 MHz and equipped with an HX-inverse probehead (University of Bremen, Bremen, Germany).

The ^{31}P-MRS experiment were performed using a 300 MHz Bruker Avance system equipped with 5-mm QNP probe (UCHSC, Denver, USA) or on a Bruker Avance WB-360 system operating at 360 MHz and equipped with an HX-inverse probehead (University of Bremen, Bremen, Germany). The Bruker systems were from Bruker BioSpin, Fremont, CA, USA or Bruker, Karlsruhe, Germany.

For ^{1}H-MRS a standard water presaturation pulse program was used for water suppression; ^{13}C-spectra were performed using composite pulse decoupling with WALTZ 16 (Table 4.10). All NMR spectra were post-processed with the 1D-WINNMR program (Bruker BioSpin, Fremont, CA), including exponential multiplication, Fourier transformation, line broadening, phase and base line correction and signal integration.

^{1}H-NMR	**PCA extracts**	**lipids**	**media**
number of scans	**128**	**64**	**32**
flip angle	**90°**	**90°**	**90°**
repetition time	**14.8 sec**	**14.8 sec**	**14.8 sec**
spectral width	**12 ppm**	**12 ppm**	**12 ppm**
data size*	**16K**	**16K**	**16K**

*zero filling to 32K

apodisation: GM: gaussian multiplication (variable parameters)

Table 4.10: Parameters used for recording of ^{1}H-NMR spectra.

^{13}C-NMR	PCA extracts	media
number of scans	20,000-30,000	1,000
flip angle	90°	90°
repetition time	3 sec	3 sec
spectral width	150 ppm	150 ppm
data size*	32K	32K

* zero filling to 64K

apodisation: EM: exponential multiplication (1-3 Hz)

^{31}P-NMR	PCA extracts
number of scans	10,000
flip angle	90°
repetition time	3.5 sec
spectral width	50 ppm
data size*	8K

* zero filling to 16K

apodisation: EM: exponential multiplication (1-2 Hz)

Table 4.10: Parameters used for recording of ^{13}C- and ^{31}P-NMR spectra.

4.3.10.4. Quantification of metabolites.

The pool size of metabolites was determined based on fully relaxed ^{1}H-NMR spectra of extracts using TSP as an external standard. The absolute concentrations of each metabolite was expressed as nmol/g wet weight and calculated by the equation:

$$\textbf{[metabolite] = \{integral x [TSP] x } V_S\textbf{\}/ wet weight}$$

where integral: Integral of respective signal; [TSP]: TSP concentration in mmol/L; V_S: sample volume in mL; wet weight: cell pellet weight in g.

For quantification of absolute concentrations of ^{13}C metabolites, calculations were made according to Zwingmann et al.[15] The ^{13}C-enrichments in C3-lactate were determined by the heteronuclear spin-coupling pattern in ^{1}H-MRS spectra as follows:

$$\textbf{[area (}^{1}\textbf{H-}^{13}\textbf{C) x 100] / [area (}^{1}\textbf{H-}^{12}\textbf{C) + area (}^{1}\textbf{H-}^{13}\textbf{C)]}$$

where the sum (area [^{1}H-^{12}C] + area [^{1}H-^{13}C]) is equivalent to the pool size of lactate.

The values were corrected for 1.1% natural abundance ^{13}C. ^{13}C-enrichments in individual carbons of amino acids were derived from ^{13}C-MRS spectra using the known ^{13}C-enrichment in lactate:

$$\mathbf{E_{Met}\,(\%) = [A_{Met} - A_{n.a.}(Met)] / A_{n.a.}(Met)] \times 1.1}$$

where A_{Met} represents ^{13}C carbon peak area of the metabolite, $A_{n.a.}$ its natural abundance signal intensity, and 1.1 is the percentage factor of the ^{13}C-isotope. The natural abundance of ^{13}C, contributing to the total intensity $A_{n.a.}$ (Met), was determined using the known ^{13}C-enrichment and natural abundance of lactate and correction for the pool size:

$$\mathbf{A_{n.a.}(Met) = \{A_{Lac} \times [Met]\}/ \{(E_{Lac} + 1) \times [Lac]\}}$$

A_{Lac} represents the carbon peak area of lactate, [Lac] or [Met] the pool sizes of lactate or metabolite of interest, respectively, and E_{Lac} the percentage ^{13}C-enrichment in lactate. The ^{13}C signal intensities were corrected for nuclear Overhauser enhancement effects by comparison with the standard mixture of amino acids.

The absolute amount of ^{13}C in specified carbon positions is the product of the pool size times the fractional ^{13}C-enrichment.

4.3.10.4. Metabolic pathway of [1-^{13}C]glucose

Biochemistry of a tumor, especially glucose uptake and metabolism, is very different from that of the normal cell: mitochondrial metabolism is impaired; and cytosolic glycolysis is elevated (Warburg effect). This makes MRS one of the most valuable techniques to evaluate cancer metabolism and efficacy of the treatment because both glycolysis and the Krebs cycle can be assessed simultaneously. After incubation of cells with [1−^{13}C]glucose, its metabolites are labeled in different carbon positions, depending on the relative contribution of the enzymatic pathways (Figure 4.11).

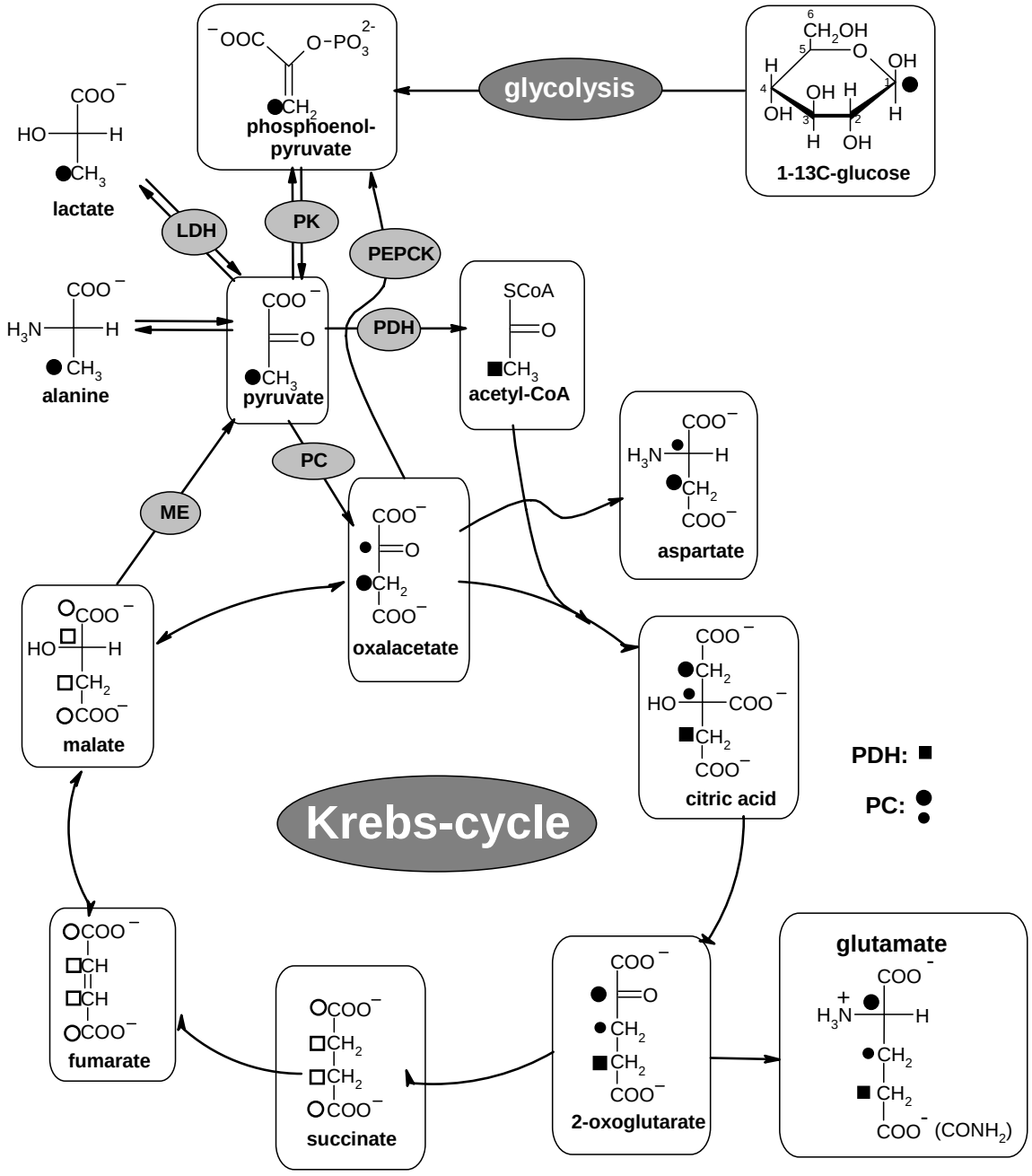

Figure 4.11: Metabolic fate of ^{13}C-label from [1−^{13}C]glucose. Label distribution in glycolytic and tricarboxylic acid (TCA) cycle intermediates during metabolism of [1−^{13}C]glucose.

4.3.10.5. 2D-NMR Spectroscopy

To verify the metabolite assignments in sensitive and resistant cell lines, a 2-dimensional 2D-H,C-HSQC (heteronuclear single quantum correlation) analysis was carried out. All 2D-measurements were performed in Bremen, Germany using a 600-MHz Bruker DRX

spectrometer system (Bruker, Karlsruhe, Germany). The experiments were acquired with 512 t1-increments and 32 scans per increment. A representative 2D-H,C-HSQC NMR spectrum is presented in Figure 4.12.

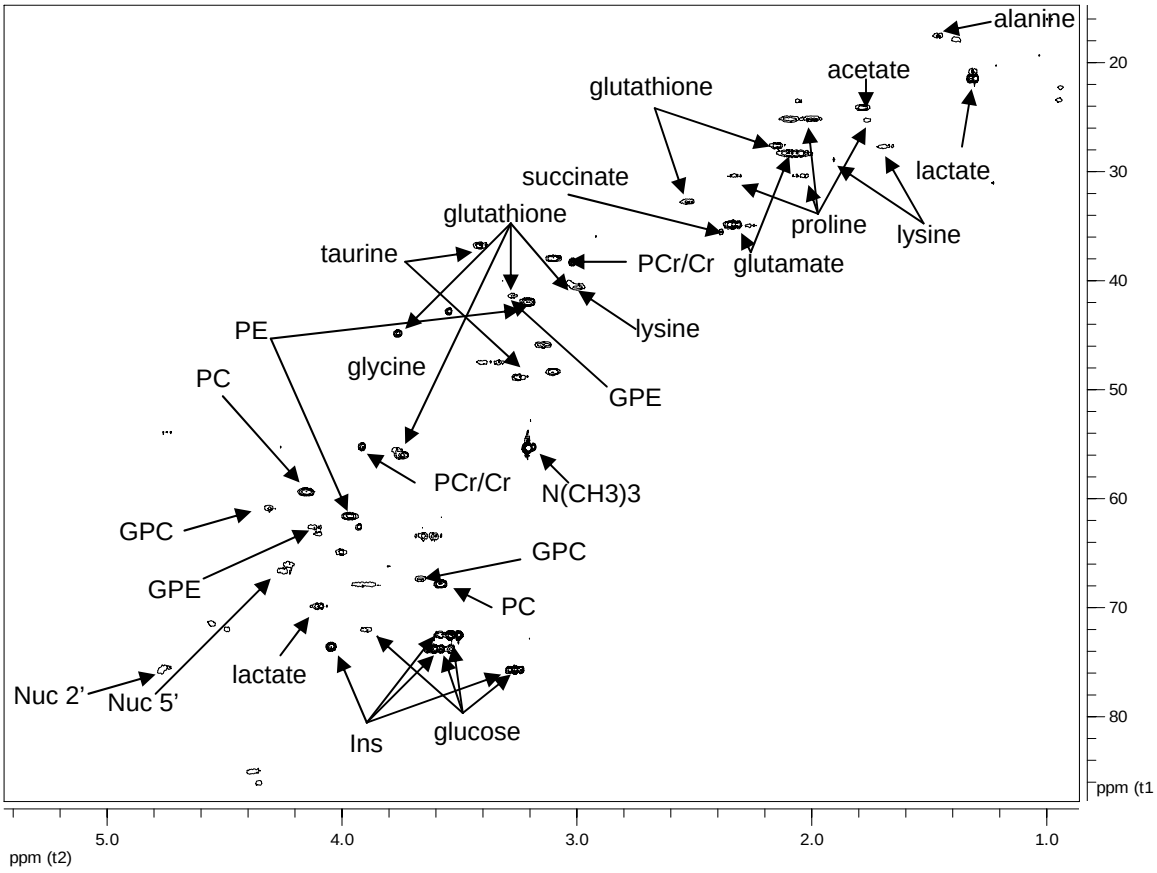

Figure 4.12: Representative 2D-H,C-HSQC (echo-antiecho) spectrum of LAMA84-R cells.

4.3.11. Statistics

All numerical data is presented as mean±standard deviation. Differences among more than two datasets were compared by one-way analysis of variance (ANOVA). Tukey's test was used as a *post-hoc* test in combination with ANOVA to test for significances between groups. Two groups were compared using a standard Student's TTest (in the case of normally distributed data) or the non-parametric Whitney-Mann's U-test (in case data was non-normally distributed). The significance level was set at $p<0.05$ for all tests (SigmaPlot-version 9.01, Systat Software, Point Richmond, CA and SPSS version 14.0, SPSS Inc., Chicago, IL).

Chapter 5

5. REFERENCES

Ackerstaff E, Pflug BR, Nelson JB, Bhujwala ZM, Detection of increased choline compounds with proton nuclear magnetic resonance spectroscopy to malignant transformation of human prostatic epithelial cells, 20011, *Cancer Res*, **61**:3599-603.

Ackerstaff E, Glunde K, Bhujwalla ZM, Choline phospholipid metabolism: A target in cancer cells?, 2003, *J Cell Biochem*, **90**:525-533.

Al-Saffar NM, Titley JC, Robertson D, et al., Apoptosis is associated with triacylglycerol accumulation in Jurkat T-cells, 2002, *Br J Cancer*, **86**:963-70.

Arias-Diaz J, Vara E, Garcia C, and Balibrea JL, Tumor necrosis factor-alpha-induced inhibition of phosphatidylcholine synthesis by human type II pneumocytes is partially mediated by prostaglandins, 1994, *J Clin Invest*, **94**: 244-250.

Arteaga CL, Epidermal growth factor receptor dependence in human tumors: more than just expression?, 2002, *Oncologist* **7**:31−39.

Asano T, Wakisaka M, Yoshinari M et al., Troglitazone enhances glycolysis and improves intracellular glucose metabolism in rat messangial cells, 2000, *Metabolism*, **49**: 308-313.

Barnes K, McIntosh E, Whetton AD, et al., Chronic myeloid leukemia: an investigation into the role of Bcr-Abl-induced abnormalities in glucose transport regulation, 2005, *Oncogene*, **24**:3257−3267.

Bennasroune A, Gardin A, Aunis D, Cremel G, Hubert P, Tyrosine kinase receptors as attractive targets for cancer therapy, 2004, *Crit Rev Oncol Hematol*, **50**: 23-38.

Bennett A and del Tacca M, Proceedings: Prostaglandins in human colonic carcinoma, 1975, *Gut*, **16**: 409.

Bennett A, Tacca MD, Stamford IF and Zebro T, Prostaglandins from tumours of human large bowel, 1977, *Br J Cancer*, **35**: 881–884.

Baselga J, Why the epidermal growth factor receptor? The rationale for cancer therapy, 2002, *Oncologist* **7**:2−8.

Bhatia R, Holtz M, Niu N, et al., Persistence of malignant hematopoietic progenitors in chronic myelogenous leukemia patients in complete cytogenetic remission following imatinib mesylate treatment, 2003, *Blood,* **101**:4701–4707.

Blankenberg FG, Storrs RW, Naumovski L, Goralski T and Spielman D, Detection of apoptotic cell death by proton nuclear magnetic resonance spectroscopy,

1996, *Blood*, **87:**1951-1956.

Blankenberg FG, Katsikis PD, Storrs RW, et al., Quantitative analysis of apoptotic cell death using proton nuclear magnetic resonance spectroscopy, 1997, *Blood*, **89**:3778-3786.

Bloch F, Hansen WW, Packard ME, Nuclear Induction, 1946, *Phys Rev*, **70**:127.

Boren J, Cascante M, Marin S, et al., Gleevec (STI571) Influences Metabolic Enzyme Activities and Glucose Carbon Flow toward Nucleic Acid and Fatty Acid Synthesis in Myeloid Tumor Cells, 2001, *J Biol Chem*, **41**:37747-37753.

Boros LG, Lee WN, Go VL, A metabolic hypothesis of cell growth and death in pancreatic cancer, 2002, *Pancreas,* **24**:26−33.

Branford S, Rudzki Z, Walsh S, et al. High frequency of point mutations clustered within the adenosine triphosphate-binding region of BCR/ABL in patients with chronic myeloid leukemia or Ph-positive acute lymphoblastic leukemia who develop imatinib (STI571) resistance, 2002, *Blood*, **99**: 3472-3475.

Buchdunger E, Zimmermann J, Mett H, et al., Inhibition of the Abl protein-tyrosine kinase in vitro and in vivo by a 2-phenylaminopyrimidine derivative, 1996, *Cancer Res,* **56**:100–104.

Buchdunger E, Cioffi CL, Law N, et al., Abl protein-tyrosine kinase inhibitor STI571 inhibits in vitro signal transduction mediated by c-kit and platelet-derived growth factor receptors, 2000, *J Pharmacol Exp Ther,* **295**:139–145.

Budd SL, Tenneti L, Lishnak T and Lipton SA, Mitochondrial and extramitochondrial apoptotic signaling pathways in cerebrocortical neurons, 2000, *Proc Natl Acad Sci USA*, **97**:6161−6166.

Bunn PA and Kelly K, New chemotherapeutic agents prolong survival and improve quality of life in non-small cell lung cancer: a review of the literature and future directions, 1998, *Clin Cancer Res*, **5**:1087-1100.

Burg MB, Molecular basis of osmotic regulation, 1995, *Am J Physiol*, **268**:F983-996.

Capdeville R, Buchdunger E, Zimmermann J, Matter A, Glivec (STI571, imatinib), a rationally developed, targeted anticancer drug, 2002, *Nat Rev Drug Discov*, **1**:493-502.

CDER, U.S. Department of Health and Human Services, Food and Drug Administration, Center for Drug Evaluation and Research and Center for Veterinary Medicine (CVM). Guidance for the Industry. Bioanalytical Method Validation, May 2001. (www.fda.gov/cder) accessed 12-28-2005.

Chandra J, Samali A, Orrenius S, Triggering and modulation of apoptosis by oxidative stress, 2000, *Free Radic Biol Med*, **29:**323-333.

Cheng T, Cao W, Wen R, Steinberg RH, LaVail MM, Prostaglandin E2 induces vascular endothelial growth factor mRNA expression in cultured rat Muller cells, 1998,

Invest Ophthalmology Visual Sciences, **39**:581-591.

Chou TC, Talalay P, Quantitative analysis of dose-effect relationships: the combined effects of multiple drugs or enzyme inhibitors, 1984, *Adv Enzyme Regul*, **22**: 27–55.

Clynes M, Daly C, NicAmhlaoibh R, Cronin D, et al., Recent developments in drug resistance and apoptosis research, 1998, *Crit Rev Oncol Hematol,* **28**:181-205.

Cohen JS, Lyon RC, Chen C, et al., Differences in phosphate metabolite levels in drug-sensitive and –resistant human breast cancer cell lines determined by ^{31}P magnetic resonance spectroscopy, 1986, *Cancer Res*, **46**: 4087-4090.

Compton MM, A biochemical hallmark of apoptosis: internucleosomal degradation of the genome, 1992, *Cancer Metastasis Rev*, **11**:105-19.

Craven RJ, Lightfoot H, and Cance WG, A decade of tyrosine kinases: from gene discovery to therapeutics, 2003, *Surgical Oncology,* **12**: 39-50.

Cullis PR and Hope MJ, Physical properties and functional roles of lipids in membranes, 1991, IN: Vance DE, Vance J, editors. Biochemistry of lipids, lipoproteins, and membranes. Amsterdam: Elsevier Science Publishers: pp 1-41.

Davidson AL, Mechanism of coupling of transport to hydrolysis in bacterial ATP-binding cassette transporters, 2002, *J Bacteriol*, **184**: 1225–1233.

Davies DD, Anaerobic metabolism and the production of organic acids, 1980, In (DD Davies ed) "The Biochemistry of Plants", Vol 2, Academic Press, New York, pp 581-611.

Desplat V, Belloc F, Lagarde V, et al., Overproduction of BCR-ABL induces apoptosis in imatinib-mesylate resistant cell lines, 2005, *Cancer*, **103**:102-110.

Di Vito M, Lenti L, Knijn A, et al., 1H NMR-visible mobile lipid domains correlate with cytoplasmic lipid bodies in apoptotic T-lymphoblastoid cells, 2001, *Biochem Biophys Acta*, **1530**:47-66.

Deininger MW, Goldman JM, Lydon N and Melo JV, The tyrosine kinase inhibitor CGP57148B selectively inhibits the growth of BCR–ABL-positive cells, 1997, *Blood,* **90**:3691–3698.

Donato NJ, Wu JY and J Stapley, BCR-ABL independence and LYN kinase overexpression in chronic myelogenous leukemia cells selected for resistance to STI571, 2003, *Blood*, **101**:690-698.

Drexler HG, Leukemia cell lines: *In vitro* models for the study of chronic myeloid leukemia, 1994, *Leukemia Res,* **18:** 919-927.

Dringen R, Gutterer JM, Hirrlinger J, Glutathione metabolism in brain metabolic interaction between astrocytes and neurons in the defense against reactive oxygen species, 2000, *Eur J Biochem*, **267**: 4912-4916.

Druker BJ, Tamura S, Buchdunger E, et al., Effects of a selective inhibitor of the Abl tyrosine kinase on the growth of Bcr-Abl positive cells, 1996, *Nat Med,* **2**:561–566.

Druker BJ, Talpaz M and Resta DJ et al., Efficacy and safety of a specific inhibitor of the BCR-ABL tyrosine kinase in chronic myeloid leukemia, 2001, *N Engl J Med*, **344**:1031-7.

Eguchi Y, Shimizu S, Tsujimoto Y, Intracellular ATP levels determine cell death fate by apoptosis or necrosis, 1997, *Cancer Res*, **57**: 1835-1840.

Elder DJE, Halton DE, Hague A and Paraskeva C, Induction of apoptotic cell death in human colorectal carcinoma cell lines by a cyclooxygenase-2 (COX-2)-selective nonsteroidal anti-inflammatory drug: independence from COX-2 protein expression, 1997, *Clin Cancer Res*, **3**, 1679–1683.

Emery PH, Zeidler TK, Kvien M, Celecoxib versus diclofenac in long-term management of rheumatoid arthritis: randomised double-blind comparison, 1999, *Lancet*, **354:** 2106-2111.

Engel RH and Evens AM, Oxidative stress and apoptosis: a new treatment paradigm in cancer, 2006, *Front Biosci*, **11**: 300-312.

Engelmann J, Henke J, Willker W, et al., Early stage monitoring of miltefosine induced apoptosis in KB cells by multinuclear NMR spectroscopy, 1996, *Anticancer Research*, **16**:1429-1440.

Escriba PV, Ferrer-Montiel AV, Farragut JA, Gonzalez-Ros JM, Role of membrane lipids in the interaction of daunomycin with plasma membranes from tumor cells: implications in drug resistance phenomena, 1990, *Biochemistry*, **29**:7275-7282.

Evelhoch JL, Gillies RJ, Karczmar GS, et al., Applications of magnetic resonance in model systems: cancer therapeutics, 2000, *Neoplasia*, **2**:152-165.

Fang G, Kim CN, Perkins CL, et al., CGP57148B (STI-571) induces differentiation and apoptosis and sensitizes Bcr-Abl-positive human leukemia cells to apoptosis due to antileukemic drugs, 2000, *Blood*, **96**:2246–2253.

Ferrara N, Alitalo K, Clinical applications of angiogenic growth factors and their inhibitors, 1999, *Nat Med*, **5**: 1359–64.

Ferté J, Analysis of the tangled relationships between P-glycoprotein-mediated multidrug resistance and the lipid phase of the cell membrane, 2000, *Eur J Biochem*, **267**:277–294.

Finstad HS, Drevon CA, Kulseth MA, et al., Cell proliferation, apoptosis and accumulation of lipid droplets in U937-1 cells incubated with eicosapentaenoic acid, 1998, *Biochem J,* **336:**451–459.

Form DM, Auerbach R, FGE2 and angiogenesis,1983, *Proc Soc Exp Biol Med*, **172**:214-218.

Fournier T, Medjoubi N-N, Porquet D, Alpha-1-acid glyciprotein, 2000, *Biochim Biophys Acta*, **1482** : 157-171.

Franks SE, Smith MR, Aria-Mendoza F, Phosphomonoester concentrations differ between chronic lymphocytic leukemia cells and normal human lymphocytes, 2002,

Leukemia Res, **26**:919-926.

Gallo O, Masini E, Bianchi B, et al., Prognostic significance of cyclooxygenase-2 pathway and angiogenesis in head and neck squamous cell carcinoma, 2002, Hum Pathol, 33: 708-714.

Gambacorti-Passerini C, Le CP, Mologni L, et al., Inhibition of the ABL kinase activity blocks the proliferation of BCR/ABL+ leukemic cells and induces apoptosis, 1997, *Blood Cells Mol Dis,* **23**:380–394.

Gambacorti-Passerini C, Barni R, Le CP et al., Role of alpha1 acid glycoprotein in the in vivo resistance of human BCR–ABL(+) leukemic cells to the abl inhibitor STI571, 2000, *J Natl Cancer Inst,* **92**:1641–1650.

Garland JM and Halestrap A, Energy Metabolism during Apoptosis: *bcl-2* promotes survival in hematopoietic cells induced to apoptose by growth factor withdrawal by stabilizing a form of metabolic arrest, 1997, *J Biol Chem*, **272**: 4680-4688.

Geilen CC, Wieder T, Reutter W, Hexadecylphosphocholine inhibits translocation of CTP:choline-phosphate cytidylyltransferase in Madin-Darby canine kidney cells, 1992, *J Biol Chem*, **267**:6719-6724.

Gerber HP, Dixit V, Ferrara N, Vascular endothelial growth factor induces expression of the antiapoptotic proteins Bcl-2 and A1 in vascular endothelial cells, 1998, *J Biol Chem*, **273**:13313–6.

Giaccone G, Herbst RS, Manegold C, et al. Gefitinib in combination with gemcitabine and cisplatin in advanced non-small-cell lung cancer: a phase III trial INTACT1, 2004, *J Clin Oncol,* **22**:777-784.

Gillies RJ, Bhujwalla ZM, Evelhoch J, et al., Applications of magnetic resonance in model systems: tumor biology and physiology, 2000, *Neoplasia*, **2**:139-51.

Goldman JM and Melo JV, Targeting the BCR-ABL tyrosine kinase in chronic myeloid leukemia, 2001, *N Engl J Med*, **344**: 1084-1086.

Goni FM and Alonso A, Structure and functional properties of diacylglycerol in membranes, 1999, *Prog Lipid Res*, **38**:1-48.

Gorre ME, Mohammed M, Ellwood K, et al., Clinical resistance to STI-571 cancer therapy caused by BCR-ABL gene mutation or amplification, 2001, *Science*, **293**: 876-880.

Gottschalk S, Anderson N, Hainz C, Eckhardt SG, Serkova NJ, Imatinib (STI571)-mediated changes in glucose metabolism in human leukemia BCR-ABL-positive cells, 2004, *Clin Cancer Res*, **10**:6661-6668.

Green DE, Leloir LF and Nocito W, Transaminases, 1945, *J Biol Chem* **161**: 559-582.

Green DR and Reed JC, Mitochondria and apoptosis, 1998, *Science*, **281**:1309-1312.

Greenlee RT, Murray T, Bolden S, Wingo PA, Cancer statistics 2000. CA Cancer,

2000, *J Clin*, **50***:* 7-33.

Griffin JL, Lehtimaki KK, Valonen PK, et al., Assignment of ^{1}H nuclear magnetic resonance visible polyunsaturated fatty acids in BT4C gliomas undergoing ganciclovir-thymidine kinase gene therapy-induced programmed cell death, 2003, *Cancer Res.*, **63**:3195-201.

Griffith J, Black J, Faerman C, et al. The structural basis for autoinhibition of FLT3 by the juxtamembrane domain, 2004, *Mol Cell,* **13**:169-178.

Griffin JL, Shockcor JP, Metabolic profiles of cancer cells, 2004, *Nat Rev Cancer*, **4**:551-61.

Groesch S, Tegeder I, Niederberger E, Braeutigam L and Geisslinger G, COX-2 independant inducation of cell cycle arrest and apoptosis in colon cancer cells by the selective COX-2 inhibitor Celecoxib, 2001, *The FASEB Journal*, **15**: 2742-2744.

Hakumaki JM, Poptani H, Sandmair AM, Yla-Herttuala S, Kauppinen RA, 1H MRS detects polyunsaturated fatty acid accumulation during gene therapy of glioma: implications for the in vivo detection of apoptosis, 1999, *Nat Med,* **5**:1323-1327.

Han SW, Kim TY, Hwang PG, et al. Predictive and prognostic impact of epidermal growth factor receptor mutation in non-small-cell lung cancer patients treated with gefitinib, 2005, *J Clin Oncol*, **23**:2493-2501.

Hanahan D, Folkman J, Patterns and emerging mechanisms of the angiogenic switch during tumorigenesis, 1996, *Cell*, **86**:353-364.

Harris AL, Hypoxia: a key regulatory factor in tumour growth, 2002, *Nat Rev Cancer*, **2**: 38–47.

Hatse S, de Clercq E and Balzarini J, Impact of 9-(2-phosphonylmethoxyethyl) adenine on (deoxy)ribonucleotide metabolism and nucleic acid synthesis in tumor cells, 1999, *FEBS Letters,* **445:**92-97.

Hayes JD and McLellan LI, Glutathione and glutathione-dependent enzymes represent a co-ordinately regulated defense against oxidative stress, 1999, *Free Radic Res*, **31**, 273-300.

Hegedus T, Orfi L, Seprodi A, et al., Interaction of tyrosine kinase inhibitors with the human multidrug transporter proteins, MDR1 and MRP1, 2002, *Biochimica et Biophysica Acta*,1**587**:318-325.

Hehlmann R, Hochhaus A, Berger U, Reiter A, Current trends in the management of chronic myelogenous leukemia, 2000, *Ann Hematol,* **79:**345-354.

Heisterkamp N, Stephenson JR, Groffen J, et al., Localization of the c-abl oncogene adjacent to a translocation break point in chronic myelocytic leukaemia, 1983, *Nature,* **306**:239–242.

Henke Joachim, Dissertation: Apoptose-Induktion in humanen Tumorzellinien durch Hexadecylphosphocholin untersucht mit multinuklearer NMR-Spektroskopie, 1996, GCA Verlag.

Herbst RS, Review of epidermal growth factor receptor biology, 2004, *Int J Rad Oncol Phys*, **59**: 21–6.

Herbst RS, Giaccone G, Schiller JH, et al., Gefitinib in combination with paclitaxel and carboplatin in advanced non-small-cell lung cancer: a phase III trial -- INTACT2, 2004, *J Clin Oncol,* **22**:785-794.

Higgins CG and Linton KJ, The ATP switch model for ABC transporters, 2004, *Nat Struct Mol Biol,* **11**: 918–926.

Hinrichs JWJ, Klappe K, van Riezen M, Kok JW, Drug resistance-associated changes in sphingolipids and ABC transporters occur in different regions of membrane domains, 2005, *J Lipid Res*, 4**6**:2367 – 2376.

Hirata A, Ogawa S, Kometani T, et al., ZD1839 (Iressa) induces antiangiogenic effects through inhibition of epidermal growth factor receptor tyrosine kinase, 2002, *Cancer Res*, **62**: 2554–60.

Hochhaus A, Kreil S, Corbin AS, et al., Molecular and chromosomal mechanisms of resistance to imatinib (STI571) therapy, 2002, *Leukemia*, **16**: 2190-2196.

Hofmann W-K, Komor M, Wassmann B, et al., Presence of the BCR-ABL mutation Glu255Lys prior to STI571 (imatinib) treatment in patients with Ph^+ acute lymphoblastic leukemia , 2003, *Blood*, **102**: 659-661.

Holyoake L, Jiang X, Jorgensen HG, et al., Primitive quiescent leukemic cells from patients with chronic myeloid leukemia spontaneously initiate factor-independent growth in vitro in association with up-regulation of expression of interleukin-3, 2001, *Blood,* **97**:720–728.

Hou C-C, Hung S-L, Kao S-H, Chen TH, Lee H-M, Celecoxib Induces Heme-Oxygenase Expression in Glomerular Mesangial Cells, 2005, *Annals of the New York Academy of Sciences***, 1042**: 235-245.

Hsi LC, Baek SJ, Eling TE, Lack of cyclooxygenase-2 activity in HT-29 human colorectal carcinoma cells, 2000, *Exp Cell Res*, **256**: 563-70.

Huang GW, Yang LY, Lu WQ, Effects of PI3K and p42/p44 MAPK on overexpression of vascular endothelial growth factor in hepatocellular carcinoma, 2004, *World J Gastroenterol*, **10**: 809–12.

Huang Y, Liu J, Wang L-Z, Zhang W-Y, Zhu X-Z, Neuroprotective effects of cyclooxygenase-2 inhibitor celecoxib against toxicity of LPS-stimulated macrophages toward motor neurons, 2005, *Acta Pharmacologica Sinica*, **26**: 952-958.

Hughes TP, Kaeda J, Branford S, et al., Frequency of major molecular responses to imatinib or interferon alfa plus cytarabine in newly diagnosed chronic myeloid leukemia, 2003, *N Engl J Med*, **349**: 1423-1432.

Idziorek T, Estaquier J, De Bels F, Ameisen JC, YOPRO-1 permits cytofluorometric analysis of programmed cell death (apoptosis) without interfering with cell viability, 1995, *J Immunol Methods*, **185**: 249-258.

Janmaat ML, Giaccone G, The epidermal growth factor receptor pathway and its inhibition as anticancer therapy, 2003, *Drugs Today (Barc),* **39**: 61–80.

Jaffe BM, Prostaglandins and cancer: An update, 1974, *Prostaglandins*, **6**: 453–461.

Johnston D, Hall H, DiLorenzo TP, Steinberg BM, Elevation of the epidermal growth factor receptor and dependant signaling in human papillomavirus-infected laryngeal papillomas, 1999, *Cancer Res,* **59**: 968-974.

Jones MK, Wang H, Peskar BM, et al., Inhibition of angiogenesis by nonsteroidal anti inflammatory drugs: insight into mechanisms and implications for cancer growth and ulcer healing., 1999, *Nature Medicine*, **5**:1418-1423.

Kan O, Baldwin SA, and Whetton AD, Apoptosis is regulated by the rate of glucose transport in an IL-3 dependent cell line, 1994, *J Exp Med*, **180**:917-923.

Kantarjian H, Sawyers C, Hochhaus A, et al., Hematologic and cytogenetic responses to imatinib mesylate in chronic myelogenous leukemia, 2002, *N Engl J Med*, **346**: 645-52.

Kantarjian HM, O'Brien S, Cortes JE, et al., Treatment of Philadelphia chromosome-positive, accelerated-phase chronic myelogenous leukemia with imatinib mesylate, 2002, *Clin Cancer Res*, **8**: 2167-2176.

Kaplan O, van Zijl PCM, Cohen JS, NMR studies of metabolism of cells and perfused organs, 1992, *NMR Basic Principles and progress*, **28**: 3-52.

Kaplan O, van Zijl PCM, Cohen JS, Information from combined ^{1}H and ^{31}P NMR studies of cell extracts: differences in cell metabolism between drug-sensitive and drug-resistant MCF-7 human breast cancer cells, 1990, *Biochem Biophys Res Commun*, **169**:383-390.

Kent C, Eukaryotic phospholipids biosynthesis, 1995, *Annu Rev Biochem*, **64**: 315-343.

Klawitter J, Schmitz V, Miljus J, et al., A New Rapid Ion-pair Reverse Phase LC/LC/MS Method for the Quantification of Nucleotides, manuscript in preparation, 2006.

Kok JW, Veldman RJ, Klappe K, et al., Differential expression of sphingolipids in MRP1 overexpressing HT29 cells, 2000, *Int J Cancer*, **87**: 172–178.

Konstantini P, Jacotot E, Decaudin D, and Kroemer G, Mitochondria as a novel target of anticancer chemotherapy, 2000, *J Nat Cancer Inst (Bethesda),* **92**:1042-1053.

Krause DS and Van Etten RA, Tyrosine Kinases as targets for cancer therapies, 2005, *N Engl J Med*, **353**(2):172-187.

Kroemer G, The proto-oncogene Bcl-2 and its role in regulating apoptosis, 1997, *Nat Med*, **3**:614-620.

Kris MG, Natale RB, Herbst RS, et al., Efficacy of gefitinib, an inhibitor of the epidermal growth factor receptor tyrosine kinase, in symptomatic patients with non-small

cell lung cancer: a randomized trial, 2003, *JAMA,* **290**:2149-2158.

Laine LS, Harper T, Simon R, et al., A randomized trial comparing the effect of rofecoxib, a cyclooxygenase 2-specific inhibitor, with that of ibuprofen on the gastroduodenal mucosa of patients with osteoarthritis, 1999, *Gastroenterology*, **117:** 776-783.

Lang F, Busch GL, Ritter M, Völkl H, Waldegger S, Gulbins E, Hussinger D, Functional significance of cell volume regulatory mechanisms, 1998, *Physiol Rev*, **78**: 247-306.

Lang F, Gulbins E, Szabo I, et al., Cell volume and the regulation of apoptotic cell death, 2004, *J Mol Recognit*, **17**: 473-480.

Lapidot A, Gopher A, A Cerebral metabolic compartmentation, 1994, *J Biol Chem*, **269**: 27198-27208.

Lavie Y, Cao H, Bursten SL, Giuliano AE, Cabot MC, Accumulation of glucosylceramides in multidrug-resistant cancer cells, 1996, *J Biol Chem*, **271**:19530–19536.

Lavie Y, Fiucci G, Liscovitch M, Up-regulation of caveolae and caveolar constituents in multidrug-resistant cancer cells, 1998, *J Biol Chem*, **273**:32380-32383.

Le Coutre P, Tassi E, Varella-Garcia M, et al., Induction of resistance to the Abelson inhibitor STI571 in human leukemic cells through gene amplification, 2000, *Blood,* **95**:1758–1766.

Lehnert M, Multidrug resistance in human cancer, 1994, *J Neurooncol,* **22**:239-243.

Leichman CG, Lenz H-J, Leichman L, et al., Quantitation of intratumoral thymidylate synthase expression predicts for disseminated colorectal cancer response and resistance to protracted infusion of 5-fluorouracil and weekly leucovorin, 1997, *J Clin Oncol*, **15**: 3223–3229.

Leist M, Single B, Castoldi AF, Kuhnle S and Nicotera P, Intracellular adenosine triphosphate (ATP) concentration: a switch in the decision between apoptosis and necrosis, 1997, *J Exp Med*, **185**:1481−1486.

Le Moyec L, Tatoud R, Degeorges A, Calabresse C, Bauza G, Eugene M, Calvo F, Proton nuclear magnetic resonance spectroscopy reveals cellular lipids involved in resistance to adriamycin and taxol by the K562 leukemia cell line, 1996, *Cancer Research*, **56**:3461-3467.

Lim S-C, Park S-Y and Do, N-Y, Correlation of cyclooxygenase-2 pathway and VEGF expression in head and neck squamous cell carcinoma, 2003, *Oncology Reports*, **10**: 1073-1079.

Listenberger LL, Han X, Lewis SE, et al., Triglyceride accumulation protects against fatty acid-induced lipotoxicity, 2003, *Proc Natl Acad Sci USA,* **100**: 3077–3082.

Liu Q, Chan STF, and Mahendran R, Nitric oxide induces cyclooxygenase

expression and inhibits cell growth in colon cancer cell lines, 2003, *Cancer Biology*, **24**: 637-642.

Liu, Z-J, Snyder R, Soma A, et al., VEGF-A and $\alpha_V\beta_3$ integrin synergistically rescue angiogenesis via N-Ras and PI3-K signaling in human microvascular endothelial cells, 2003, *The FASEB Journal*, **17**: 1931-1933.

Lundberg P, Harmsen E, Ho C, Vogel HJ, Nuclear magnetic resonance studies of cellular metabolism, 1990, *Anal Biochem*, **191**: 193-222.

Lynch T, Bell DW, Sordella R, et al., Activating mutations in the epidermal growth factor receptor underlying responsiveness of non-small-cell lung cancer to gefitinib, 2004, *N Engl J Me*d, **350**:2129-2139.

Lyon RC, Cohen JS, Faustino PJ, Megnin F, Myers CE, Glucose metabolism in drug-sensitive and drug-resistant human breast cancer cells monitored by magnetic resonance spectroscopy, 1988, *Cancer Res*, **48**:870-877.

Mahon FX, Deininger MW, Schultheis B, et al., Selection and characterization of BCR-ABL positive cell lines with differential sensitivity to the tyrosine kinase inhibitor STI571: diverse mechanisms of resistance, 2000, *Blood*, **96**:1070-1079.

Mahon FX, Belloc F, Lagarde V, et al., MDR1 gene overexpression confers resistance to imatinib mesylate in leukemia cell line models, 2003, *Blood,* **101**:2368–2373.

Mancuso A, Beardsley NJ, Wehrli S, et al., Real time detection of 13C NMR labeling kinetics in perfused EMT6 mouse mammary tumor cells and BHC9 mouse insulinomas, 2004, *Biotechnol Bioeng*, **87**: 835-848.

Mendelsohn J, Epidermal growth factor receptor inhibition by a monoclonal antibody as anticancer therapy, 1997, *Clin Cancer Res*, **3**: 2703-2707.

The Merck Manual – Second Home Edition Whitehouse Station, NJ; Merck & Co., Inc. 2003, 2004.

Meves H, Modulation of ion channels by arachidonic acid, 1994, *Prog Neurobiol,* **43**:175–86.

Miljus J, Melo JV, Anderson N, Eckhardt SG, Serkova N, MRS ability to predict resistance development to Gleevec (abstract), 2005, ISMRM, 13th scientific meeting, Miami, USA.

Miljus J, Brown JL, Kominsky DJ, et al., Metabolic Consequences of Imatinib Resistance in Human Leukemia Cells, manuscript in preparation, 2006.

Mitsudomi T, Kosaka T, Endoh H, et al., Mutations of the epidermal growth factor receptor gene predict prolonged survival after gefitinib treatment in patients with non-small-cell lung cancer with postoperative recurrence, 2005, *J Clin Oncol*, **23**:2513-2520.

Mosmann, T., Rapid Colorimetric Assay for Cellular Growth and Survival: Application to Proliferation and Cytotoxicity Assays. J. Immunol. Meth. 1983, 65, 55-63.

Mountford CE, Doran S, Lean CL, Cancer pathology in the year 2000, 1997, *Biophys Chem,* **68**:127-35.

Müller C, Schäfer P, Störtzel M, Vogt S, Weinmann W, Ion suppression effects in liquid chromatrography-electrospray-ionization transport-region collision induced dissociation mass spectrometry with different serum extraction methods for systematic toxicological analysis with mass spectra libraries, 2002, *J Chromatogr B*, **773**: 47-52.

Nagar B, Bornmann WG, Pellicena P, et al., Crystal structures of the kinase domain of c-Abl in complex with the small molecule inhibitors PD173955 and Imatinib (STI-571), 2002, *Cancer Res*, **62**: 4236–43.

Nicholson JK, Lindon JC and Holmes E, "Metabonomics": understanding the metabolic responses of living systems to pathophysiological stimuli via multivariate statistical analysis of biological NMR spectroscopic data, 1999, *Xenobiotica*, **29**, 1181-1189.

Nicholson JK, Connelly K, Lindon JC and Holmes E, Metabonomics: A platform for studying drug toxicity and gene function, 2002, *Nature Reviews Drug Discovery*, **1**:153-161.

Nicotera P & Lesia M, Energy supply and the shape of death in neuron and lymphoid cells, 1997, *Cell Death Differ*, **4:**435-442.

Nimmanapalli R, Bhalla K, Mechanisms of resistance to imatinib mesylate in Bcr-Abl-positive leukemias, 2002, *Curr Opin Oncol*, **14**:616-620.

Nowell PC and Hungerford DA, Chromosome studies on normal and leukemic human leukocytes, 1960, *J Natl Cancer Inst,* **25**:85–109.

Okada Y and Maeno E, Apoptosis, cell volume regulation and volume-regulatory chloride channels, 2001, *Comp Biochem Physiol A Mol Integr Physiol*, **130**: 377-383.

Ottmann OG, Druker BJ, Sawyers CL et al., A phase 2 study of imatinib in patients with relapsed or refractory Philadelphia chromosome-positive acute lymphoid leukemias, 2002, *Blood,* **100**:1965–1971.

Paul MK and Mukhopadhyay AK, Tyrosine kinase – Role and significance in cancer, 2004, *Int J Med Sci*, **1**(2): 101-115.

Paez JG, Janne PA, Lee JC, et al., EGFR mutations in lung cancer: correlation with clinical response to gefitinib therapy, 2004, *Science,* **304**:1497-1500.

Pao W, Miller V, Zakowski M, et al., EGF receptor gene mutations are common in lung cancers from "never smokers" and are associated with sensitivity of tumors to gefitinib and erlotinib, 2004, *Proc Natl Acad Sci USA,* **101**:13306-13311.

Figueiredo-Pereira ME, Li Z, Jansen M and Rockwell P, *N*-Acetylcysteine and Celecoxib Lessen Cadmium Cytotoxicity Which Is Associated with Cyclooxygenase-2 Up-regulation in Mouse Neuronal Cells, 2002, J Biol Chem, 277: 25283-25289.

Pricl S, Fermeglia M, Ferrone M, Tamborine E, T315I-mutated Bcr-Abl in chronic myeloid leukemia and imatinib: insights from a computational study, 2005, *Mol*

Cancer Ther, **4**: 1167-1174.

Prenen H, Stefan C, Landuyt B, Imatinib Mesylate Inhibits Glucose Uptake in Gastrointestinal Stromal Tumor Cells by Down-regulation of the Glucose Transporters Recruitment to the Plasma Membrane, 2005, *American Journal of Biochemistry and Biotechnology*, **1**:95-102.

Robertson JD & Orrenius S, Molecular mechanisms of apoptosis induced by cytotoxic chemicals, 2000, *Crit Rev Toxicol*, **30:**609-627.

Roche-Lestienne C, Soenen-Cornu V, Grardel-Duflos N, et al., Several types of mutations of the Abl gene can be found in chronic myeloid leukemia patients resistant to STI571, and the can pre-exist to the onset of treatment, 2002, *Blood,* **100:**1014-1018.

Ross BD, The biochemistry of living tissues: examination by MRS, 1992, *NMR Biomed*, **5**: 215-219.

Roumiantsev S, Shah NP, Gorre ME, et al., Clinical resistance to the kinase inhibitor STI-571 in chronic myeloid leukemia by mutation of Tyr-253 in the Abl kinase domain P-loop, 2002, *Proc Natl Acad Sci U S A*, **99**: 10700-10705.

Rowley JD, Letter: a new consistent chromosomal abnormality in chronic myelogenous leukaemia identified by quinacrine fluorescence and Giemsa staining, 1973, *Nature,* **243**: 290–293.

Salomon DS, Bradt R, Ciardiello F, Normanno N, Epidermal growth factor related peptides and their receptors in human malignancies, 1995, *Crit Rev Oncol Hematol*, **19**: 183-232.

Salonga D, Danenberg KD, Johnson M, et al., Colorectal tumors responding to 5-fluorouracil have low gene expression levels of dihydropyrimidine dehydrogenase, thymidylate synthase, and thymidine phosphorylase, 2000, *Clin Cancer Res*, **6**:1322–1327.

Savage DG and Antman KH, Imatinib mesylate – a new oral targeted therapy, 2002, *N Engl J Med,* **346:**683-693.

Sawyer TK, Novel oncogenic protein kinase inhibitors for cancer therapy, 2004, *Current Medicinal Chemistry – Anti-Cancer Agents*, **4**(5): 449-455.

Sawyers CL, Rational therapeutic intervention in cancer: kinases as drug targets, 2002, *Curr Opin Gen Develop*, **12**: 111-115.

Schlessinger J, Cell signaling by receptor tyrosine kinases, 2000, *Cell,* **13:** 211-225.

Serkova N, Brand A, Christians U, Leibfritz D, Evaluation of the effects of immunosuppressants on neuronal and glial cells in vitro by multinuclear magnetic resonance spectroscopy, 1996, *Biochim Biophys Acta*, **1314**: 93-104.

Shah NP, Nicoll JM, Nagar B, et al. Multiple BCR-ABL kinase domain mutations confer polyclonal resistance to the tyrosine kinase inhibitor imatinib (STI571) in chronic phase and blast crisis chronic myeloid leukemia, 2002, *Cancer Cell*, **2**: 117-125.

Sheng H, Shao J, Kirkland SC, et al., Inhibition of human colon cancer cell growth by selective inhibition of cyclooxygenase-2, 1997, *J Clin Investig*, **99**: 2254-9.

Shih CM, Ko WC, Yang LY, et al., Detection of Apoptosis and Necrosis in Normal Human Lung Cells Using 1H NMR Spectroscopy, 2005, *Ann N Y Acad Sci*, **1042**:488-96.

Smith KM, Yacobi R, Van Etten RA, Autoinhibition of Bcr-Abl through its SH3 domain, 2003, *Mol Cell,* **12**:27-37.

Smith TA. FDG uptake, tumour characteristics and response to therapy: a review, 1998, *Nucl Med Commun*, **19**: 97–105.

Sordella R, Bell DW, Haber DA, Settleman J, Gefitinib-sensitizing EGFR mutations in lung cancer activate anti-apoptotic pathways, 2004, *Science*, **305**:1163-1167.

Steinbach G, Lynch PM, Phillips RKS, Wallace MH, Hawk E, Gordon GB, et al., The effect of Celecoxib, a Cyclooxygenase-2 Inhibitor, in Familial Adenomatous Polyposis, 2000, *New England Journal of Medicine*, **342**: 1946-1952.

Sterin M, Cohen JS, Mardor Y, Berman E, and Ringel I, Levels of Phospholipid Metabolites in Breast Cancer Cells Treated with Antimitotic Drugs: A ^{31}P-Magnetic Resonance Spectroscopy Study, 2001, *Cancer Res*, **61**:7536-7543.

Suhardja A, Hoffman H, Role of growth factors and their receptors in proliferation of microvascular endothelial cells, 2003, *Microsc Res Tech*, **60**: 70–5.

Sun W, Haller DG, Chemotherapy for colorectal cancer, 2002, *Hematol Oncol Clin North Am,* **16**:969-994.

Talpaz M, Silver RT, Druker BJ, et al., Imatinib induces durable hematologic and cytogenetic responses in patients with accelerated phase chronic myeloid leukemia: results of a phase 2 study, 2002, *Blood*, **99**: 1928-1937.

Tipping AJ, Mahon FX, Lagarde V, Goldman JM, Melo JV, Restoration of sensitivity to STI571 in STI572-resistant chronic myeloid leukemia cells, 2001, *Blood*, **15**: 3864-3867.

Vane JR, Inhibition of prostaglandin synthesis as a mechanism of action for aspirin-like drugs, 1971, *Nature (London),* **231**:232-235.

Van der Geer P, Hunter T, Lindberg RA, Receptor protein-tyrosine kinases and their signal transduction pathways, 1994, *Annual Reviews of Cell Biology*, **10**: 251-337.

Van den Abbeele AD and Badawi RD, Use of positron emission tomography in oncology and its potential role to assess response to imatinib mesylate therapy in gastrointestinal stromal tumors (GISTs), 2000, *European Journal of Cancer*, **38**:60-66.

Van Etten RA, c-Abl regulation: a tail of two lipids, 2003, *Curr Biol,* **13**:R608-R610.

Van Etten RA, Mechanisms of transformation by the BCR–ABL oncogene: new perspectives in the post-imatinib era, 2004, *Leuk Res,* **28**(Suppl 1):S21–S28.

Van Etten RA and Shannon KM, Focus on myeloproliferative diseases and

myelodysplastic syndromes, 2004, *Cancer Cell,* **6**:547-552.

Von Bubnoff N, Schneller F, Peschel C, Duyster J, BCR-ABL gene mutations in relation to clinical resistance of Philadelphia-chromosome-positive leukemia to STI571: A prospective study, 2002, *Lancet,* **359:** 487-491.

Von Kleist S, Chany E, Burtin P, King M and Fogh J, Immunohistology of the antigenic pattern of a continuous cell line from a human colon tumor, 1975, *J Natl Cancer Inst*, **55**: 555–560.

Warburg O, On the origin of cancer cells, 1956, *Science*, **123**: 309-314.

Watanabe D, Ezoe S, Fujimoto M, et al., Suppressor of cytokine signalling-1 gene silencing in acute myeloid leukaemia and human haematopoietic cell lines, 2004, *Br J Haematol,***126**:726-735.

Williams SNO, Anthony ML, Brindle KM, Induction of apoptosis in two mammalian cell lines results in increased levels of fructose-1,6-biphosphate and CDP-cholines determined by 31P-MRS, 1998, *Magn Reson Med*, **40**:411-420.

Wosikowski K, Mattern K, Schemainda I, et al., WK175, a novel antitumor agent, decreases the nicotinamide diadenine nucleotide concentration and induces the apoptotic cascade in human leukemia cells, 2002, *Cancer Research*, **62**:1057-1062.

Wyllie AH, Kerr JFR, Currie AR, Cell death: the significance of apoptosis, 1980, *Int Rev Cytol*, **68**:251-05.

Zamaraeva MV, Sabirov RZ, Maeno E, et al., Cells die with increased cytosolic ATP during apoptosis: a bioluminescence study with intracellular luciferase, 2005, *Cell Death and Differentiation*, **12**:1390–1397.

Zeisel SH and Blusztajn JK, Choline and human nutrition, 1994, *Annu Rev Nutr*, **14**: 269-296.

Zgurskaya HI and Nikaido H, Multidrug resistance mechanism: drug efflux across two membranes, 2000, *Mol Microbiol,* **37**:219-225.